ELECTRONIC PROCESSES IN Au-CdS-In DIODES

Richard Stephen Muller

Division of Engineering and Applied Sciences

California Institute of Technology

Pasadena, California

May 1962

ACKNOWLEDGEMENTS

Special thanks for many enlightening discussions are due Dr. R. D. Middlebrook, who acted as adviser for this work. The author is indebted to the National Science Foundation and to the General Electric Foundation for fellowships held during the course of his research. The California Institute of Technology Jet Propulsion Laboratory also provided financial backing for part of the work.

Single crystals of CdS were generously donated by Dr. D. C. Reynolds of the Wright Air Development Center, Dr. J. Johnson of the Westinghouse Research Laboratory and R. W. Smith of the Radio Corporation of America Research Laboratory.

The help of Cynthia Markiewicz who typed the manuscript is gratefully acknowledged. Finally, the encouragement and aid of my wife Joyce, who helped tangibly in the preparation of the manuscript and intangibly in countless ways, is most appreciatively noted.

ABSTRACT

A study of various electronic processes in a class of solid-state diodes which function analogously to thermionic-emission vacuum tube rectifiers is made. For experimental work, such diodes were fabricated from an insulating crystal (cadmium sulfide) to which an ohmic contact (indium) and a blocking contact (gold) were affixed. The properties of the diodes that are most rigorously investigated are the equilibrium space-charge-limited current-voltage characteristic, the behavior of the blocking contact under high reverse fields, and the capacitance dependence upon crystal trapping-state kinetics. Electron trapping is demonstrated to have a marked influence on most of the electronic properties of analogue diodes. Mathematical analysis based upon the premise that these traps are volume-distributed in the crystals of CdS is corroborated by the experimental results.

An analytical method, which treats various trapping configurations with energy in a unified fashion, is employed to calculate the expected influence of traps on the space-charge-limited current characteristic. Correspondence of this analysis with experimental observations permits the deduction, in some cases, of trap densities and trap depths. The theoretical treatment of the influence of volume-distributed trapping states on terminal capacitance is also shown to be consistent with measurements designed to test the physical model. Use of this theory to interpret measured capacitance variation allowed the determination of some of the kinetic properties of trapping

states, thus demonstrating a new technique for obtaining this information. Correspondence with the results from other methods is good. Trapping-state concentrations in actual crystals are shown to constrain practical solid-state analogue devices to very small dimensions.

TABLE OF CONTENTS

CHAPTER III

CHAPTER IV

CHAPTER V

CHAPTER VI

INTRODUCTION

The noteworthy practical success that has attended a deeper understanding of the electronic properties of semiconductors has made the value of research on other solid materials keenly apparent. Temperature problems in the semiconductors have led naturally to the consideration of larger band-gap materials to see whether these, too, can be used in practical electron devices. Of course, some large band-gap materials have both been studied and used for many years because of their photosensitive properties. Although the photosensitivity of these materials was first noted as long ago as 1873 [1], very little in the way of a fundamental understanding of the responsible physical processes preceded the era of the transistor. There are good reasons for this time lag of seventy-five years between experimental observation and the beginnings of a good theoretical explanation. It has been said that the variety of electronic behavior shown by a solid increases roughly by an order of magnitude for each electron volt of its band gap. If this is a good estimate, it is evident that the insulators and most of the practical photoconductors, which have band gaps of two or more electron volts, will indeed be very complex physical systems. Complex or not, technology and the entire solid state art have advanced to such a point that large band-gap materials will be exploited in electronic devices. It is therefore a necessity to develop a physical understanding of the underlying processes which can dominate their behavior.

The increasing complexity of the large band-gap materials makes it all the more desirable that one's method of appraisal be simple. Because a complete solution of even a simple approximate model is apt to be very complex and difficult to assimilate, one is forced to look at approximations and trends. To quote Rose on this topic [2]: "Rigorous mathematical solutions can be made, if simple models are assumed. If one has confidence that materials can be fabricated with the purity demanded by these models, complete solutions are, of course, justified even if they are complex. If the materials one actually deals with are more complex than these simple models, however, then complete solutions are practically ruled out and one seeks a simple point of view from which to interpret the varied behavior of the materials. Most photoconductors appear to fall within the second 'if'."

A general characteristic of large band-gap materials is, of course, a low intrinsic free-carrier concentration. Therefore, if one seeks to make use of such a material for a practical electron device, some way must be found to increase the interior electron concentration so that appreciable currents may be drawn through it. This may be done by illumination or, as in semiconductors, by crystal doping with donor or acceptor atoms. There is, however, a third technique for increasing the free-charge population which becomes feasible only as intrinsic resistivities become very large. Under suitable conditions, there can be direct contact injection of electrons into the crystal conduction band. As discussed by Parmenter and Ruppel [3], appreciable excess charge injection into

a solid becomes possible when the carrier transit time through a region is smaller than the no-injection dielectric relaxation time in that region. This time constant for relaxation of an initial charge excess by drift processes alone is defined as the product of crystal permittivity and resistivity, $\tau = K\epsilon_0\rho_0$. For semiconductors, the dielectric relaxation time is usually in the nanosecond range or less, while for the photoconductors it can easily be in the order of milliseconds. Charge injection into photoconductors is, therefore, a very practical possibility, provided a suitable injecting contact can be found to the crystal. This mode of increasing conductivity in a region is seen to be a direct analogue to thermionic emission into a vacuum. One is led, therefore, to consider the possibility of employing it to make a new class of solid-state devices which function analogously to vacuum tubes. Much conjecture has already been published about the properties that this class of devices are expected to exhibit [4][5]. What is needed is a further experimental evaluation of the properties of materials in which this mode of operation may be exploited. Only with this experimental evidence can the simplifying viewpoints which allow one to build up a tractable, yet sufficiently accurate model be attained. The work reported in the following chapters was motivated by these considerations.

In order to look into the properties of solid-state charge injected devices, one must be able to make injecting contacts to an insulating crystal. It is because ample proof of this capability existed for CdS that this material was chosen for investigation.

Cadmium sulfide is a yellow crystalline substance which can be grown in single crystals of the close-packed-hexagonal type. It has a band gap of about 2.4 electron-volts, and has been used commercially as a photoconductive substance for years. Many of its properties have been investigated in both single-crystal and powder form, and considerable information is therefore available from previous research. In an extensive study of the properties of metallic contacts to CdS, it has been discovered that ohmic contacts can be made with either indium or gallium [6]. All other metals tested resulted in contacts which are blocking to electrons.

Before proceeding in our discussion, we shall pause to clarify these terms "ohmic" and "blocking" contact, which are used extensively in the literature on photoconductors. An ohmic contact is defined as an electrode which supplies an essentially infinite reservoir of carriers, ready to enter an insulating crystal as needed to keep the electric field zero at the contact. An "ohmic contact," therefore, is not the type of contact which is made to a solid, having a volt-ampere characteristic which is described by the adjective "ohmic." This unfortunate situation is a fact, because a solid showing a volt-ampere characteristic that is ohmic under the general use of the terminology has a field which is everywhere finite and constant and, therefore, non-zero at the contact. Thus, we shall usually avoid the term and describe a contact, having the properties mentioned above, as being injecting. Where "ohmic contact" is used, it will be in an effort at consistency with some pertinent reference. The

virtual cathode formed in front of a thermionic emitter in a vacuum diode is a familiar example of an injecting contact to the insulating vacuum space between cathode and anode. A blocking contact, on the other hand, is incapable of supplying excess electrons to an insulator and the field at such a contact is not necessarily zero. As with semiconductors, the decision as to the injecting or blocking character of a metallic contact to CdS has proven more complicated than a simple correlation between work functions of metal and insulator would suggest. Bube [1] reports the research done to date on this question.

Despite the feasibility of making injecting and blocking contacts to CdS, the development of solid-state analogue devices has not proceeded to a practical level as yet. This has been due chiefly to the relative abundance of trapping states which exist in the forbidden gap of crystals of the material. These trapping states accept most of the charge injected, and, in general, control the electronic properties of the crystal as seen externally. Moreover, it does not appear likely that it will be possible to make single crystals with such low trap populations that the effects of trapping in any large band-gap materials will be entirely negligible. Therefore, a thorough knowledge of the effects of these states is a necessity to any exploitation of analogue solid-state devices. A large portion of this report will accordingly be concerned with the influences of trapping on the electronic properties of CdS. The term "trapping state" as used in this report refers to a center located

energetically in the forbidden gap between the valence band and the conduction band, which is capable of capturing a free hole or a free electron. This definition is in accordance with common practice in semiconductor terminology and avoids the further possible distinctions about such levels, which can be made on the basis of the dominant mechanism responsible for the emptying of a filled trap. A particular experiment or phenomenon will usually make clear the role of a given trapping level, so that, for our purposes, the definition stated above will suffice. A full discussion of traps and the kinetics governing their occupation is found in Bube [1, Chapter 9]. Traps may exist only at discrete energies, or else there may be a band of trapping levels distributed more or less continuously in energy. Bube [1, p. 299] discusses some of the physical reasons for this fact. Evidence, both for traps which are continuously distributed in energy and for traps at a discrete energy level, is given in Chapter 5 of this work, and analyses for both of these cases are presented in Chapter 1.

To perform the experimental work which we shall describe, analogue diodes were constructed by affixing both injecting and blocking contacts to a single crystal of CdS. In this way, studies could be made conveniently of crystal properties under both charge injection and no-injection conditions.

In spite of extensive research on the effects of trapping in CdS, there is not complete agreement on a physical picture to

explain the experimental results. Even the spatial location of the influential trapping levels is a matter of some dispute, with at least one investigator taking the point of view that surface states control the volt-ampere characteristics under injection bias [7]. The diversity of current-voltage dependences under charge-injection conditions is so great, as we shall see, that it is not surprising that surface conditions, with their usual labile properties, should be invoked. Owing largely to the work of A. Rose and his group at RCA, a coherent theoretical explanation of the extremely varied observations has been attained in terms of bulk behavior alone. This interpretation, which assumed that the influential traps are volume distributed, will be found to describe fully the experimental work done here and will therefore be discussed in detail.

Both static and dynamic properties of the trapping states in CdS were investigated as will be described in the following chapters. Long term equilibrium volt-ampere characteristics under conditions of charge injection were studied in order to determine trapping-state densities and energy locations in the forbidden band. This technique was introduced by Rose's group at RCA, and will be the object of some discussion. A new approach was used to study the kinetic properties of trapping. Previous investigations have detected the time-dependent properties of traps through measurements of photoconductive rise and decay times, or of the properties of thermally-stimulated trap emptying [1][8]. The technique which we shall use involves a direct

detection of the trapped charge through the measurement of the diode terminal capacitance exhibited under conditions of charge injection. The capacitance is found to vary with illumination, bias voltage and measuring signal frequency in a way which can be correlated directly with the anticipated effects of varying amounts of trapped charge.

The properties of the diode blocking contact under apparent breakdown conditions were also the subject of an extensive investigation. Evidence will be given for an apparent Schottky-type high field emission over the barrier, although, as we shall see, a tunneling mechanism is not entirely ruled out. The photoconductive properties of the crystals are not the subject of an intensive quantitative study for the following reasons: first, research in this field has occupied many individuals for some time now, and a fair understanding of the quantitative effects of illumination has been attained; second, the equipment needed for such study was not readily available. In general, only the gross effects of illumination with order-of-magnitude accuracy for intensity variations was attempted.

In order to gain a clear perspective of what is to come, we shall conclude this section with a synopsis of this report, stating what was done and where it will be discussed. In Chapter 1, a complete analysis of the possible behavior of space-charge-limited currents in an insulator with traps is presented. A unified approach is used to handle various trapping

configurations with energy, which apply to the diodes studied. Chapter 2 provides a theoretical basis for the effects of trapped charge on the measured capacitance of an analogue diode. Thus, Chapters 1 and 2 are completely theoretical. In Chapter 3, the techniques used in the fabrication of the diodes which were made of CdS with gold and indium contacts are described. Chapters 4, 5 and 6 treat the measured characteristics of these diodes. Chapters 4 and 5 together discuss the complete equilibrium current-voltage behavior, with the high field effects at the gold junction the prime subject of Chapter 4. Chapter 5 describes the measurements made on the space-charge-limited currents observed in the diodes, and the deductions as to trapping properties made from them. Chapter 6 takes up the dependence of measured capacitance on various parameters and interprets this data in terms of the analysis of Chapter 2. Over-all conclusions form the final portion of the report. These will comment on the significance of the measurements and on the applicability of the various analyses presented here and in the references.

CHAPTER I

Theoretical Treatment of Space-Charge-Limited Currents in an Insulator with Traps

This chapter provides a unified theoretical basis for the properties of space-charge-limited current flow in an insulator with traps. The aim is not a mathematically rigorous treatment, because rigor in this case, unfortunately, leads to implicit equations between voltage and current and to a loss of the physical picture which underlies the observed phenomena. Instead, we shall develop the current-voltage relationships chiefly by making use of an approach developed by Lampert [9] and used by him to handle the discrete-energy trapping level. Lampert's work is here extended to various energetically-distributed trapping states in order to provide a coherent and unified structure from which to survey experimental results. Traps distributed in energy were first treated by Rose [10] in a different manner than we have used. Experimental evidence, to be presented in Chapter 5, has prompted the choice of the various energetic trapping configurations which are treated mathematically here. The spatial distribution of traps is assumed to be uniform in all cases.

The analysis to be presented is one dimensional, with x being used to denote distance. The only free-charge carriers considered to be present are electrons and recombination is taken to be negligible. The crystal is assumed to have an

injecting contact at the cathode which exists at the plane $x = 0$. The collecting electrode, which may be either injecting or blocking is called the anode and is situated at the plane $x = L$. Positive bias is defined by making the anode positive with respect to the cathode.

The over-all plan for the chapter is as follows. Section 1.1 will indicate some of the difficulties occasioned through use of a straightforward analysis, and will state conditions on the mathematical treatment which will be given in the remainder of the chapter. Section 1.2 will explain, in detail, the method of approximate analysis which will be used extensively to obtain the volt-ampere characteristic for various trapping configurations with energy. The low-voltage characteristic for a crystal containing a discrete trapping level is considered in Section 1.3. This is the only case of space-charge-limited current in a crystal with traps that can be calculated explicitly in a straightforward manner from considerations of the applicable differential equations. The direct mathematical derivation of the volt-ampere characteristic is therefore given in Section 1.3.1. In Section 1.3.2, the simplified analysis is used to treat this trapping configuration. The derivation by both methods provides a comparison which clarifies the application of the simplified method. In Section 1.4, some consideration is given to the volt-ampere characteristic of a discrete level at voltages near to that voltage which fills all the traps. The influence of the trapping parameter θ on the steepness of the

volt-ampere characteristic during trap filling is deduced by making an approximation to the true trap-filling characteristic in Section 1.4.1. Section 1.4.2 points up a limitation in the simplified method of Section 1.2, which becomes evident when it is applied to the trap-filling case of a discrete level. Two or more discrete levels are considered in Section 1.5, largely through extension of the results derived in Sections 1.3 and 1.4 for single-level trapping. Section 1.6 and its two subsections, 1.6.1 and 1.6.2, analyze the important case of energy-distributed traps through the use of the simplified viewpoint of Section 1.2. In Section 1.6.1, the configuration studied is an energetically-continuous constant trap density. In Section 1.6.2, the trap density is exponentially varying with energy. A summary of the techniques used and the results obtained in this chapter is incorporated in Section 1.7.

1.1. Comments on an Exact Approach

The procedure in the mathematical analysis of space-charge-limited currents in a solid is straightforward. The exact treatment stems from the simultaneous solution of three integro-differential equations: two of them express the definitions of potential and of drift current. The third is Poisson's equation. The interdependences, however, are such that in all but the simple, trap-free case and the case of a discrete-energy trapping level at low applied voltages, it is impossible to obtain from these an explicit relationship between current and voltage.

Lampert treats exactly the case of discrete-energy traps at all applied voltages in an appendix to his work [9], the complexity of which points up the need for a more illustrative approach. As an example, the exact equation for the current density J, derived by Lampert, takes the form:

$$J = \frac{e\mu n_a V}{L}\left\{\frac{U_a - \ln(1 + U_a)}{(1/2)U_a^2 - U_a + \ln(1 + U_a)}\right\} \qquad (1.1)$$

where U_a is defined as:

$$U_a = \frac{n_{ta} - (\bar{n}_{ta} + \bar{n}_a)}{n_a}$$

and e is the electronic charge,

μ is the electron mobility,

V is the applied voltage,

L is the anode-to-cathode spacing,

n_{ta} is the trapped-electron density at the collecting electrode (anode),

n_a is the free-electron density at the anode.

The bars refer to no-injection equilibrium values for the corresponding quantities. Yet to be inserted into equation 1.1 is the dependence of n_a on V, which will complicate the

over-all equation still further. Even without this added complexity, the form of 1.1 is too cumbersome to be of use without making approximations valid in the various regions of operation. The insight permitting these approximations comes, unfortunately, from taking other than this mathematical route to a solution. One is thus in the position of being led to an approximate method to gain facility in manipulating the exact solution to a form already known.

These considerations led Lampert to adopt a viewpoint which we shall build upon in this treatment, leaving the exact solution to be used as a check on the approximate methods. Before beginning, we should note that assumed in the analysis to be given is the condition that only drift processes contribute to the current flow. This has been proven not to lead to inaccuracies in more complete mathematical analyses which have taken account both of drift and diffusion. Shockley and Prim [11], for example, considered the effect of diffusion in a trap-free semiconductor, and showed that for applied voltages in excess of kT/e diffusion was relatively unimportant in determining the over-all characteristic. Suits [12] also considered the complete solution for a variable-width space-charge region including traps, and reached the same conclusion.

We shall also omit consideration in this chapter of two-carrier space-charge-limited currents* [3][13], because we are

* Two-carrier space-charge-limited currents would flow if holes were freely injected at one electrode and electrons at the other: the only constraint on the flow being the application of Poisson's equation.

primarily concerned with a mathematical treatment valid for the diodes studied. There has not yet been experimental verification of true two-carrier space-charge-limited currents in any materials.

1.2. The Simplified Viewpoint

The basis for the simplification proposed by Lampert lies in shifting attention from current as a function of voltage to anode charge as a function of voltage. As in the analyses of transistors and other semiconductor devices, this charge-oriented viewpoint succeeds both in providing a means for the derivation of manageable equations and in leading to a physical picture which may be readily grasped and understood.

We may begin the mathematical analysis by writing the applicable form of Poisson's equation:

$$\frac{dE}{dx} = -\frac{e}{K\epsilon_0}\left[(n - \bar{n}) + (n_t - \bar{n}_t)\right] \qquad (1.2)$$

where E is the electric field,

$K\epsilon_0$ is the permittivity of the crystal,

n is the conduction-band electron density,

n_t is the trapped-electron density,

and the bars denote no-injection values (charge-free interior).

For all values of applied positive bias, electrons are injected into the crystal such that $n > \bar{n}$ and $n_t > \bar{n}_t$, which implies that the bracket in 1.2 is always positive. Therefore, E changes monotonically from zero at the cathode, where dE/dx is negatively infinite (we assume an infinite charge reservoir for n at the cathode) to its anode value E_a (figure 1.1). Hence, E necessarily has its largest magnitude at the anode, a fact also evident from Gauss' law since the anode is the only source of electrical flux lines. Furthermore, using the fact that for an applied voltage equal to V, E is constrained by the relationship:

$$- \int_0^L E dx = V$$

it can be shown quite readily that $(V/L) \leq -E_a \leq 2(V/L)$. The proof of this inequality is due to Lampert [9]. It may be demonstrated by noting that the free-electron density n is constrained through the relationship $|J| = |e\mu nE|$ = constant. Therefore, since $|E|$ is monotonically increasing from 0 to $|E_a|$ across the diode, n must be monotonically decreasing from its cathode value. We assume, in addition to the spatial uniformity of trapping states, that n and n_t are in quasi-thermal equilibrium [9]. From this assumption, n_t also must decrease monotonically from cathode to anode. Therefore, the curve representing E must lie within the region on figure 1.1 marked I and indicated with cross-hatching. The boundaries to this region represent the case of ohmic flow and that of a

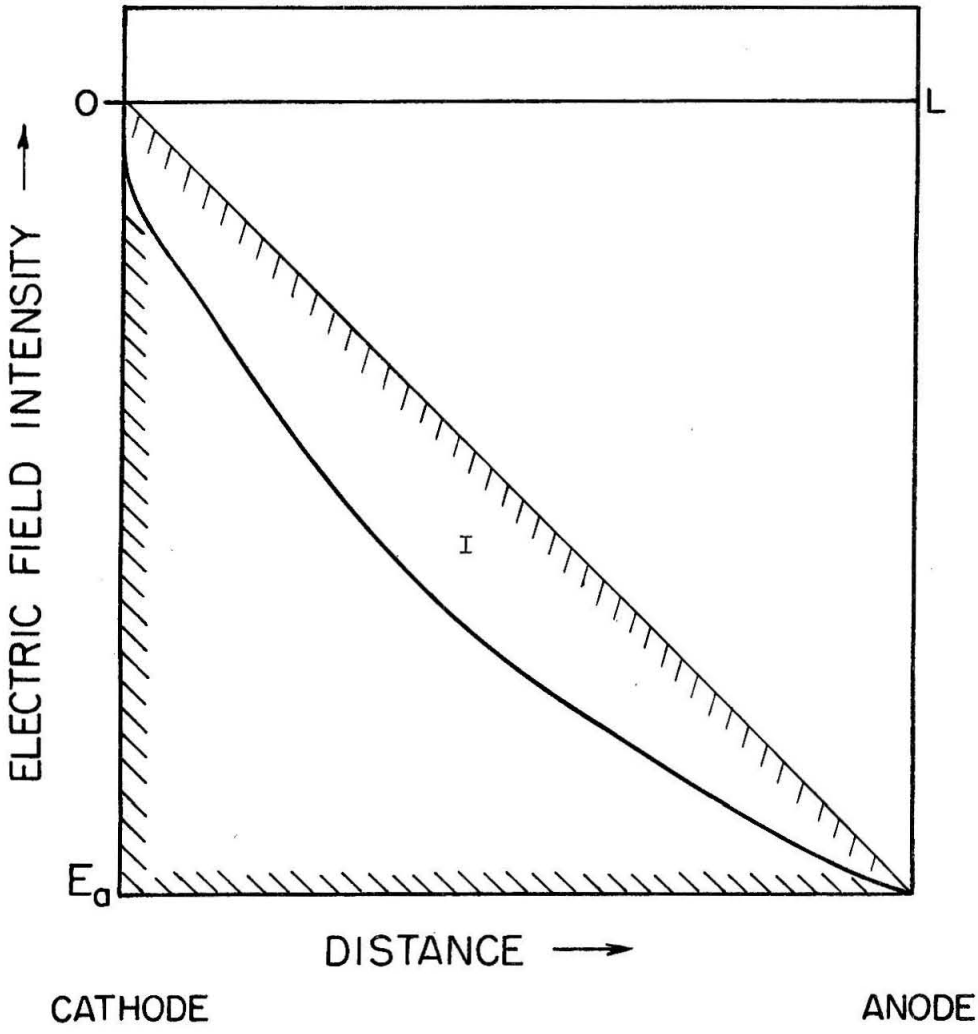

Figure 1.1. Requisite form for electric field variation with distance. Curve must lie within Region I, indicated by cross-hatched boundaries.

constant interior-charge density. Represented physically on figure 1.1, the integral constraint on E, just mentioned, states that the area between the curve standing for the field and the distance axis is fixed at V. Stating this area in terms of the boundary lines to Region I establishes the inequality. Thus, the anode field is never greater than twice the value it has for ohmic-flow conditions. This is true independently of the trapping configuration with energy.

Since drift alone is considered as an electronic-transport process, we may write:

$$J = -e\mu n_a E_a \tag{1.3}$$

Therefore, considering the inequality derived, the actual current may always be computed within a factor of two from the relationship:

$$J \approx e\mu n_a (V/L) \tag{1.4}$$

Equation 1.4 emphasizes the fact that the complex and varied behavior of insulators under conditions of charge injection is contained in the dependence of the anode free-electron density upon the applied voltage. In fact, if n_a may be obtained as an explicit function of voltage, its insertion into equation 1.4 will yield an explicit volt-ampere characteristic, valid within a factor of two.

An approximate, but very useful, method for obtaining an expression for the dependence of n_a on V follows from the integrated form of the Poisson equation. The over-all Poisson expression, equation 1.2, may be simplified in most practical cases by neglecting $\bar{n}$ and $\bar{n}_t$ since no-injection densities are necessarily small compared to injected charge densities under conditions of space-charge limitations. Integrating equation 1.2 under this assumption leads to the form:

$$-\int_0^{E_a} dE = \frac{e}{K\epsilon_0}\left[\int_0^L n\,dx + \int_0^L n_t\,dx\right]$$

or

$$-\frac{K\epsilon_0 E_a}{eL} = \frac{1}{L}\int_0^L n\,dx + \frac{1}{L}\int_0^L n_t\,dx \qquad (1.5)$$

This may be written as:

$$\nu_a = \underline{n} + \underline{n}_t \qquad (1.6)$$

where ν_a is defined as $-(K\epsilon_0 E_a)/eL$ and the underlines denote average densities. Equation 1.6 shows that ν_a physically represents the average injected-charge density inside the crystal. The inequality just derived for E_a shows us that ν_a will always be within a factor of two of the value $\nu_a = (K\epsilon_0 V)/eL^2$.

Thus, equation 1.6 provides an approximate relationship between $\underline{n}$, $\underline{n}_t$ and V when this value for ν_a is inserted into it. The electron density needed, however, to obtain the current-voltage characteristic from equation 1.4 is not the average free-charge density $\underline{n}$, but the anode free-charge density n_a. A relationship between $\underline{n}$ and n_a must, therefore, be incorporated into equation 1.6 to obtain the desired result - an expression for n_a in terms of V. The relationship we shall assume between these quantities is: $\underline{n} = n_a$ and likewise $\underline{n}_t = n_{ta}$, independently of the applied voltage. This assumption is usually closely fulfilled, but fails under certain conditions which, fortunately, may be recognized beforehand. We defer further discussion of this point until some familiarity is gained in the simplified technique here expounded. Insertion of these approximate forms for ν_a and $\underline{n}$ into equation 1.6 leads to:

$$\frac{K\epsilon_0 V}{eL^2} \approx n_a + n_{ta} \tag{1.7}$$

With equation 1.7, we have written all the expressions necessary to obtain the current-voltage characteristic through use of the simplified viewpoint. Basically, the procedure involved is to determine the dependence of n_{ta} upon n_a and to insert this into equation 1.7. In general, this dependence will be a function of the Fermi level and, thereby, also a

function of voltage. The anode free-charge density n_a is then calculated in terms of applied voltage. Having n_a in terms of V, one makes use of equation 1.4 to obtain J in terms of V. In certain cases, where extra information is available, an improvement upon the accuracy of equation 1.7 is made possible by deriving a different form through the statement of more exact relationships between ν_a and V and between $\underline{n}$ and n_a. This will be illustrated in Section 1.4.2. Much of the remainder of this chapter will be concerned with the application to various trap configurations with energy of this simplified technique for the determination of volt-ampere behavior.

1.3. Crystal with a Discrete Trapping-Level at Low Voltages

The complications arising in the analysis of the crystal with traps stem from the fact that the total space charge is divided between mobile and immobile charge. In general, the ratio between these charge densities is voltage dependent, which leads to a non-linear form for the Poisson differential equation. Fortunately, however, a special case in which a close approximation allows the equations to remain linear and explicitly solvable is applicable to many crystals. Analysis of this case both through the direct solutions of the applicable differential equations and by the method outlined in Section 1.2 provides, therefore, a useful evaluation of the latter approach. We shall begin (Section 1.3.1) by presenting the direct mathematical analysis and then (Section 1.3.2) shall illustrate the simplified approach.

1.3.1. Direct Mathematical Solution

The basic model to be considered is a crystal with a discrete trapping-level for electrons situated more than a few kT above the Fermi level (figure 1.2). Under these conditions the Maxwell-Boltzman distribution is applicable. If we assume thermal equilibrium between the free states and the trapping states, the interior Fermi level will rise with electron injection. Hence, the validity of this condition is voided as the applied voltage increases. Thus, the results of this analysis are limited to voltages low enough so that Maxwell-Boltzman statistics remain valid as a description of free and trapped charge. This constraint defines the low-voltage region.

If Maxwell-Boltzman statistics apply, the ratio of free to trapped charge is independent of both voltage and position inside the crystal. This ratio, which we shall call θ, is given by:

$$\theta = \frac{n}{n_t} = \frac{N_c}{N_t} \exp\left[-(W_C - W_T)/kT\right] \qquad (1.8)$$

where N_c is the effective density of states in the conduction band,

N_t is the density of trapping states,

W_C is the conduction-band energy,

W_T is the energy of the trapping level,

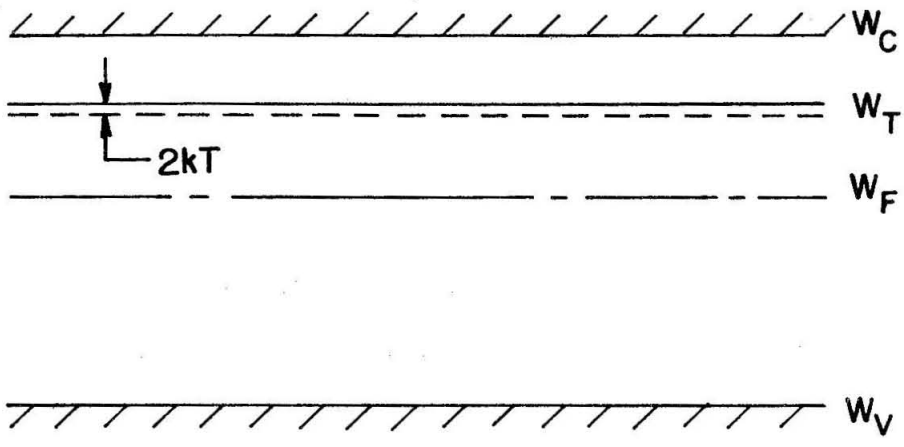

Figure 1.2.

Band structure proposed for analysis in Section 1.3. The crystal contains a discrete-energy trapping level at W_T. The Fermi level W_F is sketched in a region for which equation 1.14 is essentially accurate. The dotted line at $W = W_T - 2kT$ indicates the arbitrary 10% error point in Maxwell-Boltzman statistics at which equation 1.14 is assumed to lose accuracy (Section 1.4.1). The "trap-filling region" (Section 1.4) corresponds to W_F exceeding this magnitude.

k is Boltzman's constant,

T is the absolute temperature.

Using this definition, we may write Poisson's equation as:

$$\frac{dE}{dx} = \frac{-e}{K\epsilon_0} [n(1 + \theta^{-1}) - (\bar{n}_t + \bar{n})] \qquad (1.9)$$

For insulators such as CdS under charge-injection conditions we may expect that often $n \gg \bar{n}$ and $n_t \gg \bar{n}_t$ because the no-injection densities are so extremely small. In that case, the simplified form for equation 1.9,

$$\frac{dE}{dx} = \frac{-en(1 + \theta)}{K\epsilon_0\theta} \qquad (1.10)$$

is useful. Equation 1.10 will be used in further analysis since it is applicable in the range of voltages that is our chief interest.

At any x, it is also true that:

$$n = -\frac{J}{e\mu E} \qquad (1.11)$$

so that:

$$EdE = \frac{J(1 + \theta)}{K\epsilon_0\mu\theta}\, dx$$

Hence,

$$E = -\left[\frac{2J(1 + \theta)x}{K\epsilon_0\mu\theta}\right]^{1/2} \tag{1.12}$$

In equation 1.12, the constant of integration has been made zero by taking measurements from the virtual cathode, at which point the assumption of space-charge-limited current conditions requires the field to be zero.

Substituting 1.12 into $-\int_0^L E\,dx = V$ we obtain:

$$V = \frac{2}{3}\left[\frac{2J(1 + \theta)L^3}{K\epsilon_0\mu\theta}\right]^{1/2} \tag{1.13}$$

or,

$$J = \frac{9K\epsilon_0\mu\theta V^2}{8(1 + \theta)L^3} \tag{1.14}$$

Equation 1.14 is the relationship sought. It shows that square-law currents result in a crystal under space-charge-limited conditions provided voltages are sufficiently low so that a Boltzman factor can be used to describe the statistical population of the free and trapped states.

In practical crystals θ is almost always much less than unity, so that equation 1.14 is usually written with the demoninator $(1 + \theta)$ factor replaced by one. However, to derive the trap-free case from this solution, we must use the form given in 1.14 and allow θ to approach infinity (N_t approaches zero in equation 1.8). Under these conditions we obtain the solution of Mott and Gurney [14]:

$$J = \frac{9K\epsilon_0\mu V^2}{8L^3} \tag{1.15}$$

Equation 1.15 becomes applicable to crystals having traps at voltages exceeding that at which all traps are filled, so that further injected charge is necessarily free. This topic will be discussed more fully in the next section.

Before considering the application of the simplified viewpoint of Section 1.2 to the analysis of this problem, we shall derive some relationships from our work which will prove useful. By substituting 1.14 into 1.12, we may solve for E_a for space-charge-limited currents with a discrete trapping level. If we denote this field value by E_{asd}, we have:

$$E_{asd} = -\frac{3V}{2L} \tag{1.16}$$

which is, of course, within the limits derived in Section 1.2. From equations 1.3, 1.14 and 1.16, we may also solve for n_a in this case, again denoted by the subscripts sd.

$$n_{asd} = \frac{3K\epsilon_0\theta V}{4(1+\theta)eL^2} \tag{1.17}$$

It will be of interest to determine the ratio of the free-electron density at the anode to the average free-electron density in the crystal. Using the symbol $\underline{n}$ to denote this average density of electrons in the conduction band, we have:

$$\underline{n} = \frac{1}{L} \int_0^L n(x)dx$$

which may be written for this case, using equations 1.10 and 1.16:

$$\underline{n}_{sd} = \frac{-K\epsilon_0\theta}{(1+\theta)eL} E_{asd} = \frac{3K\epsilon_0\theta V}{2(1+\theta)eL^2}$$

Thus, from 1.17:

$$\underline{n}_{sd} = 2n_{asd} \tag{1.18}$$

Equation 1.18 implies that the average Fermi level in the crystal is only kT(ln2) ev higher in energy than the anode Fermi level. At room temperature this is just 0.018 ev. Thus, for the case here analyzed, it makes little difference whether we refer to the average or the anode Fermi level. This completes the analysis of the space-charge-limited current flow by straightforward mathematical methods.

1.3.2. Simplified Approach

We now demonstrate the derivation of the current law, equation 1.14, by the simplified techniques described in Section 1.2. To do this we refer to equation 1.7. Inherent in equation 1.7, it will be remembered, are the approximations: $\underline{n} \approx n_a$, $\underline{n}_t \approx n_{ta}$, $E_a \approx -V/L$, and $n \gg \bar{n}$. For the discrete trapping level with Maxwell-Boltzman statistics applicable as analyzed in this section, the appropriate form of equation 1.7 is:

$$\frac{K\epsilon_0 V}{eL^2} = n_a(1 + \theta^{-1})$$

Thus,

$$n_a = \frac{K\epsilon_0 \theta V}{e(1 + \theta)L^2}$$

Then, from equation 1.4 ($J \approx e\mu n_a V/L$), we have:

$$J = \frac{K\epsilon_0 \mu \theta V^2}{(1 + \theta)L^3} \tag{1.19}$$

Comparison of this form with equation 1.14 shows that use of the approximate method yields a resultant characteristic which differs from the more-exact treatment only in failing to provide the (9/8) factor of equation 1.14. The complete voltage dependence is preserved with a considerable decrease in computational effort. In more complicated cases, as we shall see, this approximate method will prove to be a very valuable technique.

Before we consider high applied voltages for this discrete trapping-level case, we should complete the low-voltage picture by noting that the behavior we have derived in equation 1.14 should not be expected at very low applied voltages. The behavior specified by equation 1.14 is the characteristic volt-ampere dependence when sufficient charge has been injected to lead to a space-charge limitation for current. For low applied voltages this will not be the case; instead the normal free-electron density inside the crystal will cause an ohmic current flow with a constant field in the interior. We may expect that the transition voltage for a change in behavior from ohmic current to space-charge-limited current occurs in the vicinity of an equality for the solution given by the two equations, the ohmic relationship, $J = e\mu\bar{n}V/L$, and equation 1.14, $J = 9K\epsilon_0\mu\theta V^2/8(1 + \theta)L^3$.

If we denote this transition voltage by the symbol V_{os}, we have:

$$V_{os} = \frac{8(1 + \theta)e\bar{n}L^2}{9\theta K\epsilon_0} \approx \frac{8e\bar{n}L^2}{9\theta K\epsilon_0} \qquad (1.20)$$

Equation 1.20 emphasizes the fact that a decreasing θ increases the voltage necessary to obtain space-charge-limited current conditions. In recapitulation, the expected volt-ampere behavior that we have derived for a crystal with a discrete trapping level is a linear dependence at voltages below V_{os} (as given in equation 1.20), with a transition to square-law currents of the form given in equation 1.14 above $V = V_{os}$.

Clearly, the space-charge-limited characteristic of equation 1.14, which rests on the assumption that the ratio n/n_t is a constant, cannot be followed indefinitely as voltage is increased. This is true because any real crystal will contain only a finite total number of traps. After these are completely filled by charge injection, the current-voltage behavior will approach asymptotically the characteristic for a trap-free crystal (equation 1.15), since, after all traps are filled, the fraction of total injected charge that is trapped decreases with voltage. As Lampert derives [9], the characteristic shows a steep rise in current with voltage between the region in which equation 1.14 is valid and the region in which equation

1.15 applies. Neither of these two asymptotic cases applies near to the voltage at which all the traps become filled. Consideration of this region of the current-voltage characteristic is the major topic of Section 1.4. Before discussing this region, we pause to note that the current-voltage behavior derived in this section is really more general in application than to the case of a discrete trapping level. Although the discussion is couched in terms of a discrete level, it is evident that all that is necessary for its validity is a constant ratio between n and n_t. This will be the case, in general, for any density of shallow traps (i.e. traps near to W_C) at low voltage excitations in a high-resistivity crystal. For a distribution of traps with energy, W_T and N_t in equation 1.8 become effective, averaged values.

1.4. Volt-Ampere Characteristic During Trap-Filling for a Discrete Level

We have noted in Section 1.3.2 that the volt-ampere characteristic near to that voltage which injects sufficient charge to fill all traps must connect the two asymptotic-behavior cases of space-charge-limited current as given in equations 1.14 and 1.15. Since most of the traps are being filled at voltages in the range connecting both of these equations, we shall call this region of the characteristic the trap-filling region. We start our analysis of the current-voltage behavior in this region by calculating, first, the value of the trap-filling voltage.

The voltage which fills all the traps may be calculated easily under the usual assumption that the trapped charge far outnumbers the free charge, so that essentially all anode electrical flux lines end on trapped charge in the interior. With this in mind, it is a problem in electrostatics to determine the voltage necessary to produce sufficient anode flux lines to link with charge in all of the traps. Since the charge configuration consists of uniformly-distributed trapped charge coupled to a planar, positive density at the anode of area A, the capacitance of the system is:

$$C = 2AK\epsilon_0/L \tag{1.21}$$

The total charge is $eALN_t$ when all possible trapped charge is coupled to the anode. Hence, the trap-filling voltage V_{TFL} is given by:

$$V_{TFL} = \frac{Q_{TFL}}{C} = \frac{eL^2N_t}{2K\epsilon_0} \tag{1.22}$$

This expression is dependent only on a uniform density of trapped charge, and is independent of the energy configuration of the trapping levels.

Above $V = V_{TFL}$ the current-voltage characteristic approaches the trap-free crystal behavior as specified in equation 1.15 since, at these higher voltages, the ratio of free to

trapped charge increases rapidly. The exact solution [9] shows that the range of validity of equation 1.15 extends down almost to $V = V_{TFL}$.

Deviation from the low-voltage asymptotic behavior of equation 1.14, on the other hand, becomes significant when Maxwell-Boltzman statistics cease to be valid in describing the ratio n/n_t. This occurs as the Fermi level inside the crystal approaches the trapping level, necessitating the use of Fermi-Dirac statistics and, thereby, incorporating a voltage dependence into the ratio n/n_t. This voltage dependence, in turn, leads to a high-power law in the trap-filling region. The volt-ampere characteristic in this region will be considered more closely in Sections 1.4.1 and 1.4.2.

1.4.1. Derivation of a Useful Approximate Form

In this section we shall consider a heuristic form of the volt-ampere characteristic during trap-filling in order to get some idea of the behavior exhibited under these conditions. The heuristic approximation is obtained by assuming a plausible characteristic to join together the two asymptotic forms (equation 1.14 and equation 1.15) which apply at low and high voltages, respectively. The asymptotic characteristics are held to be valid until their accuracy becomes poorer than an arbitrary assumed tolerance. The point at which equation 1.15 is to be joined is at $V \approx V_{TFL}$ as we have stated (from the

complete solution of reference 9). For the joining voltage to equation 1.14, we shall have to consider what voltage causes significant error in the use of Maxwell-Boltzman statistics. To determine this voltage, we start by writing the statistical relationships which are accurate through the trap-filling region. They are:

$$n_t = \frac{N_t}{1 + \exp\left[(W_T - W_F)/kT\right]} \tag{1.23}$$

and

$$n = N_c \exp\left[-(W_C - W_F)/kT\right] \tag{1.24}$$

where W_F is the Fermi level energy. From equation 1.23, we can see that the inaccuracy in the use of Maxwell-Boltzman statistics instead of Fermi-Dirac statistics is less than 10% for $(W_T - W_F) > 2kT$. If this degree of error is tolerated, then equation 1.14 may be used so long as W_F and W_T differ by $2kT$ or greater. The voltage at which $W_F = (W_T - 2kT)$ may be calculated by noting from 1.23 that for this voltage $n_t \approx (1/8)N_t$. Using the expression for the space-charge capacitance of equation 1.21, we calculate that this charge density implies an upper-limit voltage for the validity of equation 1.14, which we denote by V_j, of:

$$V_j = \frac{Q_j}{C} = \frac{1}{8}\frac{eAL^2N_t}{2K\epsilon_0} = \frac{1}{8}V_{TFL} \qquad (1.25)$$

Since the validity of 1.15 extends approximately down to the voltage $V = V_{TFL}$, this gives a range $V = (7/8)V_{TFL}$ in which neither equation 1.14 nor equation 1.15 is valid. It is tempting to use the approximate method we have outlined in Section 1.2 to obtain the characteristic in this region, but certain difficulties are presented by this attack. These difficulties are instructive and we shall, therefore, consider this approach in Section 1.4.2. However, at this juncture we shall make some speculations about the form of the characteristic during trap-filling which will also prove informative.

As we have previously noted, the exact solution [9] points up the steepness of the current-voltage characteristic during trap-filling. It would be helpful to gain some insight into the extent of this steepness as a function of the physical parameters of the trapping level. The constraint we have, thus far, is that the current-voltage relationship during trap-filling must join the two asymptotic forms, equations 1.14 and 1.15, in a voltage range roughly $(7/8)V_{TFL}$ in extent. Since we know that the fraction of total injected charge that is free increases as V approaches V_{TFL}, we can see that the actual current-voltage curve must have an increasing derivative as V approaches V_{TFL}.

A simple curve which both behaves in this fashion and satisfies the constraints just mentioned is the constant power-law curve implied by a straight line joining the two asymptotic characteristics on a logarithmic plot. Such a curve is illustrated in figure 1.3 for a θ value of 10^{-1}.

A value for θ of 10^{-1} is entirely unrealistic, but was chosen to make the graphic presentation simple; crystals usually show values for θ of approximately 10^{-5}. A diminishing value for θ translates the line corresponding to equation 1.14 downward along the current axis of figure 1.3 and parallel to itself. Thereby, a decreasing θ acts to magnify the power law during trap-filling. In fact, the power law implied by the approximation to the volt-ampere characteristic under discussion is easily calculated as a function of θ, as follows. Referring to figure 1.3, we see that V changes by a factor of 8 as J changes by a factor which can be calculated by taking the ratio of equation 1.15, evaluated at V_{TFL}, to equation 1.14, evaluated at $(1/8)V_{TFL}$. The change in J is thus $64/\theta$. The slope this yields for logarithmic current versus logarithmic voltage is $(\log 64/\theta)/(\log 8)$. Inverting the logarithms and thus converting back to J versus V, we see that the characteristic is:

$$J = \alpha V^m$$

$$\text{with } m = 2 + \frac{\log \theta^{-1}}{\log 8} \approx 2 + \log \theta^{-1} \qquad (1.26)$$

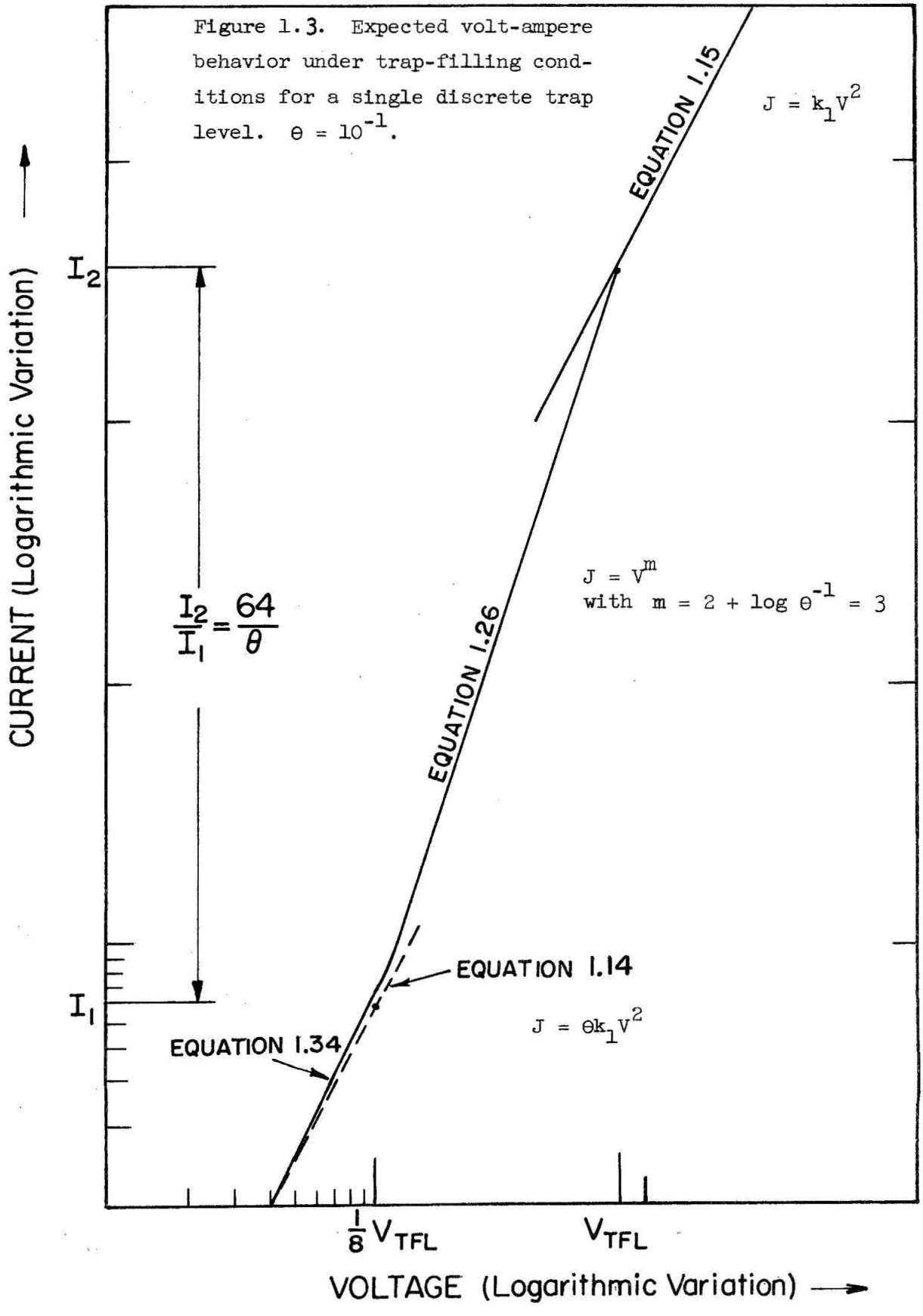

Figure 1.3. Expected volt-ampere behavior under trap-filling conditions for a single discrete trap level. $\theta = 10^{-1}$.

where α is a constant, and log signifies logarithms to the base 10. Natural logarithms are always written as ln in this report. Thus, for the case $\theta = 10^{-1}$ illustrated in figure 1.3, the trap-filling law is approximately cubic. In the more practical case, for $\theta \approx 10^{-5}$, the law would be closer to the 7th power over the approximate decade of voltage during which trap-filling invalidates the use of Maxwell-Boltzman statistics. We would note that the choice of the join point of the trap-filling law to equation 1.14 has little effect on the characteristic determined. If that point had been set at $(1/10)V_{TFL}$ instead of $(1/8)V_{TFL}$ we would have arrived at exactly the final form given in 1.26. Likewise, almost an identical form to equation 1.26 would have been obtained had one joined equation 1.15 at $V = 2V_{TFL}$. These facts make unimportant the generally arbitrary way in which the join points were chosen. The size of θ is the significant factor in determining the steepness of the trap-filling law.

No pretext is made here that equation 1.26 represents an exact solution to the applicable differential equations during trap-filling. Equation 1.26 is, rather, an approximation made chiefly to indicate the dependence of the volt-ampere characteristic in the trap-filling region on the parameter θ and to show that the characteristic in this region will indeed be steep in actual crystals.

1.4.2. Use of the Simplified Approach in the Trap-Filling Region

We shall now attempt to use the approximate method of Section 1.2 to calculate the characteristic during trap-filling. The starting point is equation 1.6 ($\nu_a = \underline{n} + \underline{n}_t$). Because we are going to join two voltage regions in which the results derived in equations 1.16 and 1.18 ($E_{asd} = -(3V/2L)$; $\underline{n}_{sd} = 2n_{asd}$) are valid, one might assume that the accuracy of the approximate form for equation 1.6, given in equation 1.7 ($(K\epsilon_0 V)/eL^2 = n_a + n_{ta}$), could be improved in this case through insertion of these values directly into equation 1.6. Under this condition, equation 1.6 becomes:

$$\nu_a = 2(n_a + n_{ta}) \tag{1.27}$$

with ν_a now given by $\nu_a = (3K\epsilon_0 V)/2eL^2$. To solve for n_a in terms of ν_a and thereby for n_a in terms of V, the relationship between n_a and n_{ta} must be inserted into 1.27. This is obtained by eliminating W_F between 1.23 and 1.24 to obtain:

$$n_{ta} = \frac{n_a N_t}{n_a + \theta N_t} \tag{1.28}$$

Inserting 1.28 into 1.27, and making the usual approximation that $\theta \ll 1$, we have:

$$n_a^2 + n_a\left(N_t - \frac{\nu_a}{2}\right) - \frac{\theta N_t \nu_a}{2} = 0 \qquad (1.29)$$

A series representation of the solution to 1.29 valid for $\nu_a < 2N_t$ is:

$$n_a = \frac{\theta N_t \nu_a}{2\left(N_t - \frac{\nu_a}{2}\right)} - \frac{\theta^2 N_t^2 \nu_a^2}{4\left(N_t - \frac{\nu_a}{2}\right)^3} + \cdots \qquad (1.30)$$

Again using equation 1.16, we may write an improved form in this case for equation 1.4:

$$J = \frac{3e\mu n_a V}{2L} \qquad (1.31)$$

Thus from 1.30, assuming all terms in the series negligible when compared to the first, we have:

$$J = \frac{3e\mu\theta V\nu_a}{4L}\left[1 - \frac{\nu_a}{2N_t}\right]^{-1} \qquad (1.32)$$

For the complete dependence upon V, we insert the definition for ν_a into 1.32 to derive:

$$J = \frac{9K\epsilon_0\mu\theta V^2}{8L^3}\left[1 - \frac{3K\epsilon_0 V}{4N_t eL^2}\right]^{-1} \tag{1.33}$$

which is more meaningfully presented when normalized to V_{TFL} through use of equation 1.22:

$$J = \frac{9K\epsilon_0\mu\theta V^2}{8L^3}\left[1 - \frac{3V}{8V_{TFL}}\right]^{-1} \tag{1.34}$$

Equation 1.34 converges asymptotically to the form 1.14 at low voltage, as expected, but obviously does not lead to the anticipated high-power law for current in the trap-filling region. This is the case despite the fact that the limits of validity of the solution in 1.30 are $\nu_a < 2N_t$. If one translates this constraint on ν_a through the definition $\nu_a = (3K\epsilon_0 V)/2eL^2$, the corresponding voltage bound is $V < 8V_{TFL}/3$. Here, however, is the step which loses physical significance because E_a changes from the value $3V/2L$ and $\underline{n}$ no longer equals $2n_a$ as the Fermi level nears the trapping level. As seen in the exact solution, and by reasoning we shall present shortly, these various factors become voltage dependent. Hence although equation 1.6 remains valid, when it is converted to functions of the anode densities as is done in writing equation 1.27 ($\nu_a = 2(n_a + n_{ta})$), the dependence of ν_a is no longer

linear with voltage. Therefore, except for the numerical coefficients, the solution 1.32 is also still valid but the higher power dependence of ν_a leads to the high-power law connecting the ranges of applicability of equations 1.14 and 1.15. Thus, the proper use of 1.34 is for voltages below the trap-filling region; that is for $V \leq (1/8)V_{TFL}$. This is illustrated on figure 1.3.

It has already been shown (Section 1.2) that under no circumstance is $E_a > 2V/L$. Therefore, the high-power law for current dependence on voltage is due mainly to the changing ratios $\underline{n}/n_a$ and $\underline{n}/n_{ta}$. Actually, it is the ratio of $\underline{n}$ to n_a that has a very large maximum near to the trap-filling voltage, because the traps physically close to the injecting electrode are filled prior to those at the anode. The exact solution [9] brings out this fact. Thus, the approximate solution procedure outlined in Section 1.2 may not be applied to this case without obtaining, in some way, the correct voltage-dependent variation for the ratio of $\underline{n}$ to n_a. The variation of $\underline{n}/n_a$ with V is not easily derived and one is therefore led, in this case, to an interpretation of the exact solution. Our interest in the volt-ampere characteristic during trap filling will not extend beyond a consideration of the influence of θ on the steepness of the relationship. Since this was determined in Section 1.4.1, we shall not pursue the topic further here. Equation 1.34 is perfectly valid in the range of voltages below $V \approx (1/8)V_{TFL}$ where all the relationships

used in deriving it are correct. In this voltage region it can properly be regarded as a corrected form for equation 1.14.

The preceding discussion was presented, and solution 1.34 derived, in order to show the problems in interpretation that may arise in using the approximate method of Section 1.2 which is based solely upon the anode field and charge density. These problems will confront one only in a case such as has just been examined, when the ratio of the average interior charge density to the anode charge density is voltage dependent. Requisite to a voltage dependence for $\underline{n}/n_a$ is an abrupt change in the energy of the electronic states that are being filled by the injected charge. For complete results in such a case, the exact solution must be considered.

This completes our consideration of the behavior of a crystal having a discrete trapping-level under conditions of charge injection. We have seen that such a crystal will show a volt-ampere characteristic consisting essentially of four voltage regions: first, an ohmic region for low applied voltages; second, a square-law region for intermediate voltages when currents flow under space-charge-limited conditions, but Maxwell-Boltzman statistics apply for free and trapped charge; third, a high-power-law region starting roughly at $V = (1/8)V_{TFL}$ and continuing until $V \approx V_{TFL}$; and fourth, a square-law region at voltages exceeding a value necessary to inject sufficient charge to fill all the traps. A sketch of the expected volt-ampere

characteristic when plotted logarithmically for a crystal with a discrete level as well as other energetic configurations of traps will be given in figure 1.6.

1.5. Two or More Discrete Energy Trapping Levels

If a crystal contains more than one monoenergetic trapping level, one would expect qualitatively that most of the phenomena sketched in Section 1.3 would occur with slight modification. Assume, for the sake of discussion, two trapping levels at energies W_{T1} and W_{T2}. For $W_F \ll W_{T1} < W_{T2}$ we may use Maxwell-Boltzman statistics to write:

$$n = \theta_1 n_{t1} = \theta_2 n_{t2} \tag{1.35}$$

where:

$$\theta_{1,2} = \frac{N_c}{N_{t1,2}} \exp\left[-(W_C - W_{T1,2})/kT\right] \tag{1.36}$$

Hence equation 1.2 becomes:

$$\frac{dE}{dx} = \frac{-en}{K\epsilon_0}\left(1 + \theta_1^{-1} + \theta_2^{-1}\right)$$

$$= \frac{-en}{K\epsilon_0}\left(1 + \theta_e^{-1}\right) \tag{1.37}$$

with:

$$\theta_e = \frac{\theta_1\theta_2}{\theta_1 + \theta_2} \tag{1.38}$$

For low applied voltages, the transition voltage from ohmic to space-charge-limited currents (equation 1.20), and the space-charge-limited relationship (equation 1.14), are not altered except that θ should be replaced in these equations by θ_e.

There will be two square-law regions of the form of equation 1.14, with θ_e characterizing the low-voltage square law and θ_2 characterizing the higher voltage square-law region. Using the reasoning described in deriving equation 1.20, we calculate that the lower trapping level would be filled at $V_{TFL1} \approx eL^2N_{t1}/2K\epsilon_0$ and the upper level would be filled at $V_{TFL2} \approx eL^2(N_{t1} + N_{t2})/2K\epsilon_0$. Deviation from the form of equation 1.14 could first be expected in this instance when the population of the lower trapping level ceases to be described by Maxwell-Boltzman statistics. From this point, $V \approx (1/8)V_{TFL1}$, until $V \approx V_{TFL1}$, a trap-filling law will be observed. An approximation, of the same sort as made in deriving equation 1.26, to describe this region yields:

$$J = \alpha V^m$$

$$\text{with} \quad m \approx 2 + \log (\theta_2/\theta_1) \tag{1.39}$$

and α a constant. Equation 1.39 says that if θ_1 approached θ_2 (which would necessitate N_{t2} being of the order of $N_{t1} \exp [(W_{T2} - W_{T1})/kT]$) the existence of the lower level would tend to be completely obscured in the space-charge-limited volt-ampere characteristic. Approximate square-law behavior could continue to be observed as the first level was being filled.

After both levels have been filled at $V_{TFL2} \approx eL^2(N_{t1} + N_{t2})/2K\epsilon_0$, the trap-free-crystal characteristic of equation 1.15 would again apply. As in the single discrete level case, it is clear that the conclusions reached about the volt-ampere behavior in the lower voltage ranges depend only upon the validity of Maxwell-Boltzman statistics - not upon the actual trap configuration with energy. The volt-ampere characteristic for a crystal with distributed states would be indistinguishable from that of a crystal with distinct levels until the voltage is raised sufficiently to invalidate the use of Maxwell-Boltzman statistics. The behavior we have described here may obviously be extended to any number of spaced trapping levels with intervening energy regions devoid of traps.

In summary, the volt-ampere behavior under charge-injection conditions that is expected for two or more energetically-discontinuous trapping levels is square-law currents diminished by a factor θ. This factor is discontinuous as the Fermi level crosses a trap energy. The trap-filling characteristic will be of a steepness dependent on the change in θ and will extend

roughly over a decade of voltage measured downward from the trap-filling voltage.

1.6. Traps Distributed in Energy

In this section we consider the space-charge-limited characteristic that will be observed when energetically-distributed trapping levels are being filled. As we have pointed out, if these levels exist at energies sufficiently above the Fermi level so that Maxwell-Boltzman statistics are applicable, the analysis of Section 1.3 is valid. When the Fermi level enters the region over which the trapping levels are energetically distributed, however, we shall see that the currents are no longer proportional to the square of the voltage. The actual behavior for two different trapping configurations with energy will be calculated through use of the procedure outlined in Section 1.2. This technique will be a great simplification over the calculations necessary for an exact treatment. In Section 1.6.1 we shall consider a uniform distribution of traps, while, in Section 1.6.2 we take up the case of traps distributed exponentially in energy.

Since we are considering the form of the volt-ampere characteristic for voltages at which the Fermi level remains within the trapping levels, any relationship between the average charge density and the anode charge density will not be a function of voltage. This follows from the fact that there is no abrupt

change in the electronic states occupied by the bulk of the injected charge while the Fermi level is in the region of the continuous trap density. Thus the problems associated with a voltage dependence for the ratio n/n_a, as pointed out in Section 1.4.2, are not met in the analysis of this section. Hence, we will make the calculations for both trapping configurations by writing the form of equation 1.7 $(K\epsilon_0 V/eL^2 = n_a + n_{ta})$ that is applicable. To do this, we must first derive the statistical relationship between n_a and n_{ta}. The analysis, therefore, will begin at this point.

1.6.1. Uniform Density of Traps with Energy

In this section we consider a uniform energy-density of traps extending from the conduction band downward to an energy W_{TL} (figure 1.4). We then define the trap density per unit energy increment as:

$$\rho_t = \frac{N_t}{(W_C - W_{TL})} \tag{1.40}$$

with N_t, the total number of traps per unit crystal volume. Thus, in an increment of energy dW in the range between W_{TL} and W_C, there are dn_t filled traps given by:

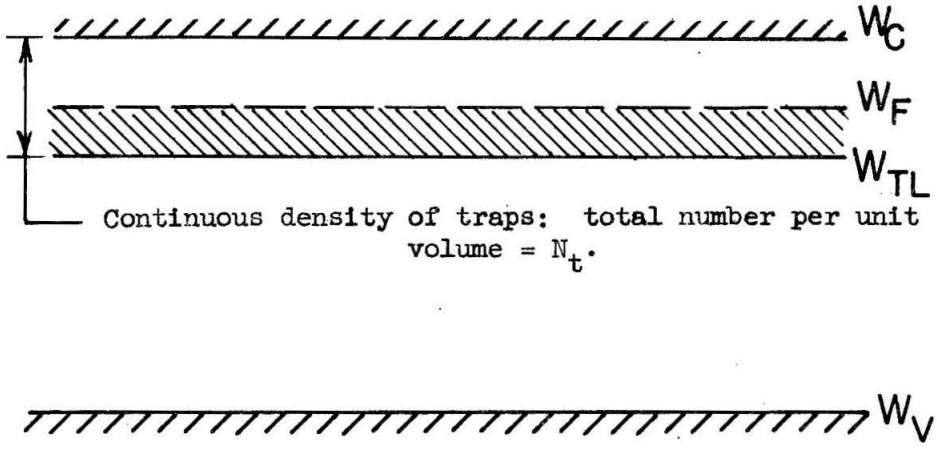

Figure 1.4. Band structure proposed for analysis in Section 1.8. The traps are distributed continuously in energy with a constant density between W_{TL} and W_C. The Fermi level is assumed always to be at energies between W_{TL} and W_C. The spatial distribution of traps is uniform.

$$dn_t = \frac{\rho_t dW}{1 + \exp[(W - W_F)/kT]} \tag{1.41}$$

We may eliminate W_F through equation 1.24 and rewrite 1.41 as:

$$dn_t = \frac{\rho_t dW}{1 + (N_c/n)\exp[(W - W_C)/kT]} \tag{1.42}$$

Upon integration of equation 1.42 between the limits W_{TL} and W_C, we obtain for n_t:

$$n_t = \rho_t\left\{(W_C - W_{TL}) - kT\ln\left[\frac{(1 + N_c/n)}{1+(N_c/n)\exp[-(W_C - W_{TL})/kT]}\right]\right\} \tag{1.43}$$

From equation 1.24 the denominator of the logarithm will approach unity rapidly as soon as W_F is a few kT above W_{TL}. Also, provided W_F is at least a few kT below W_C, $N_c \gg n$. Hence,

$$n_t \approx N_t - \rho_t kT\ln(N_c/n) \tag{1.44}$$

The next step is the insertion of equation 1.44 into equation 1.7 to obtain:

$$K\epsilon_0 V/eL^2 = n_a + N_t - \rho_t kT\ln(N_c/n_a) \tag{1.45}$$

As in the case of the discrete trapping-level, in general $n_a \ll n_{ta}$, so that from 1.45:

$$n_a \approx N_c \exp[-(N_t - K\epsilon_0 V/eL^2)/\rho_t kT] \tag{1.46}$$

Using the definition 1.40 for ρ_t, and normalizing to V_{TFL} as given in equation 1.22 ($V_{TFL} = eL^2 N_t/2K\epsilon_0$), we may write this as:

$$n_a = N_c \exp[-(W_C - W_{TL})/kT]\exp[(V/2V_{TFL})(W_C - W_{TL})/kT] \tag{1.47}$$

The dependence of n on V is more apparent if we define $N_e = N_c \exp[-(W_C - W_{TL})/kT]$ and rewrite equation 1.47 as:

$$n_a = N_e \exp\left(\frac{N_t V}{2\rho_t kTV_{TFL}}\right) \tag{1.48}$$

As a final step, we insert equation 1.48 into equation 1.4 to obtain:

$$J = \frac{e\mu N_e V}{L} \exp(\alpha V) \tag{1.49}$$

with $\alpha = N_t/2\rho_t kTV_{TFL}$. Thus J varies roughly exponentially with V for this situation of the Fermi level traversing a uniform

density of traps, a result which checks with Rose's work [10], although his analysis does not provide the value for the exponent.

1.6.2. Traps Varying Exponentially with Energy

As a second example of the behavior of space-charge-limited currents when the crystal Fermi level traverses a continuous trap density, we analyze a distribution of traps which are exponentially varying with energy in a continuous band stretching between the two energies W_{TL} and W_{TU} (figure 1.5).

The analysis is begun, as in Section 1.6.1, by deriving a relationship between n and n_t. We define a "temperature" T_c, which characterizes the trap density variation with energy, denoted by ρ_t, through the equation:

$$\rho_t = \rho_0 \exp[(W - W_{TL})/kT_c] \tag{1.50}$$

where ρ_0 is a constant density of states per unit increment of energy. Then, in an energy interval dW there are dN_t traps given by:

$$dN_t = \rho_0 \exp[(W - W_{TL})/kT_c]dW \tag{1.51}$$

Since this trap density extends between W_{TL} and W_{TU}, the total number of traps per unit volume, N_t is given by:

$$N_t = \rho_0 kT_c \left\{ \exp[(W_{TU} - W_{TL})/kT_c] - 1 \right\} \tag{1.52}$$

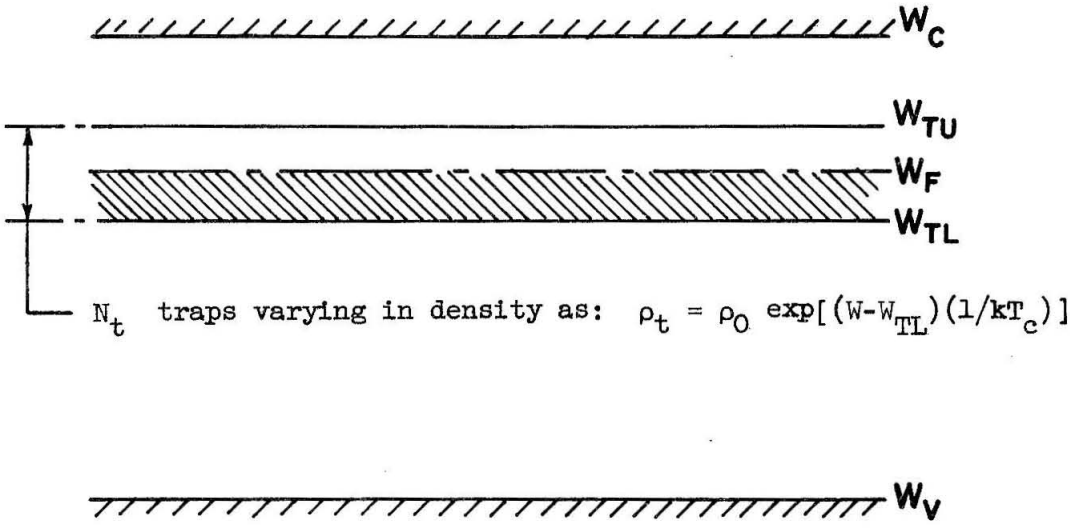

Figure 1.5

Band structure proposed for analysis in Section 1.6.2. The traps are distributed continuously between W_{TL} and W_{TU} and their density varies exponentially with energy. The Fermi level is assumed always to be between W_{TL} and W_{TU}. The spatial distribution of traps is uniform.

and, provided $(W_{TU} - W_{TL}) \gg |kT_c|$ and T_c is positive so that the trap density increases with W, only the first term is necessary.

The number of filled traps is:

$$n_t = \int_{W_{TL}}^{W_{TU}} \frac{\rho_0 \exp[(W - W_{TL})/kT_c]dW}{1 + \exp[(W - W_F)/kT]} \qquad (1.53)$$

This integral is not easily evaluated exactly, but an approximate form will preserve the important physical features. The approximate form is derived simply by assuming the Fermi distribution to be unity for $W_{TL} < W < W_F$ and zero above this value, a procedure frequently used in analysis and increasingly correct as the temperature is lowered. This may be done correctly, however, only provided $|T_c| > T$ so that the numerator in 1.53 is varying more slowly than the denominator. Whether or not this is the case in practice will have to be decided on the basis of correspondence between the conclusions implied by this step and experimental data. Under this approximation, the solution for the integral, valid for $|T_c| > T$ is:

$$n_t = \rho_0 kT_c \left\{ \exp[(W_F - W_{TL})/kT_c] - 1 \right\} \qquad (1.54)$$

Again, if $(W_F - W_{TL}) \gg |kT_c|$ and T_c is positive, the first term is sufficient. Combining the forms of equations 1.54 and

1.52, using the approximations stated, we obtain:

$$n_t \approx N_t \exp[-(W_{TU} - W_F)/kT_c] \tag{1.55}$$

To obtain the dependence of n_t on n, we first rewrite equation 1.22 $(n = N_c \exp -(W_C - W_F)/kT)$ in the form:

$$\exp (W_F/kT_c) = [n \exp(W_C/kT)/N_c]^{T/T_c} \tag{1.56}$$

We now use 1.56 to eliminate W_F from 1.55 and obtain thereby:

$$n_t = N_t(n/N_c)^{T/T_c} \exp[(W_C - W_{TU})/kT_c] \tag{1.57}$$

Equation 1.57 may be inserted into equation 1.7 to obtain n_a as a function of V. As a simplification, we again assume that $n_a \ll n_{ta}$ and thus write:

$$n_a = \left(\frac{K\epsilon_0 V}{N_t e L^2}\right)^{T_c/T} N_c \exp[-(W_C - W_{TU})/kT] \tag{1.58}$$

Again normalizing to V_{TFL} through the use of equation 1.22 this becomes:

$$n_a = N_c(V/2V_{TFL})^{T_c/T} \exp[-(W_C - W_{TU})/kT] \tag{1.59}$$

To derive J as a function of V, we again use equation 1.4 to obtain:

$$J = \frac{e\mu N_c \exp[-(W_C - W_{TU})/kT]}{(2V_{TFL})^{T_c/T_L}} V^{[(T_c/T)+1]} \qquad (1.60)$$

Equation 1.60 shows that a trap density increasing exponentially with energy (or, therefore, a trap density which decreases when moving downward energetically from the conduction band) leads to a power-law behavior that is greater than square law. The actual power for the voltage is temperature dependent.

Most of the approximations used to derive equation 1.60 will be met in practice. Perhaps the poorest of these is, however, the neglect of unity in the exact expressions for equations 1.52 and 1.54. In order to derive equation 1.60, we have specified only that $|T_c|$ needs to be greater than T. No constraints were put on the actual value for T_c which, of course, depends on the crystal properties. An increasing $|T_c|$ tends to invalidate the approximate forms for equations 1.52 and 1.54, used in deriving equation 1.55. Likewise, if the trap density is exponentially decreasing in energy (T_c negative), the neglect of unity with respect to the exponential terms in equations 1.52 and 1.54 is, of course, wholly unjustified. A solution is also possible, however, without these approximating steps. If the exact expressions for 1.52 and 1.54 are used in a series of calculations

directly analogous to those used to derive equations 1.55 through 1.60, we obtain, instead of equation 1.60, the form:

$$J = \frac{e\mu N_c}{L} \exp[-(W_C - W_{TU})/kT]V\left[1 + \frac{N_t V}{\rho_0 kT_c 2V_{TFL}}\right]^{T_c/T} \qquad (1.61)$$

Equation 1.61 is a more general solution than 1.60, useful when the trap distribution is characterized either by a negative T_c or by a large value for T_c. Equations 1.60 and 1.61 are both limited in validity to voltages less than V_{TFL} by the specification that the Fermi level lie within the range of distributed traps. For T_c negative, there are further restrictions on the validity of equation 1.61 that stem from the approximation that all charge is trapped, which was used in the application of equation 1.7. Since no observations of a behavior characteristic of negative T_c are to be presented, we shall not consider this case further. As we have noted, equation 1.61 is also valid for large T_c, that is for a more uniform distribution in energy of the traps (see equation 1.50). Therefore, using the form 1.61 we can see the smooth transition between the case of traps varying with energy, analyzed in this section, and the case of a uniform density of traps, analyzed in Section 1.6.1. Use of the identity:

$$\lim_{m \to \infty} \left(1 + \frac{ax}{m}\right)^m \equiv \exp(ax) \qquad (1.62)$$

in equation 1.61 to obtain the uniform-density case by allowing T_c to approach infinity, gives us an identical form to equation 1.49. All that is necessary is to let W_{TU} approach W_C and ρ_0 approach ρ_t to make the two cases completely comparable. Hence, we have obtained both a good check on our mathematical results and a more general relationship in equation 1.61 which contains the uniform trap-density case as well as the varying density case. The size and sign of $|T_c|$ in an actual crystal will determine whether equation 1.60 is a sufficient approximation to equation 1.61 to be applicable in a particular case.

Both equations 1.60 and 1.61 are dependent upon $|T_c|$ being greater than T, a step necessary to simplify the integration of equation 1.53. For $|T_c| < T$, the trap density becomes much more peaked in energy, provided we limit the total number of traps, as is necessary from considerations of physical realizability. Hence the distribution becomes more and more like a single level and is therefore characterized by the treatment of Section 1.3. Thus for $|T_c| < T$, J becomes proportional to V^2.

1.7. Conclusions

We have seen in this chapter that an extreme variety in current-voltage behavior is possible in a crystal with traps under conditions of charge injection. The range is from linear proportionality between J and V for slight injection, to an exponential dependence for J on V under space-charge-limited

conditions for a crystal having traps distributed uniformly with energy in the forbidden zone. The current-voltage behavior for a hypothetical crystal having a variety of interior trap-configurations with energy is sketched to logarithmic scales in figure 1.6. The regions of the characteristic are seen to be demarcated by the position of the Fermi level relative to the trapping energies.

From figure 1.6 we see that in a given crystal, not only is the type of dependence extremely varied, but so also are the magnitudes for the currents drawn in a fairly small interval of applied voltage. These can change by factors that are several powers of ten, within less than a decade change in applied voltage. The currents can also be disparate by many factors of ten in almost identical crystals at the same voltage. Faced with such variations, the researcher has at his disposal a sensitive tool for the measurement of the trapping properties of crystals. As we shall see presently, however, he has in addition almost a Pandora's box full of experimental difficulties and apparent anomalies with which to contend.

Since we have mentioned the use of space-charge-limited current measurements to elicit trapping information, we might pause to recapitulate what trap properties may be deduced by this technique and the manner of their deduction. For very low voltages, ohmic behavior can be expected in all cases because of the small free-charge density present in the crystal even under

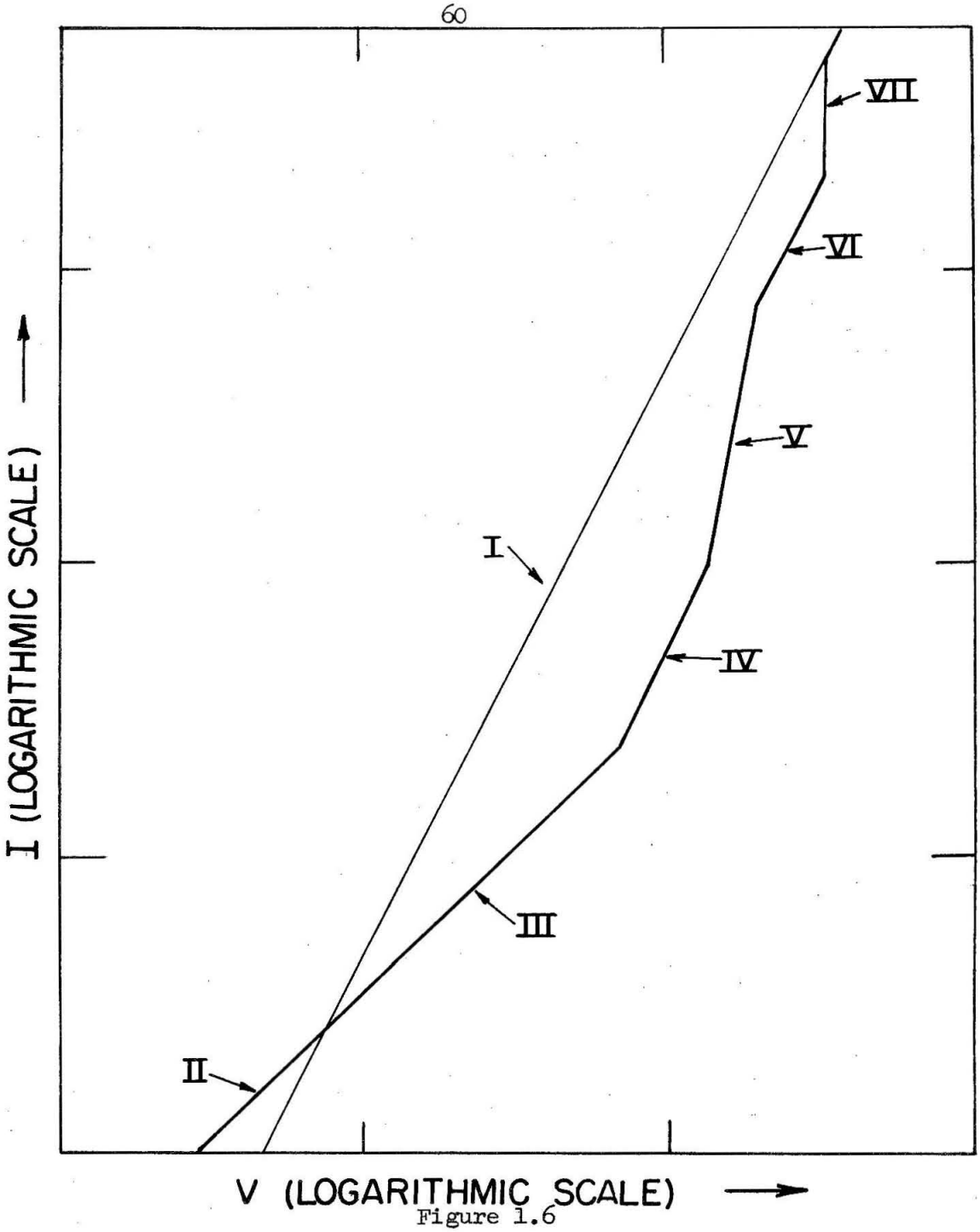

Figure 1.6

Possible behavior for space-charge-limited currents in crystals with a variety of energy levels for volume-distributed traps.

I. Space-charge-limited current for a trap-free crystal: $J = k_1 V^2$

II. Ohmic region (present also in a trap-free crystal): $J = k_2 V$

III. Extended ohmic region for a crystal with traps.

IV. Fermi level in region void of traps: $J = \theta_1 k_1 V^2$

V. Fermi level in region of continuous traps: $J = k_3 V^m$ or $J = k_4 \exp V$

VI. Fermi level again in region void of traps: $J = \theta_2 k_1 V^2$

VII. All traps in crystal filled

no-injection conditions. This ohmic behavior will, of course, indicate the position of the Fermi level without injection but cannot tell us much about any possible traps in the crystal. The voltage to which this ohmic current persists as voltage is increased, however, leads to a value for θ through equation 1.20 ($V_{os} = 8e\bar{n}L^2/9\theta K\epsilon_0$). After the onset of space-charge-limited current, one cannot discern anything about the actual trapping configuration with energy as long as Maxwell-Boltzman statistics are valid in describing the free and trapped charge densities. Nonetheless, if Maxwell-Boltzman statistics are appropriate, a check on θ as determined from the V_{os} observation is possible through a comparison of the value of θ obtained by fitting the measured square law to equation 1.14 ($J = 9K\epsilon_0\mu\theta V^2/8L^3$). When Fermi-Dirac statistics become applicable, the behavior of the characteristic will depend on the actual configuration of traps with energy. To learn the total number of traps present, and the depth of the trapping states from space-charge-limited current measurements, one must exceed the trap-filling voltage pertinent to the trapping level (or levels) in question. The trap depth is derived by solving equation 1.4 ($J = -e\mu n_a E_a$) for n_a, using this number to calculate $(W_C - W_F)$ from equation 1.24 ($n = N_c \exp[-(W_C - W_F)/kT]$) and recognizing that $W_F \approx W_T$ at $V = V_{TFL}$.

The simplified method of Section 1.2 is seen in later sections of this chapter to be a valuable tool for obtaining the significant dependence of current on voltage in a straight-

forward manner which preserves a physical picture of the sequence of events. One limitation to its use, the case of a voltage dependent $\underline{n}/n_a$, was pointed out in Section 1.4.2. The real advantage of the method is apparent if an attempt is made to handle the continuous trap-densities of Section 1.6 by writing exact forms of the Poisson equation and solving these. Any distribution of traps with energy not causing a voltage-dependent $\underline{n}/n_a$ may, in principle, be handled by the technique of Section 1.2 by proceeding in the manner illustrated in Section 1.6. In complicated cases, the integral of the equation corresponding to 1.53 may, however, become difficult or impossible to solve. Approximate methods can nonetheless be used in its evaluation, and one can thereby obtain an explicit current-voltage relationship in all cases - a distinct advantage over the direct mathematical approach.

In Chapter 5, some of the conclusions of this chapter will be put to experimental test, and others will be used to deduce the properties of diodes made with CdS. Experimental verification of a number of the deductions has already been presented, largely in the papers of Smith and Rose. Reference is made to these papers throughout the text, wherever appropriate.

CHAPTER II

Mathematical Treatment of the Capacitance due to Trapping of Electrons in Crystals Subject to Charge Injection

The previous chapter dealt with the theory of the d-c effects of traps on the crystal volt-ampere behavior. The equations derived were valid for an equilibrium condition between the trapping levels and conduction-band levels without constraints as to the time allotted to reach this equilibrium. In this chapter we shall consider theoretically one aspect of the influence that trapping levels should exert on the sinusoidal-excitation frequency dependence of the volt-ampere characteristics in a crystal. This dependence comes about because the kinetics of trap-filling and trap-emptying are determined by such properties as the trap densities and the capture cross-sections of the various energy states. These parameters are insensitive to any applied signal, and can result in a limiting amount of charge storage in the crystal if the exciting frequency is raised sufficiently.

A convenient and useful way of demonstrating the kinetic effects of trapping follows from consideration of the measured capacitance, since the capacitance is a direct function of the charge stored in a region. Trapping properties have not been studied through capacitance measurements heretofore although, as we shall see, this technique has a number of aspects which recommend its use. The analysis of this chapter will be found to be useful because sensitive means are available for measuring

capacitance on actual devices. Correspondence of these measured values with those deduced from the model proposed as representative of the physical processes in the crystals will reinforce confidence in that model. In addition, parameters such as frequency, bias voltage and illumination will be found to affect the capacitance measurements. These may be varied independently to provide quantitative information, when properly interpreted, about the actual physical processes. We shall, therefore, frame the discussion in this chapter in terms of the expected capacitance for an insulator with a uniform spatial distribution of traps subject to charge injection. Because the bulk of the injected charge in actual crystals is trapped, we shall neglect the contribution to measured capacitance of the free charge. Experimental verification of the negligibility of the contribution of the free charge to the over-all capacitance in the samples studied will be given in Chapter 6.

2.1. The Effect of Charge Injection on the Measured Capacitance of a Dielectric Crystal

The measured capacitance for a crystal into which charge may be injected will be compounded of two parts, which may profitably be considered separately. This division corresponds to the capacitance due to charge storage on the contact electrodes, and the capacitance due to charge storage in the interior of the crystal. The interior charge may, in turn, be subdivided into free and trapped components. However, unless

one applied voltages across the crystal in the range of $V = V_{TFL} = eL^2N_t/2K\epsilon_0$ as given in equation 1.22, the ratio of free to trapped charge in an actual crystal will be very small. For lower voltage excitation, one may profitably neglect the contribution of the free charge to the measured capacitance. This is the situation applicable to the experimental investigations to be described in Chapter 6 and, therefore, is the one analyzed here.

The circuit elements representing interior and electrode charge-storage will appear in a parallel connection externally and their magnitudes, with free charge neglected, will be given by the following equations:

$$C_m = C_e + C_t = \frac{1}{V}(Q_e + Q_t) \tag{2.1}$$

where C_m is the measured capacitance,

C_e is the capacitance due to charge storage on the electrodes,

C_t is the capacitance due to charge storage in the traps,

V is the impressed voltage,

Q_e is the charge stored on the electrode,

Q_t is the charge stored in the traps.

Now:

$$C_e = \frac{AK\epsilon_0}{L} = \frac{Q_e}{V} \tag{2.2}$$

where A is the junction area,

L is the electrode spacing,

$K\epsilon_0$ is the permittivity of the crystal.

C_e may be expected to be independent of frequency in the range of measurements to be considered later ($f \leq 5$mc/s) since Q_e need not enter the crystal or be trapped. The frequency variation of the relative permittivity K, due to the response of dipole-resonance modes in the material structure, should be very slight below 5mc/s. C_e will not, however, be a constant with respect to illumination because of the change in the permittivity known as the photodielectric effect. This topic will be discussed briefly for CdS in Chapter 6. The photodielectric effect has been shown experimentally to lead to an enlargement for K by factors as high as 7 in some photoconductors [1, p. 420].

The trapping capacitance $C_t = Q_t/V$, however, is a variable with frequency changes for an applied a-c excitation, since Q_t depends on the amount of charge that can be trapped and liberated in the available time. Assuming a uniform trap density in space, there is a maximum value for C_t which is derived as follows. As shown in Section 1.2, the trapped-charge density in the crystal cannot exceed the value it has at the injecting electrode. Therefore, the capacitance will be less in all cases than the capacitance of a charge system which consists of a uniform space-charge region inside the crystal coupled to a planar sheet of positive charge at the electrode. The capacitance value for such a configuration of charge, denoted by the symbol C_{tm}, is

$C_{tm} = (2AK\epsilon_0)/L = 2C_e$. In order for trapping capacitance to be as large as C_{tm} under pure a-c excitation, it would be necessary both for the stored charge to be uniform and to inject charge into the traps for both polarities of the applied voltage - hence, to have two injecting contacts to the crystal. If a crystal had one injecting contact and one blocking contact, then the trapping states could be filled only during each half cycle of a pure a-c signal and the effect of the traps on the measured capacitance would be only half that deduced above. The maximum value for trapping capacitance can be attained only provided an electron density of magnitude,

$$n_t = \frac{C_{tm}V}{eAL} = \frac{2C_eV}{eAL} \qquad (2.3)$$

can be trapped and liberated during one half cycle of the applied a-c signal. Otherwise C_t will be less than this value and will be given by:

$$C_t = \frac{eALn_{te}}{V} \qquad (2.4)$$

where n_{te} is the density of charge capable of being trapped and liberated in phase with the applied voltage V (n_{te} is the

"effective" trapped charge). Thus, under pure a-c voltage excitation, the maximum value for measured capacitance, denoted by the symbol C_{mm}, is:

$$C_{mm} = C_{tm} + C_e \tag{2.5}$$

Hence, $C_{mm} = 3C_e$ for a symmetric structure (two injecting electrodes), and $C_{mm} = 2C_e$ for a diode structure (one injecting electrode). The effects of a d-c bias on the results of this section will be discussed separately in Section 2.4. As has been pointed out, for C_t to reach the value C_{tm} there must be a uniform, interior-charge density. We may argue heuristically that a constant, trapped-charge distribution is the likely physical situation at low applied voltages, when the crystal is still in the region of ohmic behavior. Under this condition, the injected-charge density is still too small to cause an uneven distribution because of space-charge constraints. The uniform, free-charge density (implied by the ohmic volt-ampere behavior) will result in an essentially uniform, trapped-charge density. As injection is increased toward a space-charge-limiting value, the interior-charge distribution becomes non-uniform. This process is considered further in Section 2.4.

2.2. The Effect of Trapping Kinetics on the Measured Capacitance

We have established the qualitative picture of the mechanism of charge storage in traps which results in an

externally-detected capacitance in Section 2.1. In this section, we shall consider quantitatively the sequence of events responsible for this capacitance. First, in Subsection 2.2.1, we shall derive and discuss the equations representing the physical process of trap-filling and trap-emptying, since these phenomena underlie the detected a-c capacitance. Then, in Subsection 2.2.2, we shall use this derived equation to calculate the expected dependence of the measured capacitance on frequency. The analysis of this section will, therefore, provide us with a means of obtaining information about the physical properties of traps from the measurement of capacitance in actual crystals. It is assumed in this analysis that charge transport from the contacts to the traps is infinitely fast, so that the processes of electron capture and emission govern the measured capacitance. In Section 2.3, we consider separately the electron-transport process.

2.2.1. Derivation and Discussion of the Differential Equation Governing Trapping Kinetics

An electron trapping-state, as the term is used in this chapter, is a permitted electronic energy level which is filled and emptied through the conduction band. Hence, if we enumerate the mechanisms for electron transfers between free and trapped states, we shall have an equation for the trapped-charge density. If electron traps are filled from the conduction band at a rate R_F states per cm^3 per sec and emptied back into the conduction band at a rate R_E in the same units, then the differential

equation governing the trapped-charge density n_t is of the form:

$$\frac{dn_t}{dt} = R_F - R_E \tag{2.6}$$

The rate of trap-filling R_F should be proportional to the free-electron density n, the density of empty traps $(N_t - n_t)$, and a transition probability for capture of a free electron by a trap which we shall call c_f. Thus, we have:

$$R_F = n(N_t - n_t)c_f \tag{2.7}$$

In a similar manner, the rate of trap-emptying R_E should be proportional to the trap density n_t, the density of vacant free-electron states $(N_c - n)$, and a transition probability for emission of a trapped electron into the conduction band which we shall call c_e. Hence, the rate of emission is:

$$R_E = n_t(N_c - n)c_e \tag{2.8}$$

At this point, we may simplify matters without significant loss of accuracy through use of the easily satisfied approximations: $N_c \gg n$ and $N_t \gg n_t$. The first approximation is virtually always true; the second demands only that any applied voltage is appreciably less than $V_{TFL} = eL^2N_t/2K\epsilon_0$ as given in equation

1.22. Under this condition, equations 2.7 and 2.8 may be rewritten: $R_F = nN_t c_f$, and $R_E = n_t N_c c_e$. Hence, equation 2.6 may be written in the form:

$$\frac{dn_t}{dt} = -(n_t - \gamma n)N_c c_e \qquad (2.9)$$

where γ is defined by the ratio $N_c c_e / N_t c_f$. From the form of equation 2.9, we can see that γ is the ratio of the trapped-to-free charge when the conduction-band states and trapping levels are in equilibrium. Therefore, if we assume that the transition-probability ratio is independent of the excitation mode so that the thermal-equilibrium value is applicable, we may take the value n/n_t at thermal equilibrium to define γ. If Maxwell-Boltzman statistics apply to the trapping levels, we have then $\gamma = \theta^{-1}$. The quantity $N_c c_e = R_E/n_t$ is seen to be a probability per unit time for the escape of a trapped electron. We shall denote this "probability-of-escape" frequency by the symbol ν_e. For the case of a discrete trapping level in thermal equilibrium with the conduction-band states and enough above the Fermi level to be described by Maxwell-Boltzman statistics, ν_e is given by [1, p. 278]:

$$\nu_e = N_c v S_t \exp[-(W_C - W_T)/kT] \qquad (2.10)$$

where $(W_C - W_T)$ is the trap depth below the conduction band,

N_c is the effective density of conduction-band states,

v is the electron thermal velocity (10^7cm/s at 300^oK),

S_t is the capture cross-section of an empty trap for a conduction-band electron.

The physical basis for equation 2.10 is not difficult to develop. To do so, we make use of the equality of R_E and R_F at thermal equilibrium. Through the definition of ν_e, we have $R_E = n_t\nu_e$. For a discrete trapping level, the rate of trap filling R_F may be expressed in terms of the capture cross-section for a trap S_t by imagining that the free electrons are motionless and that the N_t traps per cm^3 move with the electronic thermal velocity v. Then, the volume traced out per second by each cm^3 of these "moving" traps is vN_tS_t. The number of electrons captured by the traps per second, therefore, is nvS_tN_t. Hence, c_f in equation 2.7 equals vS_t for this case. Since at equilibrium R_E equals R_F, we have: $\nu_e = nvS_tN_t/n_t$ where n/n_t has its equilibrium value. For a discrete level at thermal equilibrium, if Maxwell-Boltzman statistics are applicable, we have also $n/n_t = (N_c/N_t)\exp[-(W_C - W_T)/kT]$ (equation 1.8). Therefore, under these conditions: $\nu_e = N_cvS_t \exp[-(W_C - W_T)/kT]$ as given in equation 2.10.

For continuously-distributed trapping levels sufficiently above the Fermi level so that Maxwell-Boltzman statistics apply, an equation of the form of 2.10 can be derived for an effective value for ν_e, and the over-all trap density for the distributed

levels will be governed by equation 2.9 with γ and ν_e statistically-averaged values over the various states. Analysis in terms of equation 2.9 in the case of energetically-distributed traps corresponds to lumping together the effect of all traps in one effective level. This is, in reality, the same procedure used in the consideration of the population of the conduction-band states, which are all lumped together for most calculations into an effective density N_c, situated at the energy level W_C.

If Fermi-Dirac statistics apply for the population of the trapping-states, then the ratio n/n_t becomes dependent on the position of the Fermi level, and thereby on the applied voltage. For a small a-c signal superimposed on a d-c bias, however, n/n_t is relatively constant over a cycle, and the analysis using equation 2.9 is still meaningful. A consequence of the dependence of n/n_t on bias is that both γ and ν_e become bias-dependent.

A discussion of trapping kinetics is often couched in terms of the attempt-to-escape frequency of a trap rather than the probability-of-escape frequency. The attempt-to-escape frequency is the number of times per second that a trapped electron can absorb energy from its surroundings multiplied by a probability for that absorption. It can be shown by thermodynamic reasoning to be limited for thermal processes at room temperature to 10^{13} per sec, and to be given by the product $N_c v S_t$ [1,p. 51]. Thus, from equation 2.10 ν_e is related to

the attempt-to-escape frequency for a trapping level by the factor $\exp[-(W_C - W_T)/kT]$.

Using equation 2.10, we may rewrite equation 2.9 as:

$$\frac{dn_t}{dt} = -(n_t - \gamma n)\nu_e \qquad (2.11)$$

A special case of this form for the trapping-rate equation is given by Bube [1, p. 278]. Bube discusses the trapping behavior when n is approximately zero and there is a finite n_t at time zero, which we shall call n_{t0}. The solution for the trapped-electron density decay is then given by: $n_t = n_{t0} \exp - \nu_e t$. The rate of trap-emptying R_E is therefore: $R_E = \nu_e n_{t0} \exp - \nu_e t$. It is interesting to look at the inverse case ($n_t = 0$ at time zero with a step function in conduction-band density n of magnitude n_0 introduced at time zero). For this situation, the solution would be $n_t = \gamma n_0 (1 - \exp - \nu_e t)$ so that the rate of trap-filling R_F would be $\nu_e \gamma n_0 \exp - \nu_e t$. The ratio of $|dn_t/dt|$ in these two cases is, therefore, $\gamma n_0/n_{t0}$. If, for a comparison, we took the initial density imbalances to be equal ($n_0 = n_{t0}$), we see that the rate of change of the trap density is γ times as large for pure filling of traps as it is for pure trap-emptying. Since γ is comparable to θ^{-1} and, therefore, very large in most actual crystals, we can see that

the rates will be quite disparate for this case of equal, initial density-deviations from equilibrium.

Under charge-injection conditions, it is possible to modulate n, the density of free electrons, and thereby to change n_t according to the constraints of equation 2.11. To determine the effect that these constraints will have on the measured capacitance, therefore, one must solve equation 2.11 with the appropriate form inserted for the free-charge density. This analysis will be the topic of 2.2.2.

2.2.2. Variation of C_t with Frequency

We have derived, in equation 2.11, the relationship governing the trapped-charge density inside the crystal. Under an applied a-c voltage, the free-charge density is modulated by charge injection and extraction from the contacts. The traps are then filled and emptied via the conduction band. In order to consider the capacitance observed at the electrodes of the crystal due to this effect we must solve equation 2.11 after inserting the proper variation for n to represent free-electron injection and extraction. For a sinusoidal voltage excitation $V = V_m \cos \omega t$, the time dependence of n will depend on the nature of the contacts made to the crystal. If we consider the case of one ohmic electrode and one blocking electrode and assume proportionality between applied voltage and injected charge density, then the waveform for the conduction band density

during excitation will be a half-wave rectified sinusoid with a peak value of n_m, as in figure 2.1b. The capacitance measured at the excitation frequency will be due only to the component of trapped charge in synchronism with the applied voltage. Since equation 2.11 is a linear differential equation, we may apply the principle of superposition in its solution and therefore use a Fourier series representation for n. In this manner, we can immediately separate out that component of n which is synchronous with the applied voltage and is therefore responsible for the measured trapping capacitance. In the case now under consideration, it is the fundamental that is the component of n which is synchronous with the applied voltage. Therefore, in the following equations, we denote densities synchronous with the voltage by the subscript f. Hence, using the Fourier analysis of the waveform given in the caption to figure 2.1b, we have $n_f = (1/2)n_m \cos \omega t$, as the form to be inserted into equation 2.11. Thus:

$$\frac{dn_{tf}}{dt} = - (n_{tf} - (1/2)\, \gamma n_m \cos \omega t)\nu_e \qquad (2.12)$$

Solution of equation 2.12 for the steady-state term yields:

$$n_{tf} = \frac{(1/2)\gamma n_m}{(1 + \omega^2/\nu_e{}^2)^{1/2}} \cos (\omega t - \tan^{-1} \omega/\nu_e)$$

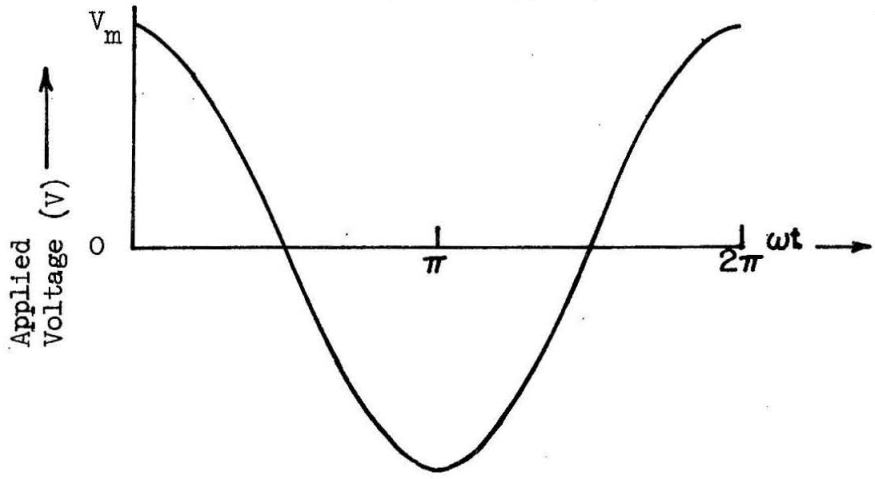

Figure 2.1a. Applied a-c voltage waveform at the collecting electrode.

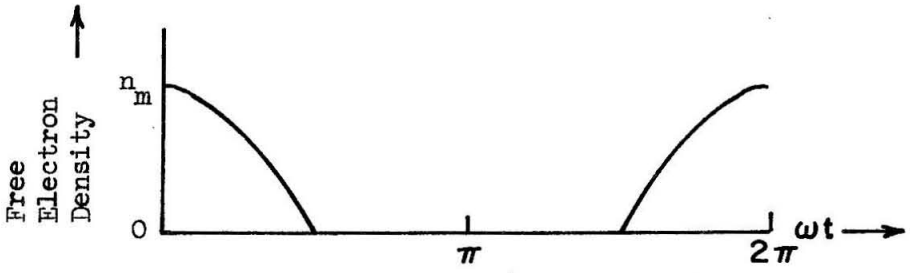

Figure 2.1b. Conduction-band density for the case of a single injecting electrode.

$$n = n_m \left[1/\pi + (1/2) \cos \omega t + (2/3\pi) \cos 2\omega t + \cdots\right]$$

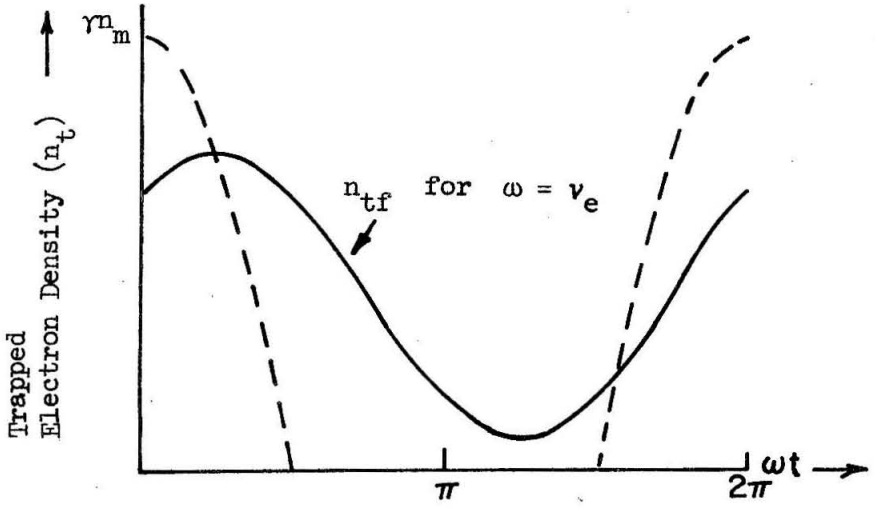

Figure 2.1c. Trapped charge density for a single injecting electrode. Dotted curve valid as ω approaches zero. Solid curve is the solution for the fundamental for n_t at $\omega \approx \nu_e$. The vertical scale is greatly contracted from that used to plot figure 2.1b.

$$n_{tf} = (1/2)\gamma n_m \left[\frac{\cos \omega t}{(1 + \omega^2/\nu_e^2)} + \frac{\omega \sin \omega t}{\nu_e(1 + \omega^2/\nu_e^2)} \right] \qquad (2.13)$$

The value of n_{tf} at $\omega \approx \nu_e$ is plotted in figure 2.1c.

Before interpreting equation 2.13, we pause to note that the entire problem as considered thus far is completely analogous to the solution for the charge stored on the capacitance in the circuit of figure 2.2a. If the voltage source in figure 2.2a were taken to be proportional to the conduction-band density multiplied by γ, and the natural relaxation time-constant RC for the circuit were proportional to ν_e^{-1}, then Q_C, the charge stored on the capacitor, would be described exactly by equation 2.11. Hence, the frequency analysis we have just performed could have been done equally well in terms of this analogue circuit.

Thinking in terms of the equivalent circuit suggests the use of the phasor diagram of figure 2.2b to represent the two terms of the solution for the trap population obtained in equation 2.13. The first term in this solution represents trapped charge in phase with the applied voltage, and hence its magnitude is proportional to the capacitance variation with frequency. The second term is 90° out of phase with the applied voltage, and therefore has a derivative in phase with it. Hence, this term represents a current in phase with the voltage, and therefore implies a conductance for the device due to traffic

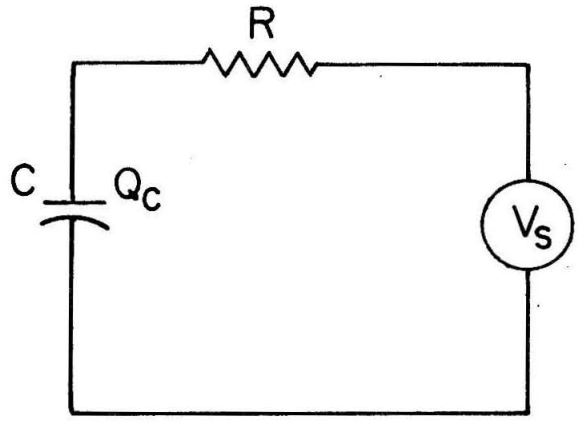

Figure 2.2a

Circuit showing behavior analogous to trap-filling. The charge Q_C, stored on the capacitor, is analogous to the density of filled traps n_t, provided that ν_e^{-1} is taken to be proportional to the time constant RC and V_S is taken to be proportional to γn.

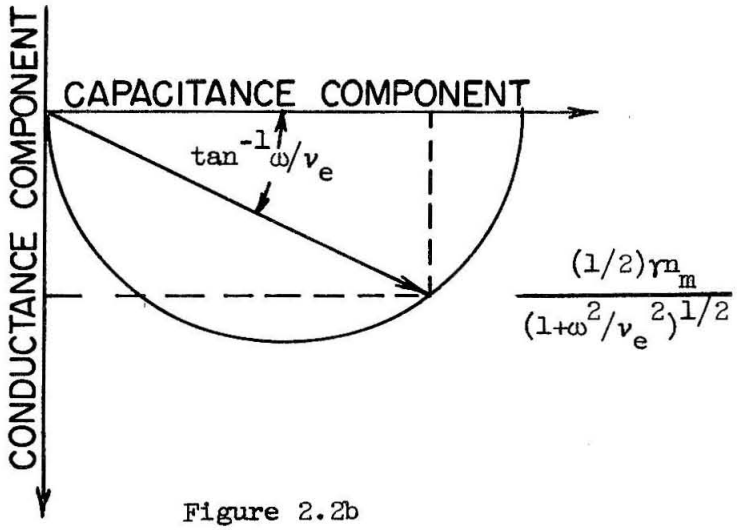

Figure 2.2b

Phasor diagram representing the time-variant components of the trapped-charge density. The component of trapped charge in phase with the applied voltage results in a terminal capacitance; the trapped charge in quadrature with the applied voltage results in a conductance component.

between the traps and the conduction band. The conductance term is seen to have a maximum at $\omega = \nu_e$, or, as seems quite reasonable, when the probability-of-escape frequency equals the driving frequency. This term would account for only a portion of the total conductance as measured at the terminals, however, since it does not represent the charge actually traversing the crystal for collection at the opposite electrode.

To express the result for n_{tf} in equation 2.13 in terms of the trapping capacitance measured at the terminals, we recognize that the portion of this solution in phase with the applied voltage represents the quantity that we have called n_{te} in equation 2.4. Thus, if we use the symbol C_t' to denote the low frequency value of the trapping capacitance, we have from equation 2.4:

$$C_t' = \frac{eAL\gamma n_m}{2V} = \frac{eAL\eta}{2} \qquad (2.14)$$

where we have defined a new constant $\eta \equiv \gamma n_m/V$. This definition serves to lump together the assumed proportionality constant between n_m and V with the proportionality constant between n_t and n, which has already been defined by the symbol γ. Since C_t' was shown in Section 2.1 to have a maximum value of: $C_{tm}' = AK\epsilon_o/L = C_e$ for a single injecting electrode, we may use equation 2.14 to derive a limiting value for η. This is $\eta_m = 2K\epsilon_o/L$. For η less than η_m, C_t' will be less than C_e.

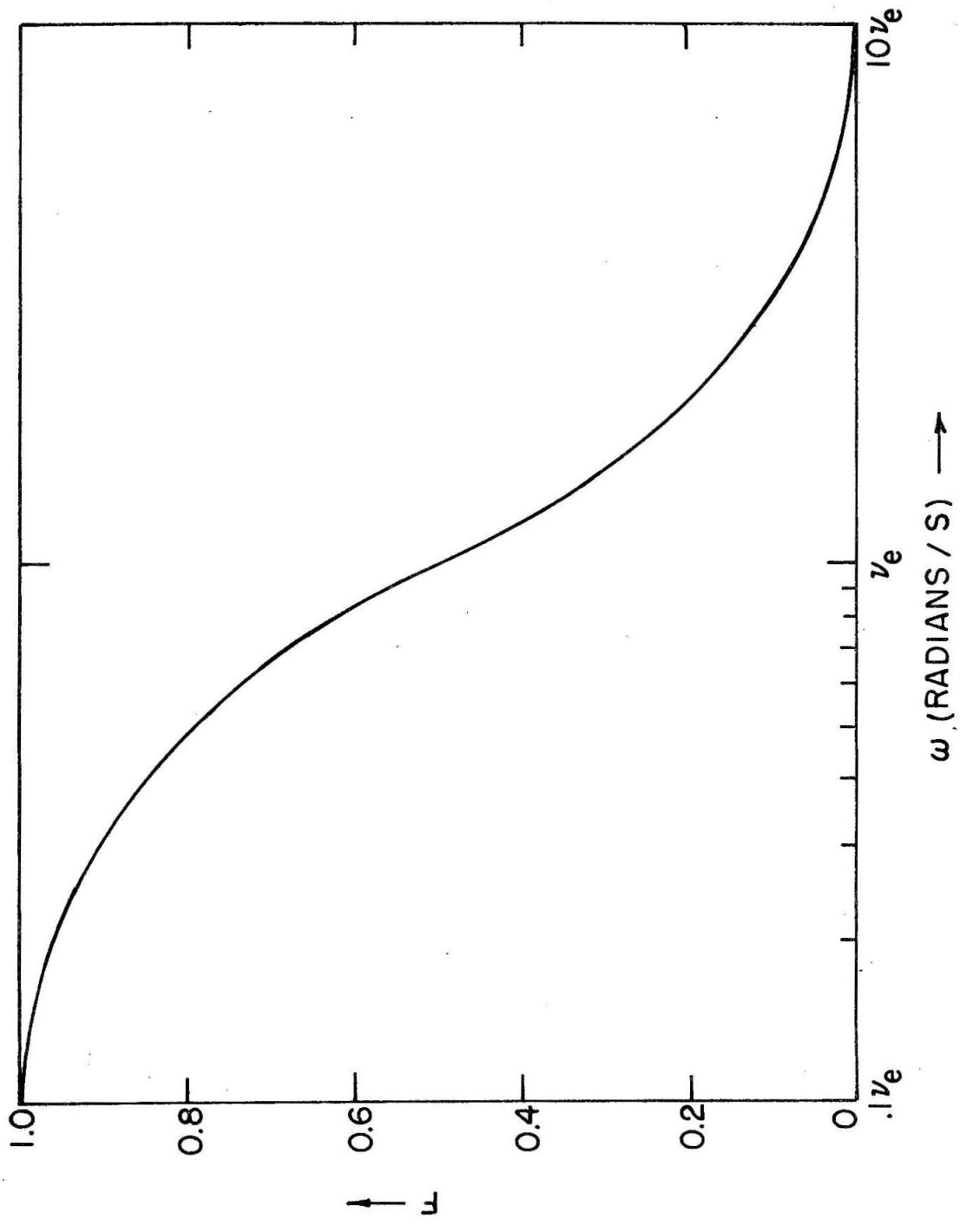

Figure 2.3

The function $F = 1/(1 + \omega^2/\nu_e^2)$ plotted versus logarithmic frequency. The trapping capacitance is given by: $C_t = C_t'F$.

For $\eta = \eta_m$, $C_t' = C_e$. In terms of C_t', the over-all frequency-variant expression we have derived for the trapping capacitance is:

$$C_t = C_t' \frac{1}{1 + \omega^2/\nu_e^2} \tag{2.15}$$

The trapping capacitance should therefore drop from its low frequency magnitude C_t' when the voltage driving function is raised in frequency to a value near to the probability-of-escape frequency of the trapping level. Figure 2.3 is a plot on semilogarithmic paper of the frequency dependence as represented in equation 2.15. The figure shows that the drop in capacitance due to trapping limitations will be spread over about two decades of frequency centered roughly at the probability-of-escape frequency ν_e.

We have discussed, thus far, the case of a single injecting electrode to the crystal. We shall now speculate about the situation with two injecting electrodes. When there is little or no applied bias, the case of two injecting electrodes presents some peculiarities which should be pointed out. The conduction-band density for two injecting contacts and a pure a-c applied voltage ($V = V_m \cos \omega t$) will be a full-wave rectified sinusoid as sketched in figure 2.4a. The Fourier analysis of such a wave contains no fundamental as can be seen in the representation

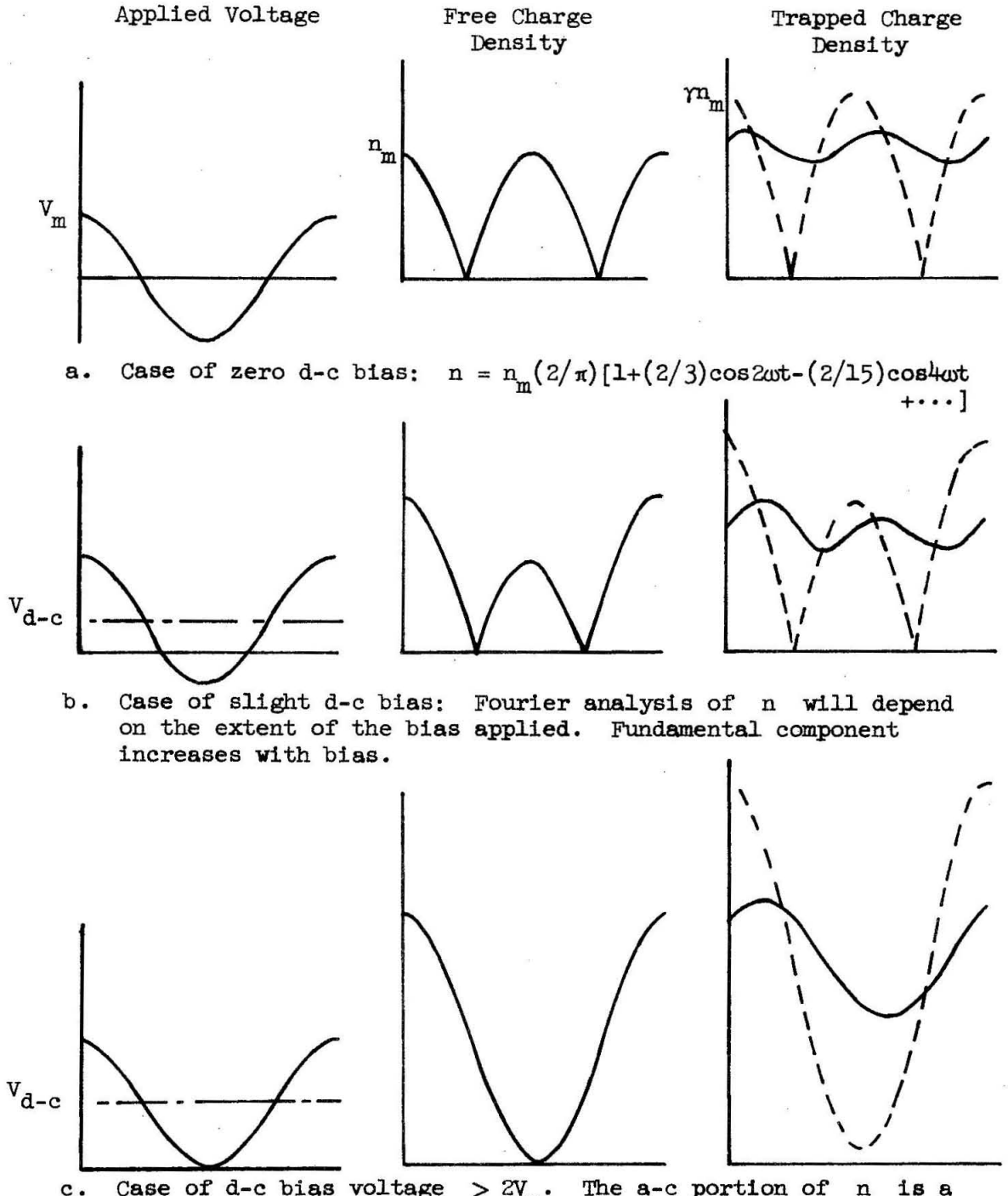

a. Case of zero d-c bias: $n = n_m(2/\pi)[1+(2/3)\cos 2\omega t-(2/15)\cos 4\omega t +\cdots]$

b. Case of slight d-c bias: Fourier analysis of n will depend on the extent of the bias applied. Fundamental component increases with bias.

c. Case of d-c bias voltage $> 2V_m$. The a-c portion of n is a pure cosine waveform at the applied frequency of V.

Figure 2.4. The voltage waveform, conduction-band density, and trap density for a crystal with two injecting contacts and various values of applied d-c bias. The abscissa is a full cycle of the variable ωt in all cases. The vertical scale for the trapped-charge density is much contracted over that for the free-charge density. The dotted curves for n_t represent the solution at very low frequencies; the solid lines represent the solution at $\omega \approx \nu_e$.

given in the caption to figure 2.4a. The trap density is, therefore, forced to respond to twice the applied signal frequency in addition to higher harmonics. Again using the linear property of the fundamental equation (2.11), we calculate that the response of each harmonic is given by an equation of the form of 2.13. Thus, the over-all trap density is represented by:

$$n_t = \frac{2\gamma n_m}{\pi}\left[1 + \frac{2\cos(2\omega t - \tan^{-1}2\omega/\nu_e)}{3(1 + (2\omega)^2/\nu_e^2)^{1/2}} - \frac{2\cos(4\omega t - \tan^{-1}4\omega/\nu_e)}{15(1 + (4\omega)^2/\nu_e^2)^{1/2}} + \cdots\right] \qquad (2.16)$$

In order to convert this form for n_t into the trapping capacitance variation, we would expect to separate out the portion of n_t that is synchronous with the applied voltage. Since equation 2.16 has no component at the fundamental frequency, however, a first conclusion might be that the trapping capacitance, in this case, is zero. The error in this conclusion is evident when one considers the behavior at low frequencies when it is certain that n_t contributes to the capacitance. The root of this conceptual problem is in the fact that the trapped charge is always negative; whereas electrode-stored charge, as in a normal capacitor, may change sign. The density n_t of equation 2.16 is set up by charge injection from each of two electrodes during a single complete cycle.

The capacitance actually measured is defined by the ratio of the charge stored in a region to the voltage difference between the terminal from which the flux lines linking that charge emanate and the edge of the charge storage region. Thus, one must consider, in this case, not the original sinusoidal variation in voltage, but rather a rectified full-wave sinusoid representative of the flux pattern causing the trapped-charge build-up over a full cycle. The use of the absolute value for V is consistent with the fact that the actual driving function for the trap density as inserted into equation 2.11 is not the applied voltage V, but the free-charge density n. The latter is inherently positive and is proportional to the absolute value for V. Thus, the a-c portion of the trapped-charge density that is in-phase with the conduction-band density and, therefore, with the a-c portion of the absolute applied voltage will be represented by an external trapping capacitance. For this case, therefore:

$$C_t = \frac{eAL\gamma n_m}{V_m} \frac{\left(\frac{2}{3(1+(2\omega)^2/\nu_e^2)} - \frac{2}{15(1+(4\omega)^2/\nu_e^2)} + \cdots \right)}{(2/3 - 2/15 + 2/35 - 2/63 + \ldots.)} \qquad (2.17)$$

The series in the denominator of equation 2.17 can easily be summed by noting that $n = (2/\pi)n_m[1 + (2/3)\cos 2\omega t - (2/15)\cos 4\omega t + \cdots] = n_m$ at $t = 0$. Hence, the denominator of

equation 2.17 equals $(\pi/2) - 1$. Equation 2.17 gives the proper low and high-frequency magnitudes for C_t; $C_t = eAL\gamma n_m/V_m$ at low frequencies and zero at high frequencies. The over-all frequency dependence is seen to be complex, although the various components of the a-c portion of n_t go to zero quite rapidly. Since the double-frequency component is five times as large as the second harmonic, the frequency variation will be approximately:

$$C_t = \frac{C_t''}{(1 + (2\omega)^2/\nu_e^2)} \qquad (2.18)$$

where C_t'' has a maximum value of $2C_e$, as determined in Section 2.1. Thus, from equation 2.18, the observed trapping capacitance should cut off in the vicinity of $\omega = \nu_e/2$ for the case of pure a-c applied to a crystal with two ohmic contacts. The behavior of equation 2.18 is, of course, the same as was sketched in figure 2.3 except that the frequency scale in the graph is shifted a factor of two to the right.

D-C bias will affect these conclusions by changing the waveform which represents n. As sketched in figure 2.4, an increasing d-c bias acts to increase the fundamental component of the waveform for n. This is a smooth process, culminating in the a-c portion of n being pure fundamental at biases greater than $2V_m$ (figure 2.4c). The variation of C_t with

frequency for two ohmic contacts is, therefore, represented with fair accuracy by equation 2.18 under no bias and exactly by equation 2.15 for biases greater than $2V_m$. In the intermediate bias case such as is represented by figure 2.4b, no simple frequency variation applies. For an intermediate bias, the variation of C_t with frequency must be obtained by finding the response of all components of n_t to the Fourier-analyzed waveform for n. The ratio of this response that is in phase with the absolute voltage to the a-c portion of the absolute value of applied voltage gives the magnitude of the trapping capacitance. This analysis which corresponds to the calculations just performed in deriving equation 2.17, will not be of sufficient interest to be carried out here.

In summary, the detected trapping capacitance of a crystal will be frequency dependent and will fall rapidly in the vicinity of an applied radial frequency equal to the probability-of-escape frequency for the traps. In the special case of two ohmic electrodes with no d-c bias, the capacitance roll-off will be effective at a radian frequency roughly one half the probability-of-escape frequency. As bias is applied in this case, however, the roll-off of capacitance will move to higher frequencies until it is strongest in the immediate vicinity of the probability-of-escape frequency.

2.3. Transit-Time Effect

In considering the kinetics of the trapping states in Section 2.3, we analyzed the constraints on the trapping

capacitance imposed by the state-transition kinetics between the conduction band and trapping levels. One must also consider the process of physical transport of the electrons from the injecting contacts to the vicinity of the traps. Since the electrons must be introduced at the electrodes and collected there again, they must traverse the crystal to the region of the traps. If the capacitance-measuring frequency is raised until the quarter-cycle-time* approaches the transit time through the crystal, there will clearly be a decrease in C_t due to lack of sufficient time for this transport, regardless of the crystal trapping kinetics. For low voltage excitations, if the crystal behaves ohmically, there will be a uniform field across the crystal so that the transit time T_{tr} is given by:

$$T_{tr} = L/v = L^2/\mu V \qquad (2.19)$$

where v_f is the electron velocity due to the applied field.

For very small applied measuring voltages, transit-time effects can be observed at surprisingly low frequencies. For example, if 10mv is used as the capacitance-charging voltage for a 10 micron crystal of CdS ($\mu \approx 200 cm^2/volts$), equation 2.19 yields 0.5 microsecond for the transit time. Since this number is to be compared to a quarter-cycle-time of the impressed voltage, the effect should be apparent, for this hypothetical

---

* This is the length of time for which a given contact is injecting electrons.

case, at 500kc/s. The calculation performed is, of course, only approximate since V, and therefore T_{tr}, are actually time variant in equation 2.19.

A mathematical treatment of the actual behavior of the trapping capacitance under a transit-time limitation demands a solution for the x-dependence of the trapped-charge distribution. This analysis will not be necessary in considering the experimental data and will not be given here.

2.4. Effects of a Bias Voltage

In Section 2.2.2, one effect of an applied d-c bias was discussed. There, it was shown that the frequency dependence of C_t for the case of two ohmic contacts to the crystal will be altered by an applied d-c voltage. There are certainly other ways in which an applied bias can affect the trapping capacitance. A discussion of these other effects of bias voltage on C_t is the subject of this section.

First, we note that in order to achieve the maximum, measured capacitance of equation 2.5, a spatially uniform, trapped-charge density is necessary. The discussion of Section 2.1 indicated that such a density can be achieved only for small voltages in the range in which the crystal is behaving ohmically: that is, for voltages much lower than $V_{os} = 8e\bar{n}L^2/9\theta K\epsilon_0$ (equation 1.20). If the crystal is subjected to higher voltages, so that charge injection tends toward a space-charge-limitation,

then the spatial arrangement of the electrons is altered from the uniform density that was assumed in Section 2.1. This results in a diminution of the maximum value for C_t. The extent of the deviation from a uniform charge density at varying degrees of injection and for each trapping configuration with energy must be worked out separately. For the discrete trapping level showing a space-charge-limited characteristic, much of the work has been done in Section 1.3 so that it is a simple matter to calculate the effect on C_t in this case. The average trapped-charge density is, using equations 1.17 and 1.18: $\underline{n}_t = 3AK\epsilon_0 V/2eL^2$, instead of $\underline{n}_t = 2AK\epsilon_0 V/eL^2$ as in Section 2.1. Thus, the maximum capacitance is reduced by $AK\epsilon_0/2L = (1/2)C_e$, to $C_{mm} = (5/2)C_e$. For lower values of injected charge than that causing a space-charge-limited characteristic, the reduction in C_{tm} can be expected to be less than $(1/2)C_e$.

Assuming that ν_e and γ in equation 2.9 are specified by thermal-equilibrium conditions, some further conclusions about other effects of bias may be made. We shall discuss these conclusions in the following paragraphs.

Provided that trapping is by a discrete level so that the probability-of-escape frequency ν_e is accurately described by equation 2.10, we would not expect any variation in the frequency dependence of C_t with bias due to a change in ν_e. If, however, ν_e is an effective value obtained from an

averaging process over a group of energy-distributed traps whose occupancy is subject to Fermi-Dirac statistics, then bias could conceivably affect its value. This will occur because a bias voltage acts to raise the interior Fermi level and, thereby, to alter the statistics governing the averaged value for ν_e. Of course, if the crystal contains one blocking and one ohmic contact, then bias in the reverse direction so as to attempt injection from the blocking contact will yield a zero trapping capacitance. If, however, the diode structure is biased to inject electrons from the contact capable of injection, the crystal trapping capacitance should be the same as that for a symmetric structure.

The magnitude of the terminal capacitance might also be influenced by d-c bias. Both C_t' in equation 2.15 and C_t'' in equation 2.18 are seen to be proportional to γ, the ratio between n_t and n under equilibrium conditions. If the average value of the Fermi level in the crystal is enough below the trapping levels so that Maxwell-Boltzman statistics apply, γ equals θ^{-1} (with θ defined in equation 1.8) and is independent of voltage. In general, however, γ is a function both of voltage and of illumination. The variation of γ with voltage has been discussed briefly in Chapter 1. It will be described more fully in Chapter 5 along with the dependence on illumination.

A sketch of possible behavior with bias voltage due to γ changes at a low applied frequency is given in figure 2.5.

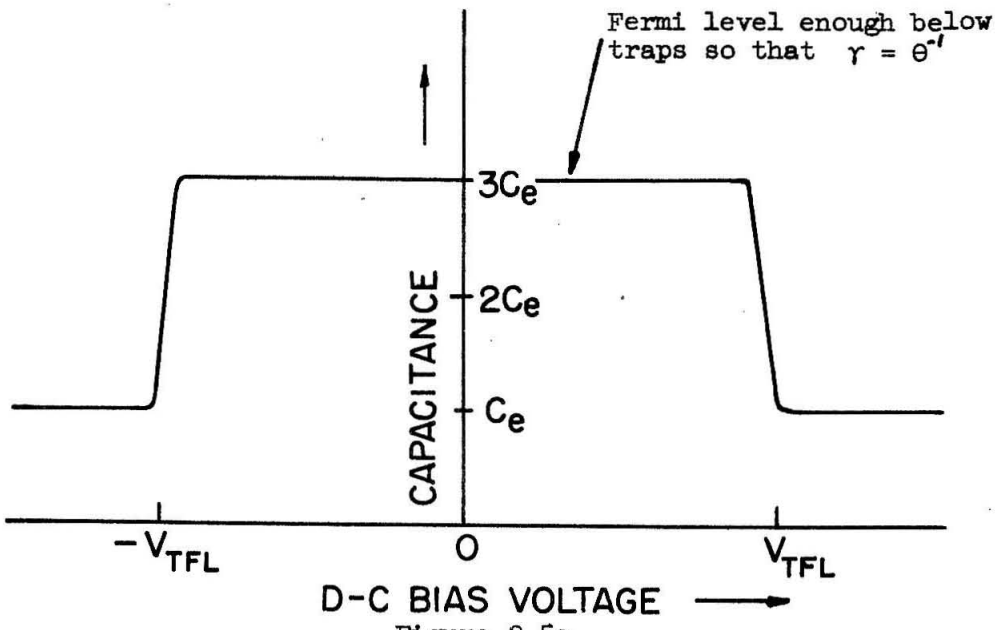

Figure 2.5a

Expected variation of measured capacitance under sinusoidal excitation with a d-c bias for a crystal with traps and two injecting electrodes for the case that $C_t = C_{tm} = 2C_e$. The values for capacitance at biases $\approx V_{TFL}$ are heuristic since the applicability of the analysis in terms of equation 2.9 fails for $n_t \rightarrow N_t$.

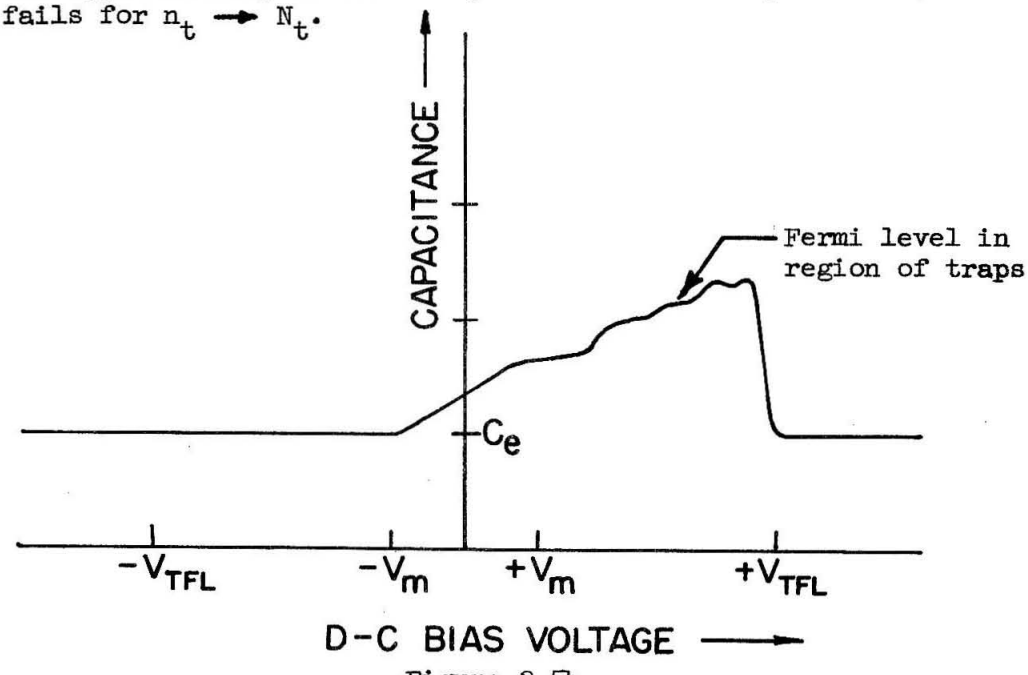

Figure 2.5b

Expected variation of measured capacitance under sinusoidal excitation with a d-c bias for a crystal with traps and one injecting contact. Polarity of the bias voltage is that of the collecting electrode with respect to the injecting electrode. Applied a-c voltage is $V = V_m \cos \omega t$.

In figure 2.5a, the case of two injecting electrodes is sketched with the supposition that $\gamma = \theta^{-1}$. In 2.5b, the single injecting electrode is considered for the hypothetical case that both γ and ν_e are voltage-dependent (Fermi-Dirac statistics applicable to energetically-distributed traps). For both figures, the applied voltage is assumed to be $V = V_m \cos \omega t$. The cut-off of C_e at $\pm V_{TFL} = N_t e L^2 / 2K\epsilon_0$ (equation 1.22) occurs because above this voltage magnitude, all the traps become terminals for the electrical flux lines generated by the d-c component of voltage and are therefore insensitive to the a-c signal. Thus C_t approaches zero at all frequencies under this condition. In this voltage region, however, the free charge becomes significant in increasing the measured capacitance. The analysis of the capacitance due to free charge in this region of voltage excitation is straightforward, but will not be applicable to our work and is therefore not given here.

It is also possible for the contact injection efficiency, which relates the injected free charge to the voltage applied, to vary with a d-c bias as well as with other parameters such as illumination. This quantity, defined as n_m/V_m, was lumped together with γ to form the over-all proportionality η, between trapped charge and applied voltage in the discussion of Section 2.2.2. A variation in n_m/V_m could result, for example, from a very limited charge reservoir at the virtual cathode of an emitting surface. Instead of discussing all the

possible alternatives for contact behavior at this time, we shall reserve comment on this subject until we present experimental results.

2.5. Conclusions

We have seen, in this chapter, that the capacitance exhibited externally as a result of charge storage in traps has a characteristic behavior which can provide information about trapping properties. Before we recapitulate the expected behavior of the capacitance due to traps and discuss the information about the trapping levels that this behavior will divulge, we should consider whether the expected magnitudes for C_t will be detectable in any experimental measurements. Since the maximum trapping capacitance C_{tm} is equal to $2C_e$ where $C_e = AK\epsilon_0/L$ is the electrode capacitance, any crystal must be thin to achieve a measurable value for C_t. As will be discussed in Chapter 6, about the smallest exciting voltage that could be used across the capacitance to measure it in a bridge circuit was 10mv. If a crystal of $1mm^2$ cross-sectional area and 10 microns thickness were used and a voltage of 10mv applied, it would take a trapped-charge density of about 6×10^{10} electrons cm^{-3} to contribute 1 picofarad of capacitance. Not only is 1 picofarad a detectable capacitance but also the injected, trapped-charge density can reasonably be expected to reach and exceed 6×10^{10} electrons cm^{-3} in many actual crystals at this voltage. Therefore, for crystals in the size

range considered, C_t is measurable and one could expect to test the conclusions made in this chapter experimentally. Actually, in Chapter 6 when measurements are discussed, we shall see that even smaller trapped charge densities than this are detectable.

We shall conclude this chapter by enumerating the information that measurements of C_t should provide on the basis of the theoretical framework we have provided. The analysis of Section 2.1 showed us that under no circumstances can we expect C_t to exceed twice the electrode capacitance C_e. This value $C_{tm} = 2C_e$ will occur only for injection into the traps from both contacts and for a uniform interior-charge density. For a single injecting contact, C_t will be limited to values below C_e. Hence, observation of either of these alternatives will indicate the nature of the contacts to the dielectric crystal. The frequency behavior of C_t, analyzed in Section 2.2, is chiefly governed by the value of the probability-of-escape frequency. In most cases C_t will drop rapidly as impressed radial frequencies are raised to the neighborhood of ν_e. Correspondence of the observed behavior of C_t with frequency with the predictions of Section 2.2 will allow a deduction of the value of ν_e. If ν_e is given by equation 2.10 ($\nu_e = N_c v S_t \exp[-(W_C - W_T)/kT]$) and the trap depth in that equation is known independently, a value for the capture cross-section may be obtained. As seen in Section 2.5, the behavior of C_t with d-c bias will indicate the energy configuration of the traps which are responsible for the measured capacitance. Finally,

the over-all correspondence of measurements on actual samples with this analysis will act to reinforce confidence in our physical model, which emphasizes the importance of volume-distributed, interior trapping states.

From this discussion, we can see that much information can be obtained from observations of the trapped charge through capacitance measurements. The practical aspect of this statement will be made evident in the experimental results of Chapter 6.

CHAPTER III

Diode Fabrication

This chapter forms a bridge between the theoretical analyses of the properties of an insulator with traps, described in Chapters 1 and 2, and the experimental work with CdS to be interpreted in Chapters 4 through 6. It is concerned with providing the details of the processes involved in the preparation of diodes made from single-crystal CdS. These diodes were made bi-polar by exploiting the differing contact properties of gold and indium to CdS. Although much research has been done on the properties of metallic contacts to CdS, success in making injecting contacts in the absence of illumination has been reported only with indium and gallium. The effect of illumination on the blocking character of the other metals is not fully determined, yet. We shall give some evidence in Chapter 6 bearing on this subject. Good blocking contacts have been made using copper, silver and gold [15]. In order to study the properties of both injecting and non-injecting contacts to CdS crystals, therefore, it was decided to make a diode structure by affixing electrodes of indium and gold to the monocrystals. Indium was chosen instead of gallium for the injecting contact because of the convenience of acquiring and handling it. Gold was chosen as the material for the blocking contact for much the same reasons, in addition to the fact that it promised to form a non-reactive, stable electrode. In the diode fabrication, as

we shall see, extensive care was necessary to achieve duplicable results.

3.1. General Description of the Types of Diodes Constructed

There were two basic types of diodes made and investigated as described in the later chapters. The diode types are distinguished by the nature of the single-crystal CdS material used. Some units were cut from large crystals, and then lapped and etched before the contacts were attached. Others were made from small, thin platelets which were condensed in a vapor diffusion furnace using the method of Frerichs' as described by Bube and Thomsen [16]. Those made from large crystals were generally of larger area and width (approximately $25mm^2$ x 0.1mm) than the small platelets which had cross-sectional areas in the range of $0.5mm^2$ and thicknesses of about 10 microns. Handling of the small crystals, which were extremely fragile, was much facilitated through the use of a "Penfield Eductor Pickup." This is a commercial unit which holds small samples with the very light vacuum created at the end of a shaped hypodermic needle through a Venturi action on escaping compressed air.

The preparation of the surface of the crystal prior to the attachment of electrodes is a very important part of the process of diode construction. As evidence of this fact we shall discuss briefly at the end of this report some data taken on the photovoltage observed for these diodes. The

photovoltage data showed conclusively that the contact properties of gold on CdS will be dependent on the state of the surface of the material. Crystals from the same lot, processed in identical fashion, showed a value for photovoltage at a given illumination which varied considerably. In a few instances, the photovoltage was even of an inverse polarity from that detected for the majority of crystals. That this is a surface effect is evident from the similarity in behavior of the same diodes under space-charge-limited flow conditions (described in Chapter 5), which is definitely a bulk phenomenon. To minimize any influence of differing surface conditions, therefore, it is necessary to treat the material in a set manner, keeping all preparation variations to a minimum. As described in Section 3.2, practically no surface preparation was attempted on the small platelets. Under these conditions it is not too surprising that the contact properties of these samples varied somewhat. A far greater degree of uniformity prevailed inthe photovoltage data taken for the large crystals, which had a more extensive surface preparation.

The small platelets were of special interest for at least three reasons. First, they were truly monocrystalline and hence the analyses made under this assumption are justified for these platelets. It is not certain that the larger crystals were monocrystalline, since on many of them there were lines which looked suspiciously like grain boundaries. Second, the thinness of the small platelets enabled high fields to be easily impressed

upon them with a small, laboratory d-c supply. The platelets for which results were obtained were in the range of 10 microns in width, so that fields of a million volts per meter were easy to obtain. At these fields certain interesting phenomena were noted which will be described more fully in Chapter 4. Third, the thinness of the platelets also permitted the exploration of trapping properties through capacitance measurements. The experiments reported in Chapter 6 would have been impossible with the larger crystals. Because of these three attributes, we shall find that most of the discussion to be given resulted from experiments on the thin-platelet crystals.

3.2. Crystal Preparation

Preparation of the small crystals for the attachment of contacts was limited to a surface cleansing with de-ionized water followed by swabbing with di-chloromethane. The extreme fragility of the crystals would certainly have made more extensive surface preparations difficult. It was felt, however, that they were unnecessary since these samples had no surface abrasion performed on them and since CdS appears to be a relatively inactive material. The experiments of Smith [17][18] at RCA and by Wright [4] at Birmingham on CdS platelets were done on similarly-prepared crystals.

The large single-crystals were first cut with a diamond saw and lapped with successively finer garnet powders culminating in

W-12 grit. Care was needed in these operations, especially in the use of the diamond saw, owing to the structural weakness of the material. It is advisable to set the automatic feed of the saw at its slowest speed to minimize breakage. The CdS crystals used had a close-packed-hexagonal crystallography and had far more strength across the hexagonal axis than along it. All samples were cut across this axis (001 plane). For this mechanical work the samples were waxed to a supporting substrate. They were then removed from the substrate and etched. A suitable etch appears to be six-normal hydrochloric acid. The rate of material removal is high, so that only a short time should be allowed in the etch bath. After etching, the crystals were quenched in de-ionized water and swabbed with di-chloro-methane. They were then ready for the attachment of electrodes.

3.3. Construction of the Diodes

A great deal of experimentation and trial preceded the successful construction of diodes. The chief problems lay in achieving mechanical strength, and in providing sufficient electrical insulation for the extremely thin wafers in order to avoid leakage paths around the crystal.

Based upon the procedure reported by Wright [4], initial effort was directed toward making alloyed contacts of indium directly to the CdS surface. This was successful in some instances, especially in the work on the large crystals, but proved difficult to implement with the small platelets. The

procedure followed for the alloying began by placement of a small indium pellet on a copper substrate with the CdS crystal perched above it. A hot plate then provided sufficient heat to melt the indium and thereby make a binding contact between the CdS and the copper. An acid flux at this point acted to increase the mechanical strength of the joint without apparent electrical effect.

Chiefly owing to mechanical difficulties with the small platelet crystals, later efforts were directed toward making the indium contacts by evaporating the electrode material in a vacuum chamber. This evaporation was performed at a fairly poor vacuum (approximately 10^{-5}mm of mercury) from an overhead tungsten filament. A silver paste was then used to attach the CdS platelet to the copper substrate. The electrical path into the crystal thus consisted of a copper plate, conducting silver-paste, and then indium evaporated to the CdS. The silver paste was very poor in its mechanical strength, but rigidity was provided for the mount by the Fibreglas insulation as will be described. Figure 3.1 is a schematic diagram of the construction used and should prove helpful as a reference as the description proceeds. It should be emphasized that this figure is not intended as a pictorial representation nor is it drawn to scale.

With the crystal in place on the copper substrate, a layer of Fibreglas, a very hard, inert, air-drying, commercial resin, was laid to its edges covering the copper completely in the

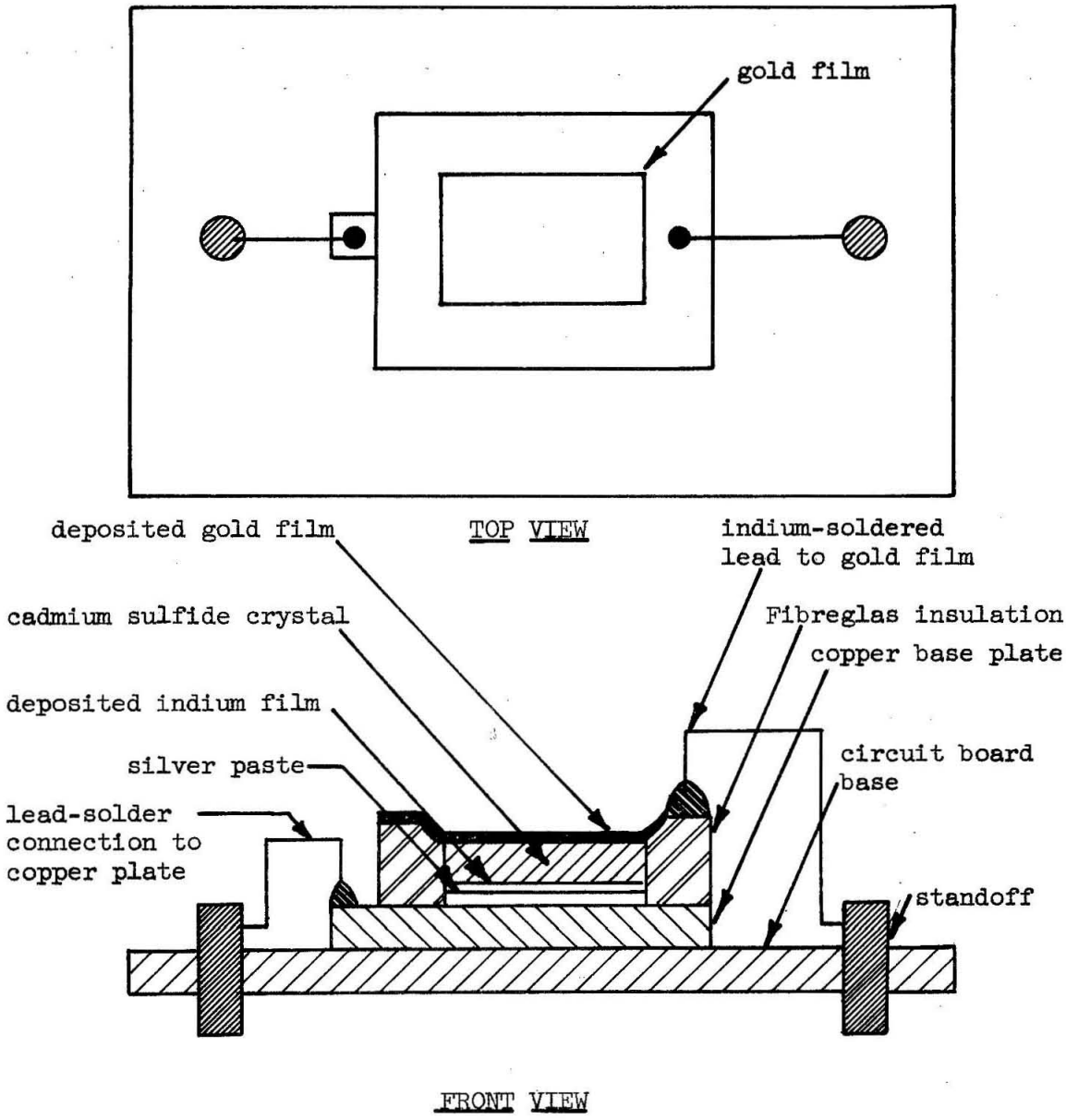

Figure 3.1

Schematic drawing of the construction of the Au-CdS-In diodes. The drawing is not to scale and not representative of shapes - all crystals are actually of an irregular shape.

vicinity of each unit (there were often more than one crystal on a single substrate). The Fibreglas had enough surface tension to form a neat fillet at the edge of the crystal without running over the crystal itself, provided care was taken in this operation. The Fibreglas was permitted to dry for at least 24 hours before any further operations were performed. The next step was to treat the exposed surface of the CdS as was described in Section 3.2, etching the larger cut pieces and cleansing the small platelet surfaces. The Fibreglas is capable of withstanding the etch for short periods of time.

After this, the entire assembly was placed in a vacuum chamber and the system pumped to about 5×10^{-7} mm of mercury. It was left at this vacuum for at least an hour before evaporating any material. The gold evaporation was done from an elevated tungsten filament onto the assemblage, which was masked so that only the crystal face and the Fibreglas adjacent to it were coated. To ensure a clean surface on the evaporative source material, the first metal evaporated was caught on a shutter used to shield the diode structures. The final step in the process was lead attachment to the gold substrate. Early work was done by making this contact with a micro-manipulator until it was discovered that very fine wires could be soldered with pure indium to the portion of the gold film overlapping the crystal onto the Fibreglas. The copper plate was then glued to a circuit board, the wires from the gold film attached to stand-offs, and leads attached from other stand-offs to the plate itself. This

produced a portable, rigid structure suitable for electrical tests. As made, the units could stand only moderate temperature changes. Heating was limited by the melting point of indium (156.4°C) and cooling by the effects of unequal coefficients of expansion. The Fibreglas would crack from the copper at low temperatures and the crystal contact to the copper base would break due to the relative motion. Lack of facilities and units prohibited a complete study of the permissible excursion to lower temperatures. As a precautionary measure, completed diodes were stored in an evacuated dessicator, although later experience suggests that this is not necessary.

3.4. Material Sources and Properties

Cadmium sulfide is now of some commercial value, and there are, accordingly, a number of chemical supply houses from which it is available in single-crystal form. On the advice of R. L. Williams of RCA, relatively large (5 gram) single crystals of the material were purchased from the Eagle Picher Company of Cincinnati, Ohio. Other single-crystal samples of roughly the same size and character were generously supplied by D. C. Reynolds of the Wright Air Development Center in Dayton, Ohio. Eagle Picher sells CdS doped with chlorine to give a range of room-light resistivities, and various values were obtained for study. Chlorine and the other halides act as donors in CdS. They are ionized at room temperature and can cause significant increases in dark conductivity. The halides are thought to be incorporated substitutionally for

sulfur in the crystal lattice. Trivalent cations such as aluminum, gallium and indium appear to substitute for cadmium in the lattice and also act to increase the conductivity of CdS. Copper and silver, on the other hand, provide energy states low in the band gap, and thereby decrease the conductivity of the crystal. Since copper and silver have opposite effects from the halides on the conduction-band population, elements from the two groups are sometimes incorporated one after another in a crystal to establish a given resistivity [1].

The addition of copper or silver after a halide is a useful technique in the condensation of the thin-platelet crystals. While it is possible to grow the crystals from pure vapors of H_2S and cadmium, the presence of a halogen seems to enhance their growth [6]. Therefore, high resistivity thin-platelet crystals are sometimes made through compensation of the incorporated halogen by copper or silver. Both pure crystals and crystals doped with chlorine followed by copper were studied. These were obtained through the generosity of R. W. Smith of the RCA Princeton Laboratories, and of J. E. Johnson who is at the Westinghouse Research Center in Pittsburgh, Pennsylvania.

Both the gold and indium used in making contacts to the CdS were chemically-pure grades, available from almost any chemical supplier. The Fibreglas resin used as an insulating material is available at a number of hardware stores, chiefly those dealing in marine products.

3.5. Measurement of Thin-Platelet Dimensions

It is necessary to establish the physical dimensions of the crystals accurately in order to check the electrical measurements with theory. The diode construction made measurement of the sample area fairly straightforward. With vapor-deposited contacts it was relatively simple to obtain this value by making use of the graduated eyepiece in a metallurgical microscope. The procedure was to estimate the outline of a rectangle approximating the sample area, and to read the dimensions directly from the eyepiece calibration. The approximate error from such a procedure is estimated at a maximum of 10% of the linear measurement. Most small platelets had a cross-sectional area of about half a square mm, known with a precision estimated at ± 20%.

Measurement of the crystal thickness was more difficult. Before any of the operations used in fabricating the samples were started, all platelets were measured with a micrometer. This proved satisfactory for the large samples, but it was a fairly gross technique for the small samples since the crystal surfaces were in general not planar, but had small spines on them. Also, most of these samples had thicknesses in the range of ten microns. This is a rather small measurement to make accurately with a micrometer. Especially in the case of alloyed junctions, it was not certain whether the electrical contact existed at the physical surface or, perhaps, below it due to some in-diffusion of the metals. Wright [4] gives evidence that some diffusion

occurred from the contacts of one of his samples. For these reasons the thickness used in all calculations for the thin platelet was the one deduced from the capacitance measurements. In the discussion concerning capacitance measurements in Chapter 6, the interpretation of the capacitance data is explained, as is the technique of making measurements. Thicknesses deduced from measured capacitance were about 50% lower than those measured initially with the micrometer.

The errors involved in the calculation of thickness from measured capacitance are due to:

a. The added stray capacitance from the lead attachments. As described in Section 3.3, it was necessary to overlap the gold film onto the Fibreglas in order to provide a place for soldering the leads. This overlap necessarily adds some capacitance in parallel to that of the sample. The size of this added capacitance is dependent on the area of the overlapping gold film and the thickness of the insulating Fibreglas. Although some test measurements of capacitance measured across the Fibreglas film alone ran as high at 1.3pf, it is felt that a good average for this value would be closer to 1pf. Accordingly, in

deducing thickness 1pf was subtracted from the measured value for the capacitance of all diodes. It follows, therefore, that the probable percentage errors are highest in samples for which the measured capacitance is lowest.

b. Inapplicability of the simple formula $L = C/AK\epsilon_0$, with L the crystal thickness, C the measured capacitance, A the junction area, and $K\epsilon_0$ the crystal permittivity. Error in the application of this formula would arise due to lack of surface planarity or uniformity of electrodes or crystal. Owing to the extreme thinness of the samples, this source of inaccuracy is not likely to be great. In any case the simple equation would give an average thickness, which should be the most useful in further calculations.

c. Error in the measurements of C or A. The expected precision for the area has already been discussed. The discussion of the precision of capacitance measurements is given in Chapter 6. In the worst case, their inaccuracy might lead to about 30% error in L.

d. Error in the value for the relative permittivity. We shall see in the complete discussion of capacitance measurements in Chapter 6 that the permittivity in CdS is a function of illumination. Bube [1, page 276] comments also on the variation of K with trap densities in CdS. This being the case, it is not surprising that the dark values given in various references differ by as much as 10% from the value 10.5, which was used in this study.

In summary, it is not expected that the total error in the thickness measurement exceeds 50%. Table 3.1 tabulates the high frequency capacitance and dimensions for the diodes for which mathematical analysis will be presented later in the text.

TABLE 3.1

Diode #	Capacitance pf	Thickness μ	Area m^2	Volume m^3
13-4	4.0	13.5	5.8×10^{-7}	7.9×10^{-12}
13-5	2.15	13.85	3.2×10^{-7}	4.4×10^{-12}
13-7	5.74	9.71	6.0×10^{-7}	5.8×10^{-12}

3.6. Control of Gold Film Deposition Thickness

In studying illumination effects on the completed diodes, light was directed through the gold contact. By this means,

information was sought bearing upon the assertion of Williams and Bube that the photovoltaic effect at a metallic blocking contact to CdS results from optically-stimulated photoemission from the metal into the crystal [15]. To test this theory, and also to obtain a correct evaluation of photoconductive data, it was necessary to control the thickness of the gold film.

This was done by monitoring the resistance of a square of the deposited material placed in the vacuum at the same distance from the source as the diode on which deposition was taking place. Research done by Wilkinson and reported by Holland [19, page 237] showed that the dependence of the resistivity on film thickness for gold on glass may be fitted empirically by the equation:

$$\rho_{film} = \rho_{bulk} (1 + 1230/L) \qquad (3.1)$$

with ρ standing for the resistivity, and L, the thickness of the film in angstroms. Using 3.1 and the relationship $\rho = RL$ for a square gauge, one can solve for the requisite resistance measured across the terminals for any desired film thickness. The evaporating metal is then simply cut off by the shutter when this resistance is reached.

The precision of this method is somewhat limited due to fluctuations of film thickness over the square area, and inaccuracy in the exact distances from source to sample and source to gauge.

However, the primary goal was a means of knowing relative thicknesses for the gold film on various samples. It is felt that this end was served adequately by the method.

3.7. Conclusions

With the hindsight available from many trials at diode construction, some observations on working with CdS may be made. If work is done on samples cut from large crystals, the minimum thickness for the sawn wafer should be about .02 inches. CdS does not appear to have sufficient structural rigidity for thinner cuts without fracturing. It is easy to reduce the thickness considerably below the cut dimension by hand-lapping, so that the minimum saw cut is not a thinness limitation. The fact that the lapped crystals are not overly fragile suggests that the problem in diamond sawing is blade vibration. Care was observed to minimize this effect but even with such care, twenty mils seemed the lower limit for a reasonable yield of samples. These statements apply to cuts across the crystal axis (001 plane); essentially no success was achieved in diamond sawing along the axis.

Vapor-deposited metallic contacts are recommended wherever possible. This technique not only permits accurate geometric control, but is as gentle as possible to the crystal. In addition, by building substrate heaters into the vacuum system, any desired heat treating can be done within an inert milieu.

In heat treating the CdS in this fashion, it was found that vapor-deposited, indium contacts were capable of electron injection even in the complete absence of alloying.

The final mounting of the crystal for experimental test is an important part of the fabrication procedure. The mounting technique described in Section 3.3 represents the result of a number of attempts, most of which were only partially successful. The mounting finally adopted could serve well for a number of different experiments with only slight modifications. Its main and most useful features are the use of Fibreglas to hold the sample and the employment of indium-soldered wires to make connections to the vapor-deposited contact films. Most other investigators of the properties of CdS have worked with samples that had surfaces exposed to air except underneath the metallic contacts. From the agreement between their results and those which we shall present in Chapter 5, we can state that the resin ambient does not significantly alter the properties governing charge injection into the crystal. If anything, the surface of the crystal contacting the Fibreglas should be more stable than if it were exposed to air so that, even in experiments where surface properties were more important, the Fibreglas support could be valuable.

CHAPTER IV

CdS Diode Equilibrium Current-Voltage Characteristic: I. Gold Contact Negative

In this chapter we shall begin the discussion of the electrical measurements made on the CdS diodes fabricated in the manner described in Chapter 3. The current-voltage characteristic for the diodes under equilibrium conditions will be the subject both of this chapter and of Chapter 5. Much of the discussion in these two chapters is framed in terms of the measured characteristics of diode 13-5, a thin-platelet unit which behaved similarly to most of the diodes of its type that were tested. Other diodes are discussed with reference to differences from diode 13-5. Figure 4.1 is the overall volt-ampere curve for diode 13-5, plotted to linear scales. The voltage polarity is that of the gold contact. Figure 4.1 divides quite neatly into three distinct regions, which are best discussed separately. These regions are demarcated by Roman numerals on the plot. Regions I and II are discussed in this chapter, although the latter is common to both positive and negative excitation for the gold film. Region III is discussed in Chapter 5.

As all of the diodes made were light sensitive, the measurements not concerned with photoelectric effects were made in the dark. In discussing experimental results, it will always be specifically stated where this was not so.

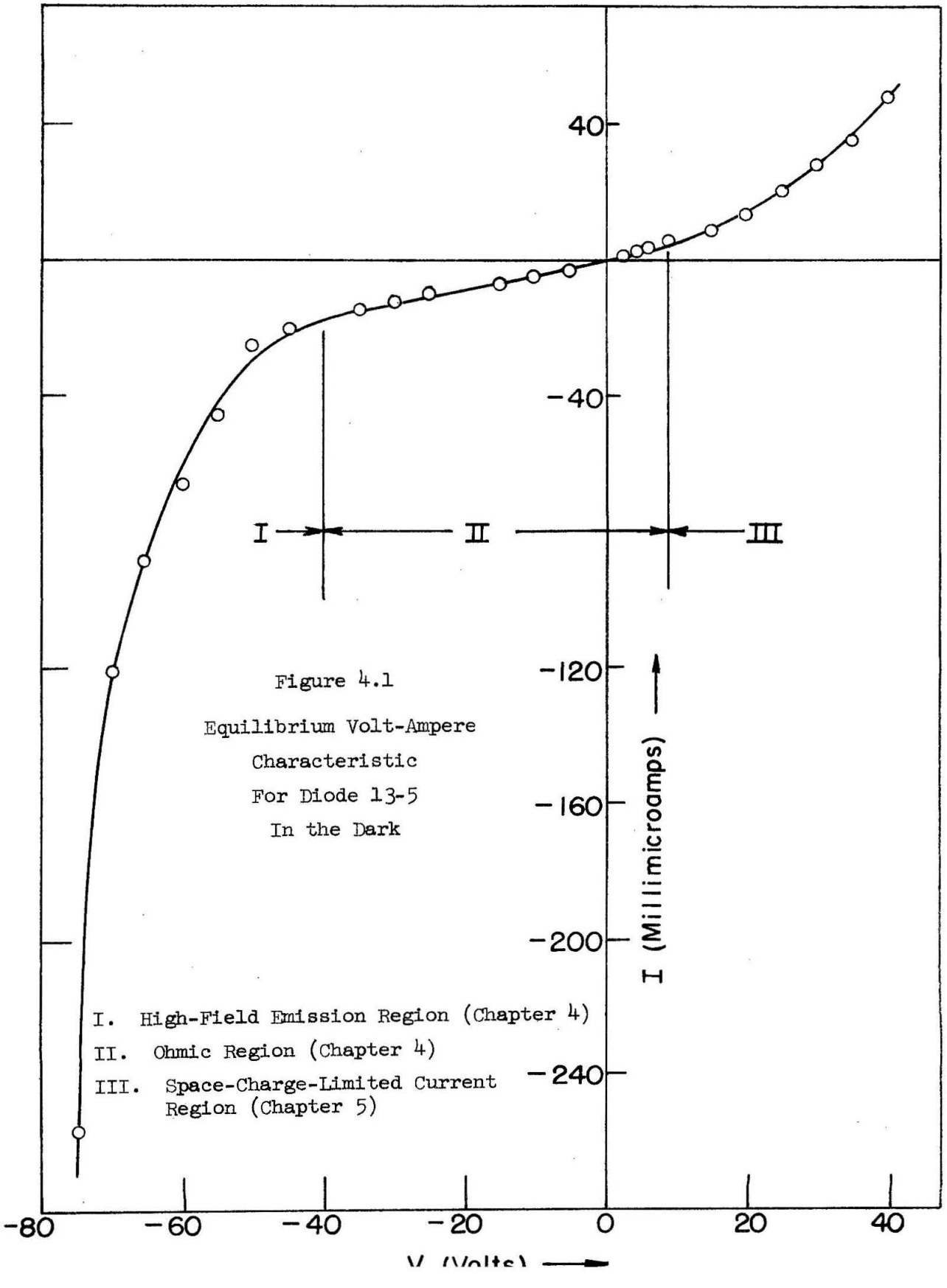

Figure 4.1

Equilibrium Volt-Ampere Characteristic For Diode 13-5 In the Dark

I. High-Field Emission Region (Chapter 4)

II. Ohmic Region (Chapter 4)

III. Space-Charge-Limited Current Region (Chapter 5)

4.1. Dark Conductivity

At low applied voltages, either positive or negative, figure 4.1 shows that the crystal exhibits an ohmic behavior indicative of an extremely high resistivity. From this portion of the characteristic, which we have labeled Region II, we may deduce the free-electron density in the crystal.

Making use of the standard formula for the resistance value deduced from the slope of figure 4.1 in Region II together with the diode dimensions given in Table 3.1, we may calculate the crystal resistivity. The indicated resistance, 2.5×10^9 ohms, implies a dark resistivity value of 5.78×10^9 ohm-cm. Assuming a mobility for electrons in CdS of $200^* cm^2$/volt-sec., this resistance indicates a dark electron concentration of $5.4 \times 10^6 cm^{-3}$. The dark resistivity value for diode 13-5 is within a factor of three of that measured for the three other pure samples checked. Some of the diodes doped with chlorine and copper as described in Section 3.4 had dark resistivities an order of magnitude greater than this.

It is pertinent at this point to see what value one would expect for the intrinsic electron density in a perfect crystal of CdS, in order to decide whether the observed density can be accounted for through normal excitation processes from the CdS

---

* There is not yet general agreement among investigators on the value of the electron mobility in CdS. (There is absolutely none on a value for the hole mobility.) Values range from $10 cm^2$/volt-sec. [20] to 200 [1, p. 269]. The latter value is used here since it is most current and is given by Bube after a search of the literature on the properties of CdS.

valence band or whether it is due to ionized donor centers.

For an intrinsic material the electron density is given by:

$$n = N_c \exp - \left(\frac{W_g}{2kT}\right) \tag{4.1}$$

where W_g is the gap energy and N_c is the effective density of states in the conduction band. From Bube [1], $W_g = 2.4$ev for CdS. The quantity N_c is given by:

$$N_c = 2\left(\frac{2\pi m_e kT}{h^2}\right)^{3/2} \tag{4.2}$$

where m_e is the effective mass of electrons in the conduction band and h is Planck's constant. Bube [1] gives an ellipsoidal average of $m_e = .14m_r$ for CdS, where m_r is the electron rest mass. Using these values, we calculate:

$$N_c = 1.38 \times 10^{18} cm^{-3}$$

at $T = 300^{\circ}K$. Hence we obtain $n = 1.93 \times 10^{-3} cm^{-3}$ for intrinsic CdS. Comparison of this extremely low density with the value $5.4 \times 10^{6} cm^{-3}$, deduced from measurements, assures that the measured electron density is due to effective donor centers, and

that the Fermi level interior to the crystal is not located at the band-gap center. Assuming that all the effective donor centers are ionized, we can carry these calculations one step further and determine the depth of the Fermi level in the actual crystal below the conduction band edge through the relationship:

$$W_C - W_F = kT \ln\left(\frac{N_c}{N_d}\right) \qquad (4.3)$$

with N_d the effective donor density. For sample 13-5, if we take for N_d the measured electron density $n = 5.4 \times 10^6 cm^{-3}$, we obtain from equation 4.3: $W_C - W_F = .656ev$. Hence the actual Fermi level is distinctly elevated from its 1.2ev depth in intrinsic material. This has been a general finding among investigators of the properties of "pure" crystals of CdS.

4.2. High Field Characteristic

As the gold film contact to the CdS is made progressively more negative, a departure from ohmic behavior begins to become evident at applied voltages in the neighborhood of 40 volts. This is the portion of figure 4.1 which we have called Region I. From the crystal thickness in Table 3.1 we see that the average field at the edge of Region I is 3×10^4 volts/cm.

At such high fields a number of phenomena are possible, including various types of crystal breakdown. Further considerations are necessary to deduce what mechanism is responsible

for the characteristic obtained.

A possible explanation of the mechanism leading to departure from ohmic behavior suggests itself when the data of figure 4.1 is replotted with logarithmic current, the ordinate, and the square root of voltage, the abscissa. With such a representation the experimental data in Region I becomes an extremely good fit to a straight line. Such a plot for sample 13-5 is given in figure 4.2. The $\exp(\alpha V^{1/2})$ dependence of current implied by this curve is reminiscent of the Schottky* high-field variation for thermionic emission into a vacuum. This leads one to believe that the gold film is indeed acting as an electron emitter into the CdS at high-fields, and that its effective emission work function is being decreased through the action of the high electric field.

Besides Schottky emission, consideration of at least one other solid-state phenomenon has been shown to lead to an $\exp(\alpha V^{1/2})$ dependence for current. Henisch [22, p. 202] derives such a dependence for electrons tunneling through the top of a variable-width barrier under the influence of a high field. This hypothesis does not appear likely to explain the results presented here both on theoretical and experimental grounds, for the following reasons:

1. The hypothesis is based on the assumption that the space-charge region is of variable width as in a back-biased

* See, for example, Spangenberg [21, p. 156].

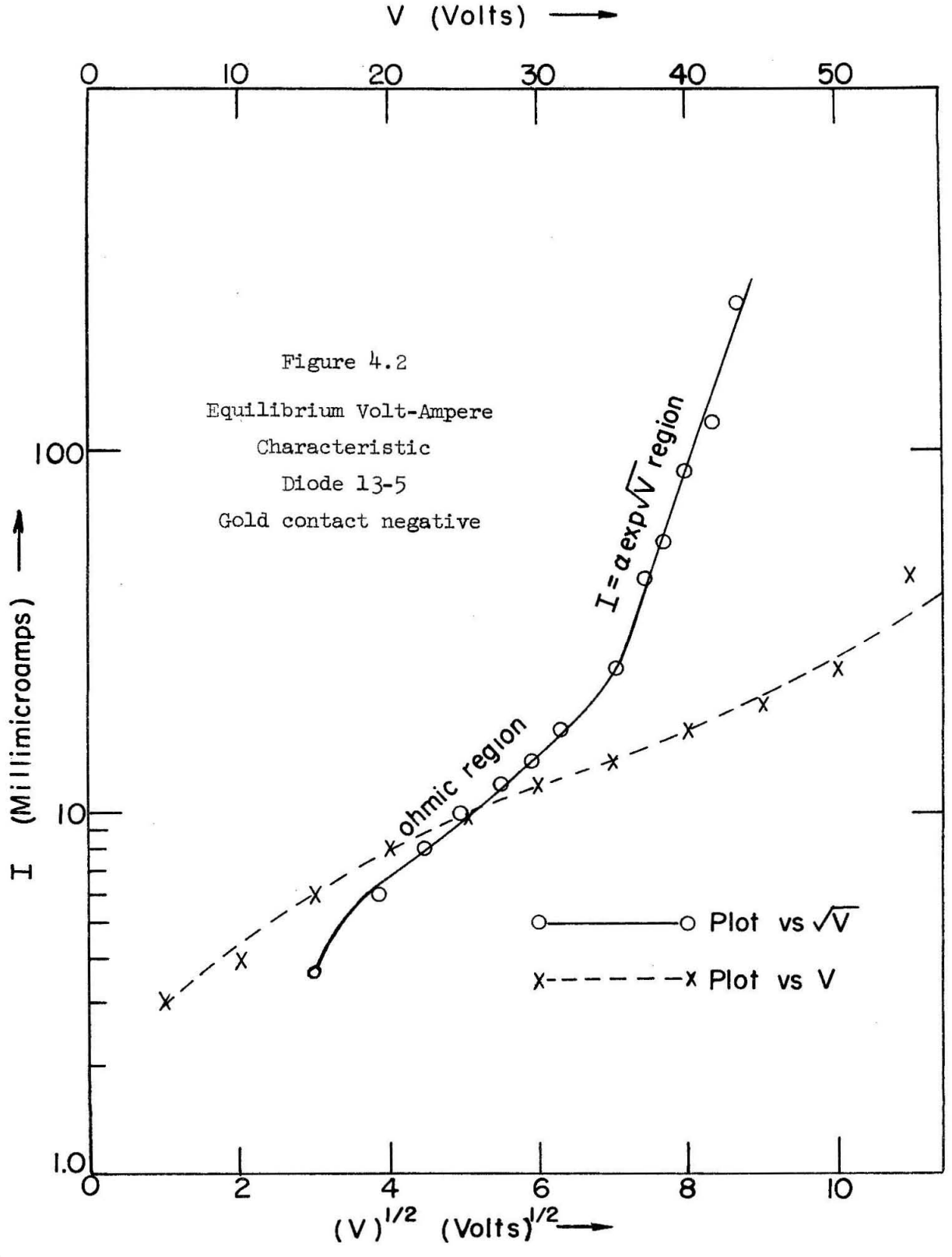

Figure 4.2

Equilibrium Volt-Ampere Characteristic

Diode 13-5

Gold contact negative

p-n junction. The observed conductivity is so low that one would expect the space-charge region to extend the length of the crystal at any reasonable applied voltage. Therefore, it seems unlikely that one can justify the postulate that tunneling is through a variable-width barrier unless a marked surface concentration of donor states is present.*

2. The theory for the tunneling mechanism as given by Henisch results in an expected variation of current with voltage of the form:

$$J = J_0 \exp\left[\frac{ex_c}{kT}\left[\frac{2eVN_d}{K\epsilon_0}\right]^{1/2}\right] \qquad (4.4)$$

where J_0 is the low-voltage, junction saturation current,

N_d is the effective donor-state density near to the contact,

x_c is a critical thickness for tunneling such that a barrier is assumed completely opaque to tunneling electrons for $w > x_c$ and completely transparent to tunneling electrons for $w < x_c$, with w the barrier width for electrons of a given energy. A reasonable value for x_c is: $x_c = 10^{-9}m = 10A^{\circ}$.

* If the barrier width were not variable, then the Fowler-Nordheim [23] treatment for tunnel emission would apply. This predicts a variation of current proportional to $\exp(K/E)$, with E, the applied electric field and is, therefore, inconsistent with the measured data.

Insertion of the calculated donor density $N_d = 5.4 \times 10^{6} cm^{-3}$ from Section 4.1 into this equation leads to a coefficient for $V^{1/2}$ in the exponential of the order of $10^{-6} volts^{-1/2}$. As we shall see shortly in the analysis of the experimental data, the measured value for this coefficient is of the order of unity. Hence, the disparity is a factor of about a million between experiment and this theory. One might object to the use of a bulk donor density in the calculation, arguing that surface-state donor densities might differ significantly from those in the bulk. However, the necessary hypothesized donor density to insert into equation 4.4 to match theory to experiment is roughly $10^{18} cm^{-3}$. Such a density of donor states is unlikely, but cannot be dismissed as impossible.

Returning to the consideration of an analogue behavior in solids to field emission over a barrier into a vacuum, we note that some reported research has already succeeded in an apparent observation of this phenomenon. The mechanism was invoked by Vermilyea [24] with apparent success to explain experimental data on the volt-ampere characteristics that had been measured by Charlesby on thin films of ZrO_2. The simplest approach to follow in the calculation is to assume, as did Vermilyea, a behavior of the electrons emitted from the gold film analogous to the well-documented vacuum situation [21]. Provided both that our analogy is correct and that the distances involved are significantly larger than the material lattice spacing, this classical treatment should be valid.

Consideration of the image-force potential of an emitted electron, together with the potential related to the applied field E, results in the apparent diminishing of the emission work function by the value:

$$e\Delta\phi = -\frac{e}{2}\sqrt{\frac{eE}{\pi K\epsilon_0}} \tag{4.5}$$

Hence the actual current emitted would be given by:

$$J = J_0 \exp\left[-\frac{e}{kT}\left(\phi_0 - \frac{1}{2}\sqrt{\frac{eE}{\pi K\epsilon_0}}\right)\right] \tag{4.6}$$

where ϕ_0 is the emission work function with no applied field. If the anode potential is so high, or the current density so low, that space charge has a negligible effect on the potential distribution between the electrodes, then the potential gradient at the cathode surface depends only on the anode potential and on the geometry of the electrodes. In general, under these conditions, we may write:

$$E = \beta\frac{V}{L} \tag{4.7}$$

where β is a geometrical constant which assumes the value unity in the case of absolutely plane, parallel electrodes with no fringing effects. Inserting equation 4.7 into equation 4.6, we write:

$$\ln J = \ln J_0 - \frac{e}{kT}\phi_0 + \frac{e}{2kT}\left(\frac{e\beta V}{\pi K \epsilon_0 L}\right)^{1/2} \qquad (4.8)$$

which implies that a logarithmic plot for either the current density J, or the current I, should be linear versus the square root of the applied voltage. The slope of such a graph, if plotted on usual base 10 semi-log paper should be the coefficient of $V^{1/2}$ in equation 4.8, multiplied by the reciprocal of ln 10, or:

$$\frac{d(\log I)}{d\sqrt{V}} = \frac{1}{2.3} \times \frac{e}{2kT}\left(\frac{e\beta}{\pi K \epsilon_0 L}\right) \qquad (4.9)$$

At $300^{\circ}K$, this value is $2 \times 10^{-4}(\beta/L)^{1/2}$ for CdS in the MKS system of units. For sample 13-5, therefore, the theoretical slope implied is $0.053(\beta)^{1/2}$ volts$^{-1/2}$. From figure 4.2, the measured slope for diode 13-5 is 0.625 volts$^{-1/2}$. This value is typical of the order of magnitude for other measured samples, the slopes ranging from 0.37 volts$^{-1/2}$ to 0.77 volts$^{-1/2}$ (crystal thicknesses were roughly equal).

The measured characteristic, therefore, implies that the constant β, which relates the apparent field in the vicinity of the emitting electrode to the average field in the interior, is 139. In Section 4.4, we shall consider the possible causes for such a large apparent cathode field. Thus, at 40 volts, where the apparent field emission becomes evident, $E_{cathode} = 4 \times 10^6$ volts/cm.

4.3. Calculation of Field-Emission Voltage

In principle, one should also be able to calculate the voltage at which incipient field emission will take place. This is done by assuming the validity of the Richardson equation [21], and equating the emission rate it implies to a drift flow of electrons whose density is obtained from a thermal equilibrium between the metal and the insulator. Such a calculation sets equal the maximum electron transfer-rate across the junction and the electron flow-rate away from the junction. The resultant equation is:

$$\frac{e\mu N_c \beta V_f \exp(-eV_B/kT)}{L} = A_e T^2 \exp(-eV_B/kT) \qquad (4.10)$$

in which the exponential factor accounts for the barrier height eV_B, at the blocking metal-insulator junction, and V_f is the applied voltage at incipient field emission. A_e is the

Richardson factor which is calculated by expressing the average density of electrons with velocities oriented out of the crystal and with energies above the emission work function. Ideally, A_e has the value 120 amps $cm^{-2}\ {}^{o}K^{-2}$. The absolute temperature is denoted by T, N_c is the density of states in the insulator conduction band, and the other symbols have their usual definitions.

Solving equation 4.10 for V_f, we obtain:

$$V_f = \frac{A_e T^2 L}{\beta e \mu N_c} \tag{4.11}$$

The value to use for A_e in this equation, as well as that for β, is questionable. As an example, for vacuum emitters, the "constant" A_e has been determined experimentally to vary from .01 times the theoretical value for oxide emitters to 72 times its theoretical value for tungsten as an emitter [21]. If we assume that A_e is 30 times its theoretical value for the situation under consideration (this appears to be typical for the noble metals), and the β of 139 deduced from the measured slope of the breakdown characteristic, equation 4.11 yields V_f = 78 volts. This is a factor of two higher than the voltage measured for sample 13-5, which is not too surprising, when we consider the approximations that are involved. Figure 4.3 is a sketch of a potential configuration near to the gold contact

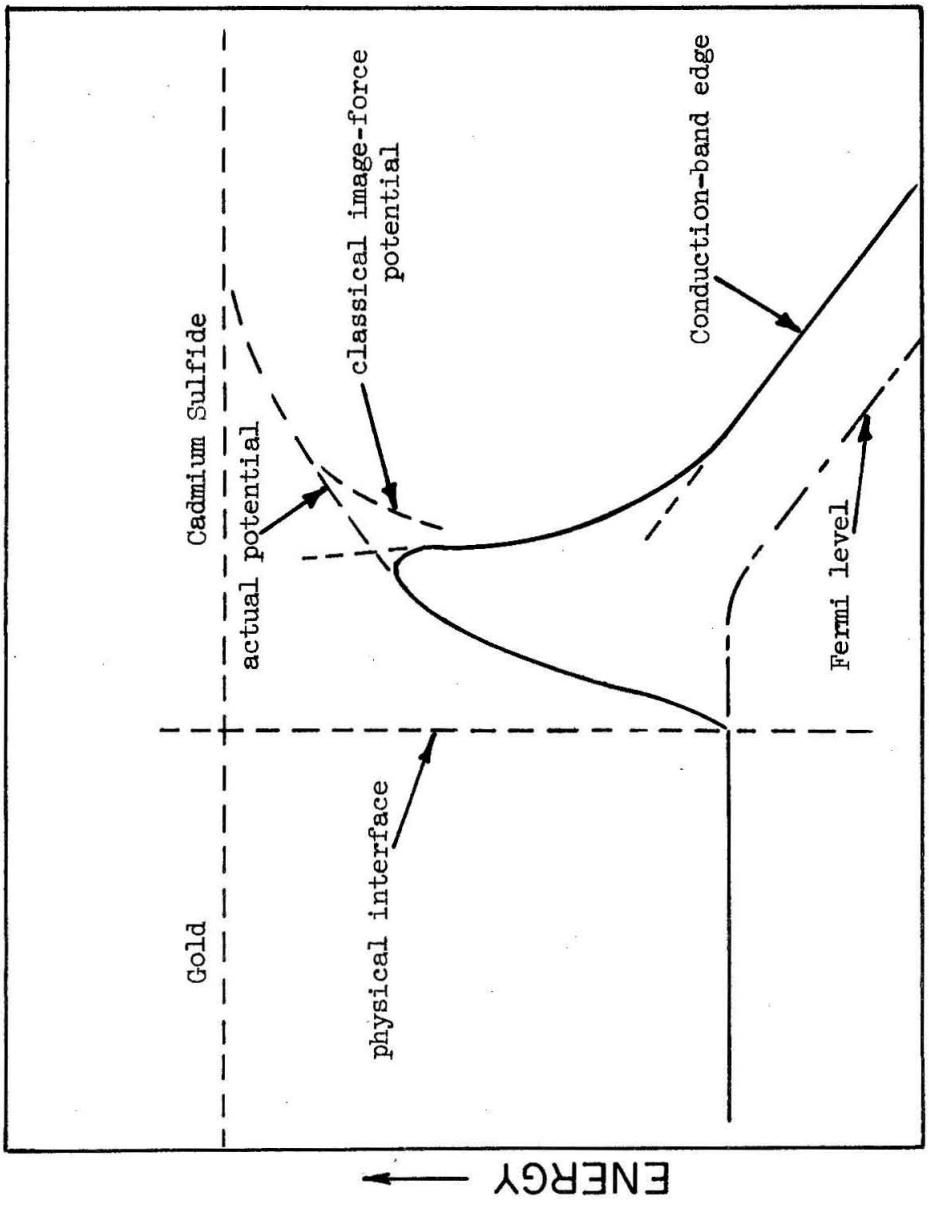

Figure 4.3

Sketch of the potential energy configuration near to the blocking contact as deduced from experimental observations.

which would cause a behavior such as we have noted. The steep maximum near to the gold contact indicates the high emitter field. Possible causes for this field are the subject of the next section.

4.4. Causes of the High Contact Field

There are at least two causes to which might be ascribed the rather large ratio between the apparent field at the cathode and the average field in the interior. First, the image-force consideration involves a distance from the cathode to the potential maximum given by [21]:

$$x_m = \frac{1}{4}\sqrt{\frac{e}{\pi K \epsilon_0 E}} \qquad (4.12)$$

Using the calculated E for diode 13-5 this gives $x_m = 2.92A^{\circ}$. Since this number is of the order of a lattice constant, there is certainly doubt as to the validity of the classical image force treatment. It is, however, the same order of magnitude as in Vermilyea's case [24]. In the case of emission into a vacuum, agreement with simple image-force theory is quoted as being found down to $x_m = 19A^{\circ}$ by Parker [25, p. 176].

The low value calculated for x_m provides one possible explanation for the magnitude of β. If one applied the method of images down to infinitesimal dimensions from the cathode, the

force holding an electron inside the metal would approach infinity and there could consequently be no emission. Hence, when the distance of the image from the plane of the metallic emitter begins to shrink to lattice-constant size, the actual force must be less than that calculated by the method of images. In the procedure used in our calculations this would necessarily show up as a higher effective electric field than that calculated from electrostatics; hence, we would expect to find β some number greater than unity with its value varying inversely with x_m.

Theoretical considerations of the actual potential in the immediate vicinity of a metal-vacuum interface have been reported in a number of papers with a fairly up-to-date summary presented in the work of Cutler and Gibbons [26]. In a quantum-mechanical treatment these authors concluded that a corrected image force potential could be used in the classical manner at small distances from an emitting surface. Their corrected potential differs from the actual potential by 3% or greater in a length characteristic of the emitting surface. This length, which is denoted here by λ, is defined in terms of the electron potential-well depth (W_a) by the formula:

$$\lambda \approx \frac{0.16e^2}{K\epsilon_0 W_a} \qquad \text{(MKS)} \qquad (4.13)$$

This equation and other work in reference 26 are hard to apply to the situation under consideration here, since the actual surface conditions are unknown. In equation 4.13, for example, both the well depth and the value to use for K at small distances from a surface are in question. If one supposed a case where W_a were just the difference between the work function of gold (4.5ev) and the electron affinity of CdS ($\approx$ 3.5ev), and that K, following the considerations of MacDonald [27], was about one fifth the bulk value*, λ may be calculated from equation 4.13 to be 14.5 angstroms. Thus, for the treatment of the observations here discussed, a corrected form of the potential is warranted. We have already conjectured that this corrected potential would act to cause a value larger than unity for the observed β. Because of a lack of more fundamental knowledge of the interface, however, further calculations using reference 26 appear too arbitrary to be useful.

The second possible cause for the large apparent cathode field stems from the fact that the planarity of the surface most certainly does not approach the magnitude calculated for x_m from equation 4.12. Thus, the concept of an image in a perfectly-

* The modification of K is necessary near to the surface since the relative permittivity measures the average electrical polarizability over all space. MacDonald's work was done with electrolyte-metal capacitance measurements and his deduction as to the size of K came from considerations of the implied width of the surface barrier. Therefore we use here only an analogy. His paper is quoted as evidence that K decreases near the interface. As a first consideration one might think the contrary: that the influence of the metal surface - where K becomes infinite, would be to increase, rather than to decrease the relative permittivity in the crystal.

conducting plane surface is not satisfactory. More probably the surface consists of small protuberances that act to increase the fields locally. This conclusion is strengthened by the observation of a similar effect in atomic film emitters for vacuum tubes. A theoretical analysis by Langmuir and Compton in 1930 (described by Parker [25]) of a specialized model was able to account on this basis for a higher observed variation of emission with voltage than is given by the simple theory for such emitters.

More currently, Spangenberg [21] states that the results of experimental tests of the Schottky effect on a large number of vacuum cathodes have indicated high slopes for $\log I$ versus $V^{1/2}$ than that predicted by the simple image-force theory which regards the cathode field as equal to V/L.

It would not be instructive to attempt to contrive a specialized emission model to obtain β theoretically, since it would be a completely ad hoc theory. Conditions so close to the surface may be of such a complexity that there are simply too many alternatives.

4.5. Conclusions

The characteristic of the diodes under reverse bias as determined experimentally is an ohmic behavior until average fields of the order of 2×10^4 volts/cm are reached in the crystal. As voltage is increased from the value causing this average field strength, a sharp increase in current which varies

as $\exp \alpha V^{1/2}$ with α a constant, is noted. The observed behavior suggests strongly that Schottky emission is taking place from the gold film into the interior of the sample. As discussed in Section 4.2 there is some possibility of the breakdown being due to a tunneling effect but this requires the postulate of a large density of donor states near to the surface. Correspondence of measurements with theory for the Schottky-emission hypothesis demands that the ratio β of the actual field near the blocking contact to the average applied field be of the order of one hundred. Various physical grounds do exist which tend to justify such a value for β.

Current varying as $\exp \alpha V^{1/2}$ was observed in all five thin platelet diodes tested for this effect. Three of these failed under continued high voltage excitation in the range of an average field of 5×10^4 volts/cm. In failing, the units suddenly assumed a higher apparent conductivity which persisted at all voltages and for either polarity of voltage. Unfortunately, the thicknesses of these crystals were only known via the relatively inaccurate micrometer measurements, described in Chapter 3, making a rigorous test of the constancy of β in equation 4.9 impossible. For the two remaining diodes, the value of β was within 30% of the β obtained for diode 13-5, when calculated from the measured slope of the curve corresponding to figure 4.2, through equation 2.9.

A recent paper by Williams [28] reported experiments on the effects of high fields on CdS as imposed at an electrolyte-

CdS interface. Williams observed a breakdown field which resulted in a short-circuit type of failure for his samples. The breakdown field for seven samples averaged 2×10^6 volts/cm. This value corresponds closely to the cathode field of 4×10^6 volts/cm deduced in Section 4.2. Three diodes, as noted above, failed in the same manner as did Williams' samples under average fields about 0.01 times this value. This correspondence is further evidence of the apparent high fields deduced to exist near to the cathode. The most likely source of the breakdown, according to Williams, is electron tunneling from valence to conduction band.

CHAPTER V

CdS Diode Equilibrium Current-Voltage Characteristic: II. Gold Contact Positive

In this chapter we shall complete the discussion of the equilibrium current-voltage characteristics for the CdS diodes. In Chapter IV, we considered the diode behavior both under high reverse bias and under low biases in the forward and reverse direction, corresponding respectively to Regions I and II in figure 4.1. The portion of the characteristic still to be investigated is that which we have labelled Region III in figure 4.1. We shall see that this region, which is confined to positive applied voltages for the gold contact, harbors a rich variety of behavior both in apparently similar diodes and in a single diode under slight parameter variations. The lower boundary for Region III is set by a departure from ohmic behavior. Both this point and the nature of the characteristic for diode 13-5 in Region III become more evident when the data of figure 4.1 are replotted onto logarithmic scales, as is done in figure 5.1. In figure 5.1, it is revealed plainly that the characteristic for diode 13-5 goes from a proportional behavior (45° slope) at low voltages to a square law behavior (26.6° slope) at higher voltages. As can be seen, the data fit of measured points for diode 13-5 is extremely good to both of these lines. From the theory, developed in Chapter 1, this is the simplest characteristic which can be observed under space-charge-limited current-flow conditions. The theory of space-charge-limited injection will

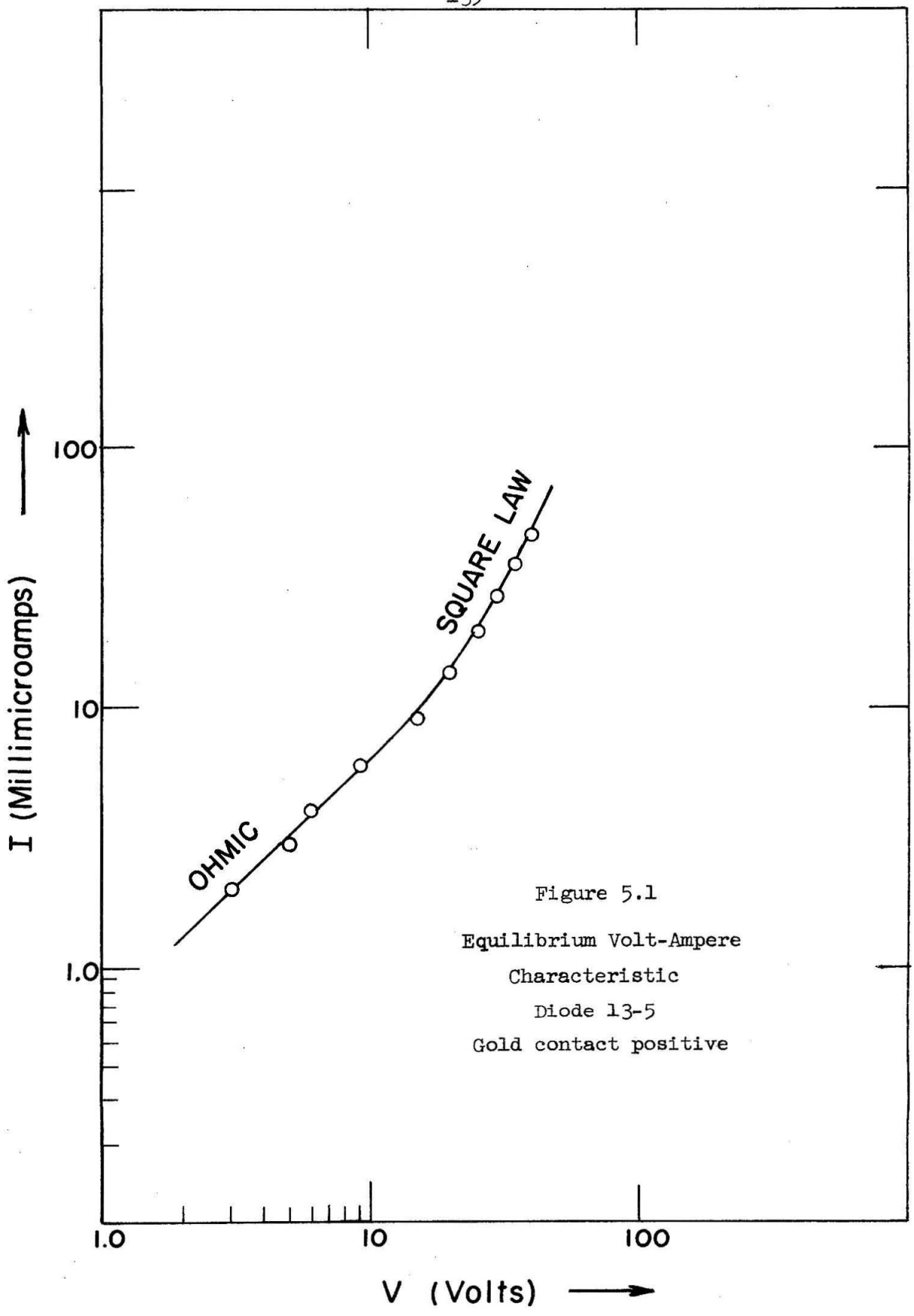

Figure 5.1

Equilibrium Volt-Ampere Characteristic

Diode 13-5

Gold contact positive

be applied in this chapter to the characteristics shown by diode 13-5, and to the characteristics measured for another diode whose behavior was more complex. The fit between theory and experiment, as we shall find, is good. In order to orient our thinking we shall begin the chapter with a résumé of the properties of space-charge-limited currents. This résumé, the topic of Section 5.1, will emphasize the physical processes which are operative and therefore will act as a supplement to the quantitative theory of Chapter 1. Succeeding sections will present and interpret experimental results obtained on the diodes.

5.1. Space-Charge-Limited Current in Solids: Qualitative Discussion

The evidence from figure 5.1 is that indium is capable of acting as an electron injector into CdS. At low voltages there are essentially only the carriers normally present in the material conduction band, and an Ohm's law behavior results. At higher voltages, electron injection from the indium begins to occur to an appreciable degree, and the interior assumes a net negative charge. The amount of charge injected is governed by a simultaneous solution of Poisson's equation and an equation expressing the rate of charge transport across the crystal, subject to the applied voltage as a boundary condition.

The possibility of sufficient space charge being injected into insulators to lead to a space-charge-limited flow condition

was first suggested and analyzed by Mott and Gurney [14]. The authors applied an analogous attack to that used to deduce Child's law for space-charge-limited currents in vacuum. The differing dependence of the motion of the charge carriers through the field ($v = \mu E$ in a solid; $v = (2eV/m)^{1/2}$ for a vacuum) leads to a square-law dependence for current on voltage in the crystal case, instead of the 3/2 power law of the vacuum case. If perfect crystals were available, so that an insulator could be characterized as having electronic energy states permitted only in the various bands, the solution of Mott and Gurney would be applicable. Their solution:

$$J = \frac{9K\epsilon_0\mu V^2}{8L^3} \tag{5.1}$$

is approached in the behavior of actual crystals only when the free charge in the conduction band becomes the significant component of the total charge injected into the solid. Equation 5.1 was derived in Section 1.3.

Actual crystals are not devoid of permitted states in the so-called forbidden band. In fact, the large band-gap materials such as CdS, into which one could expect to inject significant charge, are characterized by an appreciable density of forbidden gap states. The relative importance of these states is naturally enhanced by a decreasing density of free electrons. States in

the forbidden gap, which provide energy levels that immobilize injected charge, act to modify significantly the dependence of current on voltage from the form of equation 5.1. Those gap states which are in thermal equilibrium with the conduction band, and which are filled and emptied through the conduction band, are called electron trapping states. The bulk of the injected charge will be found, in most cases, to reside in these trapping states. By postulating the energy configuration of the trapping states, it is possible to deduce the expected dependence of current upon voltage under space-charge-limited conditions. A mathematical analysis for the trapping-level configurations pertinent to the diodes studied was given in Chapter 1. The discussion in that chapter also outlined the procedure to follow in deducing the effects of any type of trapping configuration on space-charge-limited current flow. The theoretical treatment of Chapter 1 showed that it is possible to obtain volt-ampere characteristics, in crystals susceptible to space charge injection, ranging from linear to an exponential dependence. The behavior of a given crystal will be specified by its trapping configuration with energy and the position of the Fermi level relative to that trapping configuration.

The governing condition for the type of volt-ampere behavior observed under space-charge-limited conditions is the statistical relationship between free and trapped charge. Since only the free charge contributes to the observed current, while the total charge is made up of free plus trapped charge, their

inter-relationship has a direct bearing on the volt-ampere characteristic obtained.

The simplest case for a crystal with traps is that in which there is a voltage-independent proportionality between the free and trapped charge. This occurs when the Fermi level is sufficiently below the trapping levels in the band gap so that Maxwell-Boltzman statistics apply. Under these conditions, the trap-free current (given by equation 5.1), is reduced by a factor equal to the ratio of free to trapped charge. When Fermi-Dirac statistics must be used for the free and trapped charge populations, the ratio of n to n_t becomes a function of voltage and higher power than square-law currents result.

Because of the rapid variation of the Fermi-Dirac distribution function in the region of the Fermi level, the bulk of the traps for a discrete-energy trapping level are filled when Maxwell-Boltzman statistics are not applicable. This leads to a high power law between voltage and current near to that voltage which fills all traps. A physical insight into the reason for this behavior comes from the realization that the position of the Fermi level interior to the crystal should be of no consequence with regard to the injection of electrons from the cathode. That is, the number of electrons injected for each increment of voltage should undergo no sharp discontinuity as the Fermi level begins to approach the trapping level. When the Fermi level is below the trapping level, almost all injected electrons are trapped; when the Fermi level is above the trapping

level, almost all injected electrons are free. Since the neutral crystal usually contains enormously more trapping states than free electrons we can see that as the trapping level is traversed by the Fermi level, there will be a sharp increase in current.

If a crystal is characterized by trapping densities distributed over a range of energies, then a power-law higher than of order 2 will be observed for the volt-ampere characteristic while the Fermi level is within this range. An exponential behavior results in the special case of a continuous constant density.

One would expect that all these characteristics would lead to less current at a given voltage than that predicted for the simple trap-free crystal. This is true because all of the space charge is mobile in the trap-free case but only a portion of it is free to move in the actual crystal. Figure 1.6 illustrated the possible behavior of a crystal containing a variety of trapping levels, as discussed in this section and analyzed in Chapter 1. Figure 1.6 makes it graphically evident that, at a given voltage, the largest currents are drawn in a crystal which is free of traps.

5.2. Complications in Measurements

In the early course of the experimental work for this investigation, especially with units such as will be described in Section 5.5, certain "hysteresis" phenomena were noted. Diodes

would apparently change their characteristics under low-frequency a-c operation after roughly five minutes of what appeared to be an equilibrium condition. This behavior, which has been noted by other investigators, has its explanation in the discussion of Section 5.1. In the case of low-frequency a-c measurements, there is a slow build-up of interior charge by the signal through charge injection into traps from the contacts. These traps discharge slowly, and the net result is a general straightening of any diode non-linearity. That is, the traps act to keep the conduction band charge more nearly constant, and therefore to make the crystal more like a resistor. The slow discharge from traps is evident also in d-c measurements if data are taken for a volt-ampere characteristic by lowering the voltage from some high value at which an equilibrium current has been established. Unless sufficient time is allotted for equilibrium at each of the lower voltages, an ohmic characteristic is likely to be measured. For a typical chlorine-copper doped diode, a sufficient time is about two and one-half days per point (in the dark). These observations concur with the findings of R. W. Smith* at RCA.

This persistence of a non-equilibrium condition, when coupled with the extremely variable behavior of space-charge-limited currents noted in Section 5.1, can cause not only inconsistent current-voltage points, but even an inconsistent current-voltage relationship between data taken at different times. This arises because one crystal may contain trap configurations

* Personal communication. See also Ruppel and Smith [29]

of varying types spaced at intervals throughout the energy band gap. If all these groups of levels are in thermal equilibrium with the conduction band, the Fermi-Dirac distribution function acts to enhance the importance of those trapping states near to the Fermi level relative to the others. Since the time to reach an equilibrium is often very long, the position of this Fermi level may depend on prior excitation of the diode. Thus, there is the possibility of a given crystal showing a variety of differing space-charge-limited characteristics, dependent upon its history. This was encountered in some of the investigations performed, before it was realized that times as long as fifty hours are sometimes needed for an equilibrium situation to be achieved.

5.3. General Observations on the Diodes Studied

Measurements, which may be interpreted in terms of the theory of space-charge-limited currents were obtained for all five of the small thin-platelet diodes studied. Three of these had no intentional impurities, while two had been doped with chlorine followed by copper as described in Section 3.4. The equilibrium characteristic observed most often under space-charge-limited conditions was a proportionality between current and the square of the applied voltage. In all cases, however, the current observed was less than that given by equation 5.1.

From the discussion of Section 5.1, and the more complete mathematical analysis presented in Chapter 1, this behavior indicates that usually the position of the Fermi level throughout the excitation was in a trap-free zone in the band gap and sufficiently below the trapping levels that Maxwell-Boltzman statistics were applicable.

To bring out the salient features of the observations in the remainder of this chapter, we shall discuss at length the results for two small platelet diodes (13-5 and 13-4), the former for which the gold-film-negative behavior has already been discussed, and the latter for which an apparent distribution of traps in energy was observed. Diode 13-5 was made from a pure crystal of CdS, while diode 13-4 was doped both with chlorine and copper. Experimental measurements will be interpreted in terms of the mathematical treatment given in Chapter 1.

In the experimental work, most of the current measurements were at very low levels, especially for diode 13-4. As seen in its characteristic (figure 5.3), currents in the picoampere range resulted for applied voltages below about 0.2 volts. Since the measurements of figure 5.3 were at the lowest level, their accuracy is the most critical. The precision of the measurements presented in figure 5.3 is nonetheless believed to be very good, since all readings were recorded on a Varian oscillograph until an equilibrium

condition was clearly indicated. The ammeter used was a Hewlett Packard 425A, which has current ranges from 10×10^{-12} amperes to 3×10^{-3} amperes. This instrument was checked and found accurate down to the nanoampere region by a Multiflex galvonometer which had a sensitivity limited to 4×10^{-9} amperes. Owing to the long measuring times and the shielding of leads, dark measurements were felt to be accurate to within 2×10^{-12} amperes, a precision which makes significant measuring error possible in only the lowest point on figure 5.4 (3×10^{-12} amperes). Voltage readings were not nearly as critical since they were not required below 0.1 volt. They were taken on a Kintel voltmeter.

5.4. Characteristic for Diode 13-5

The square-law current-voltage characteristic observed at high voltages for diode 13-5 implies, from Chapter 1, that the trapping levels in the crystal are described by Maxwell-Boltzman statistics. The traps may exist either at a discrete energy or else be distributed energetically, but their energies are not closer than approximately $2kT$ to the Fermi level in the range of voltages studied. The discussion in this section will refer to the traps as if they existed at a discrete energy which corresponds, if the traps are in reality energetically-distributed, to lumping them into an effective density at an effective energy level.

According to the analysis of Chapter 1, ohmic behavior in a crystal should give way to space-charge-limited behavior when the excess free-electron density at the collecting electrode (in this case, the gold electrode) approaches the dark density $\bar{n}$ of electrons in the crystal. The voltage at which this occurs is given by equation 1.20: $V_{os} = (8e\bar{n}L^2(1 + \theta))/(9\theta K\epsilon_0)$. If we use the dark electron density deduced in Chapter 4, $\bar{n} = 5.4 \times 10^6 cm^{-3}$, and assume a trap-free crystal*, we calculate from equation 1.20 that a transition to space-charge-limited currents should occur at $V_{os} = 2.37 \times 10^{-6}$ volts for diode 13-5. From figure 5.1, the observed value for V_{os} is 19 volts, so that it is clear that the crystal is not trap-free. Therefore, we may use equation 1.20 to calculate θ:

$$\theta = \frac{2.37 \times 10^{-6}}{19} = 1.25 \times 10^{-7}$$

We have an immediate check on this value, since θ can also be computed from the measured current after the inception of square-law behavior through equation 1.14. Thus:

$$\theta = \frac{8JL^3}{9K\epsilon_0\mu V^2}$$

---

* For the trap-free crystal, θ approaches infinity in equation 1.20.

Using the measured point, V = 30 volts, I = 27na, from figure 5.1 in this equation together with the diode area from Table 3.1, we obtain

$$\theta = 1.19 \times 10^{-7}$$

These two values for θ are in remarkable agreement. A "best" value for θ would probably be an average between the two, or $\theta = 1.22 \times 10^{-7}$. We may also calculate the average trap density in the region of the square-law currents. From equations 1.8, 1.17 and 1.18, we have:

$$\underline{n}_t = \frac{3K\epsilon_0 V}{2eL^2} \qquad (5.2)$$

where $\underline{n}_t$ denotes the average trap density, as in Chapter 1. Hence, in the region of the transition to square-law currents for diode 13-5, $\underline{n}_t \approx 10^{14} cm^{-3}$. If these are deep traps, such that their occupancy probability is high, this number is a good estimate of the actual trap density. However, if these are relatively shallow traps which are not filled with high probability, then we cannot yet draw a conclusion as to the actual trap density. Nonetheless, we can derive an inequality pertaining to the trap density. This is possible because data was accumulated for voltages as high as 40 volts applied to the diode, without observation of the steep rise in current which is characteristic

of passage of the Fermi level through the trapping energy. As we saw in Section 1.4, filling of discrete energy traps should cause a noticeable deviation from square-law behavior in the vicinity of $V = (1/8)V_{TFL}$, with $V_{TFL} = eL^2N_t/2K\epsilon_0$ as derived in equation 1.22. Since square-law currents are observed for applied voltages up to at least 40 volts for diode 13-5, we may expect that $V_{TFL} > 320$ volts for this diode. If we express this inequality in terms of N_t through equation 1.22, we may write:

$$N_t > \frac{2K\epsilon_0(320)}{eL^2}$$

Putting numbers into this equation, we obtain $N_t > 1.9 \times 10^{15} cm^{-3}$ for diode 13-5. Having established this inequality, we are in a position to calculate the maximum depth of the discrete trapping level. To do this, we note that the postulate of thermal equilibrium between conduction band and trapping level, coupled with the comparatively low energy of the Fermi level, allows us to write a Boltzman factor for the statistical weighting of the filled states at the conduction-band and trapping levels. From the Boltzman factor, we have:

$$W_C - W_T = kT\ln\left[\frac{n_t N_c}{N_t n}\right] \qquad (5.3)$$

A minimum value for N_t, when inserted into equation 5.3, will yield a maximum value for the trap depth $(W_C - W_T)$. The ratio n/n_t has been defined in equation 1.8 as θ. Therefore, we have:

$$W_C - W_T < kT\ln\left[\frac{N_c}{\theta N_t'}\right]$$

with N_t' representing the minimum value determined for N_t. Hence, for diode 13-5, we calculate: $W_C - W_T < 0.56$ev. This inequality does not stipulate a very shallow trapping level. We shall see in Chapter 6, however, that the depth of the discrete level in diode 13-5 is appreciably less than this limiting value.

The current-voltage characteristic for diode 13-5 was found to be linear even under low-intensity illumination conditions. From the data of figure 4.1, it is evident that if $\bar{n}$ were increased only by as much as a factor of two from its dark value through illumination, V_{os} would be increased to 38 volts and ohmic behavior would prevail over the range of voltage studied. The observed conductivity increase at low illumination indicated roughly a factor of ten increase in $\bar{n}$, so that the measured ohmic behavior is expected.

5.5. Characteristic for Diode 13-4

Quite a different behavior from what was observed for diode 13-5 resulted when a positive bias was applied to the

gold terminal for diode 13-4. This sample was also more light-sensitive than was diode 13-5. As discussed in Section 5.3, extreme care was necessary to obtain reproducible measurements for this diode. The dark characteristics were taken from what appeared to be equilibrium conditions (five hours of the same reading) although this necessitated oscillograph records as long as fifty hours, especially at the lower voltages. The resultant dark volt-ampere characteristic is presented in figure 5.2, along with some measurements taken in the light which will be discussed presently.

In contrast to the behavior of diode 13-5, we note in figure 5.2 that there is apparently no region in which diode 13-4 behaves ohmically under forward bias. The dark characteristic consists of a region in which the current is proportional to voltage raised to the power 4.7, followed by a square-law region at voltages above $V \approx 4.6$ volts. The square-law behavior may be attributed to the same phenomenon noted in Section 5.4 in explaining the characteristic for diode 13-5. The measured currents correspond to a θ value, as calculated from equation 1.14, of 1.6×10^{-5}.

Readings were attempted above $V = 12$ volts in the dark to add to the data on the square-law behavior, but these resulted in erratic current pulses superimposed on a projected square-law value. These pulses lasted for variable lengths of time and greatly exceeded the square-law value. This apparent breakdown

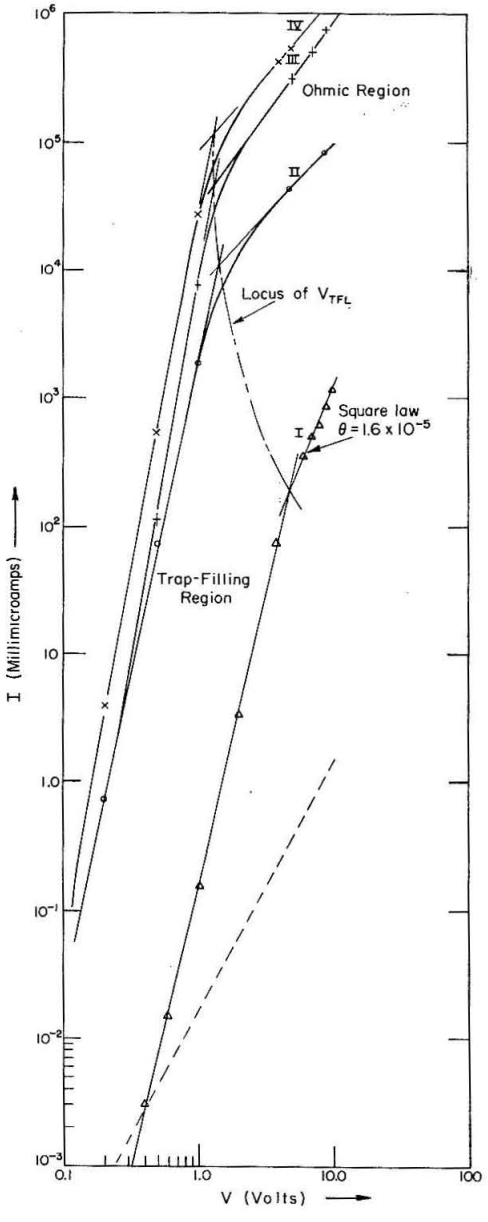

Figure 5.2

Equilibrium volt-ampere characteristic for diode 13-4 at various levels of illumination with the gold contact positive. Curve I - dark; Curve II - illumination ≈ 2 candles/ft^2; Curve III - illumination ≈ 8 candles/ft^2; Curve IV - illumination ≈ 20 candles/ft^2. The power law in the trap-filling region is $J \approx \alpha V^{4.7}$. The dashed line represents the lower square-law region implied by the data if the trapping level being filled is discrete ($\theta = 6.0 \times 10^{-8}$, Section 5.5).

occurs at an average field strength of approximately 10^4 volts per cm. It was not studied further, because it was felt that it might be destructive to the sample.

The high power dependence of current in the low voltage range is suggestive of a case in which trap-filling is taking place. The energy configuration of the level or levels being filled, however, is uncertain at this point. It is possible that the high power law results either from a discrete-energy trapping state, or a density of states distributed in energy.

If the characteristic were the result of filling a discrete-energy trapping level then, since less than trap-free currents are measured in the eventual square-law region, the level is below shallower traps and the analysis of Section 1.5 would apply. In Section 1.5, we derived an approximate equation (equation 1.39) for the exponent of the voltage in the voltage range which connects the two square-law regions that stem from the discrete levels. From equation 1.39 and the observed 4.7 power law we have:

$$2 + \log \theta_2/\theta_1 = 4.7$$

with θ_2 the ratio of free to trapped charge in the shallower level and θ_1 its counterpart for the deeper level. Hence $\theta_1 = \theta_2/845$ or, using the value $\theta_2 = 1.6 \times 10^{-5}$ just determined: $\theta_1 = 6.05 \times 10^{-8}$. The characteristic corresponding to this θ_1

value is shown dashed in figure 5.2. It was not possible to take data at a sufficiently low current level to ascertain directly whether or not the diode followed this variation. Because of the extreme linearity of the high-power-law characteristic on the log-log plot of figure 5.2, one might expect that, as an alternative to the explanation just given, the traps being filled are continuous in energy.* The exponent on V would then imply a density that varied exponentially with energy. Mathematical analysis of such a case has been carried out in Section 1.6 and will be applied to the present case more fully in Section 5.7. Briefly, this type of trapping configuration with energy results in a characteristic $J = \alpha V^m$, where $m = ((T_c/T) + 1)$, T_c is a "temperature" characteristic of the trap distribution and greater than T, and α is a constant. It is tempting to check for the applicability of this equation directly through temperature variation, but the environmental range necessary for an unequivocal test would damage the diodes. A rigorous differentiation between these possibilities may be achieved, however, through observation of the trap-filling characteristic under illuminated conditions.

Accordingly, three more sets of volt-ampere data were taken for this diode, under illuminated conditions. The data

* The power law for a discrete level was an approximation and one would expect the measured points to deviate somewhat from it, especially near the join point to the square-law characteristic. A more complete discussion of this topic was given in Section 1.4.

obtained are also plotted in figure 5.2. The first set was taken at a very low light intensity (approximately 2 candles/ ft^2) while the other two were taken at factors of illumination four and ten times this amount respectively. The evident difference in the lighted and dark curves is the marked increase in current at a given voltage. This increase amounted to approximately a factor of 10^4 at the lowest illumination and increased from this factor. What is not evident in the figures is the enormous decrease in the time necessary to reach an equilibrium for the points on the curve. Whereas dark values were not in equilibrium until times of the order of tens of hours, even the lowest level of illumination produced an equilibrium situation within a few minutes. The lighted curves, while duplicating the low-voltage, 4.7-power relationship for current as a function of voltage, show ohmic behavior in the higher ranges. We note also that the voltage at which the characteristic departs from the high power law decreases with illumination; although the variation is clearly not uniform.

These observations, especially the large current increase under trap-filling conditions, cannot result from the effects of a discrete energy trapping level. The 10^4 factor increase in current demands a corresponding shift in the Fermi level. Since the characteristic behavior stays the same after this shift, trap-filling must still be taking place under illuminated conditions. A single level would be almost insensitive to light in its current-voltage behavior as long as the Fermi

level were in the vicinity of the trapping level. For discrete-level trapping, all of the photo-excited electrons would pour into the traps without significantly raising the Fermi level - hence without increasing the conduction-band concentration. This will be discussed further in the theoretical analysis of Section 5.6.

5.6. Theoretical Explanation of the Observations on Diode 13-4

The measured results described in Section 5.5 are consistent with a model based upon the theoretical framework for photoconductor behavior proposed by Rose [30]. The observations suggest a band-gap structure for the CdS as sketched in figure 5.3a. The gap states are of three types: shallow traps, which may be distributed in energy or else exist at a discrete level; traps which are distributed in energy in roughly exponential fashion; and finally, states that have been called "primary centers" by Rose. The primary centers are electron states, low-lying in energy, through which almost all recombination takes place; that is, by far the most likely mechanism for the recombination of an electron-hole pair is the annihilation of a trapped hole in a primary center by a conduction-band electron. The specific structure of the primary centers is not indicated since it is still a matter of conjecture; hence, they are indicated only by cross-hatch in figure 5.3. For this same reason, the shallow-trap structure is also indicated by cross-hatching.

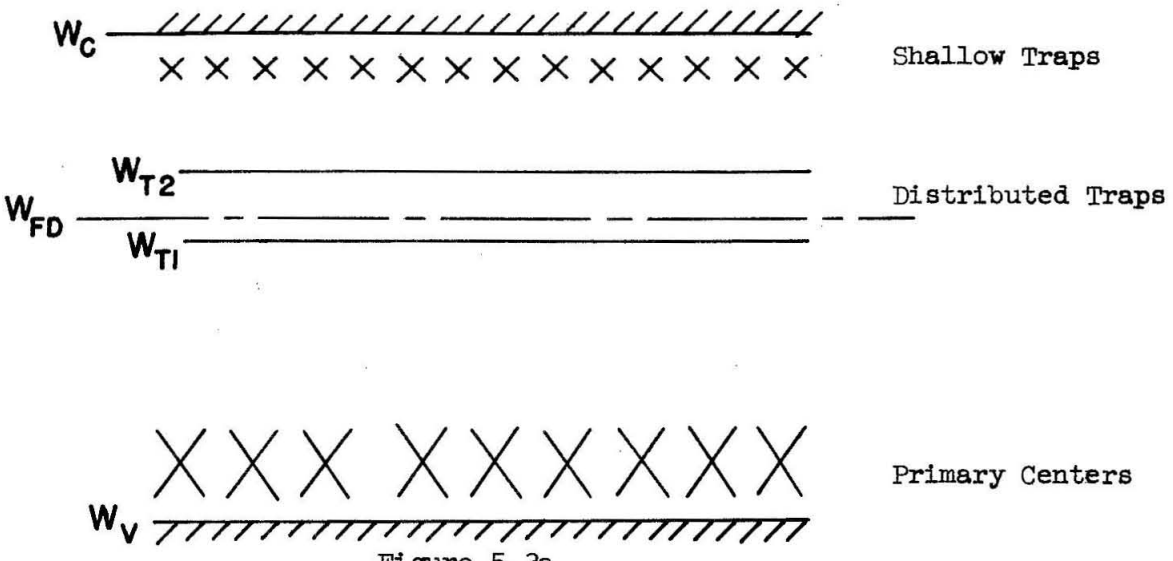

Figure 5.3a

Crystal band-structure proposed to explain the observed current-voltage characteristic for diode 13-4. The symbol W_{FD} indicates the dark position of the Fermi level.

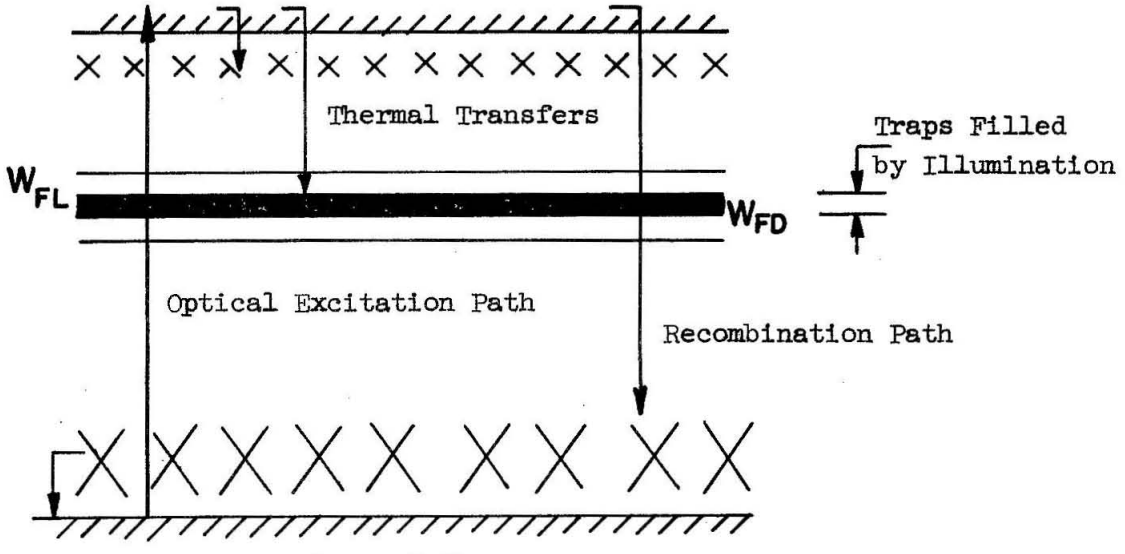

Figure 5.3b

Interpretation of the effect of illumination on the populations of the various gap states.

Under dark conditions with no applied voltage, there is thermal equilibrium between all states in the crystal and a single Fermi level (labeled W_{FD} in figure 5.3a) describes the state populations. The Fermi level can be expected to lie either within the trapping density or else on its lower edge from the evidence of high-power-law currents in the dark at very low applied voltages (figure 5.2). Visible-spectrum illumination, which matches roughly the band gap of CdS (2.4ev) creates hole-electron pairs in the material. Almost all the holes are trapped immediately* by primary centers with which the free holes are in thermal equilibrium. Electrons in the conduction band come to a thermal equilibrium with the shallow traps. Thus, when illuminated, the crystal may be described by two quasi-Fermi levels situated in the vicinity of the conduction and valence bands. The description of the use of the two Fermi levels and the requirements for their validity are described extensively by Bube [1, Chap. 3]. According to Bube, the Fermi level for electrons W_{Fn} is defined by the equation $W_{Fn} = W_C - kT\ln(N_c/n)$, with a similar relationship holding for the Fermi level for holes W_{Fp}. Since, experimentally, the free holes are insignificant under lighted or dark conditions, we shall not be interested in W_{Fp} and,

* Speculation as to why this is true has not led to conclusive results as yet. Experimentally, no-one has reported accurate measurements of free-hole lifetimes in CdS to date, although Rose [30] speculates on an estimated τ_p of approximately 10^{-10} seconds. One reason for this result, suggested by some researchers, is that the valence band in CdS is at such a low energy that an atomistic model, in which all electrons are effectively trapped, is more applicable than the band model for the valence states in the material.

therefore, shall refer to W_{Fn} simply as W_F in further discussion. In figure 5.3, $W_{Fn} = W_F$ is sketched under both dark and illuminated conditions and labelled W_{FD} and W_{FL} for these respective situations. These symbols will be used to facilitate the discussion of the effects of illumination.

When the crystal is illuminated, the relative populations of the primary centers and of the conduction band are not in thermal equilibrium. Recombination traffic flowing from the conduction band through the primary centers balances the effective flow of electrons from these centers due to the illumination. The population of the primary centers is thus a function of the recombination parameters describing them, and of the intensity and frequency of the illumination.

The net effect of the light, therefore, is to raise the Fermi level in the crystal and to fill the traps existing between the old and new Fermi levels with electrons that had been in the primary centers (figure 5.3b). The crystal is still electrically neutral, however, since the net charge has not been increased, but only redistributed energetically. It is, of course, still subject to space-charge limitations for voltage-injected electrons. Since the traps existing between the dark and the illuminated Fermi level are now filled, one would suspect that the voltage necessary to inject sufficient charge for trap-filling would decrease. This effect is noted in figure 5.2, where the variation indicates that the phenomenon is non-linear with illumination.

A complete explanation of the shortening of the observed decay times demands a rather lengthy exposition of the role of the various band states as a function of the separation of the hole and electron Fermi levels through photo-excitation. This treatment is given in its entirety by Rose [31], together with much experimental verification. The essential points in the argument may be recounted as follows. The long decay time for photoconductivity results from the fact that an equilibrium condition is arrived at only after all the electrons are in the states prescribed by the Fermi-Dirac distribution function. The transition probabilities are such that essentially all electrons captured by states above the Fermi level must return to the conduction band before going to any other state. An individual electron's journey through the various gap states is terminated effectively only when it is captured by states below a demarcation level. In most practical instances this demarcation level is very close to the steady-state Fermi level. Hence, a given electron may be trapped and freed many times before the conduction-band population finally assumes an equilibrium condition. The time to reach an equilibrium will thus be a large factor greater than the lifetime of a free electron, which measures only the time spent in the conduction band. The net result of a complete analysis of this process is that the actual decay time is greater than the free-carrier lifetime roughly by the ratio of filled, shallow traps (i.e. traps above the steady-state Fermi level) to free electrons. In the case

of diode 13-4, current measurements show that n_t/n changes by a factor of about 10^4 between lighted and darkened conditions, which accounts for the response time variation from tens of hours to tens of seconds.

The ohmic behavior in the illuminated condition after the continuous density of trapping states is filled results from the relatively large population of electrons in the conduction band. From the dark characteristic we know that the Fermi level moves from the traps distributed continuously in energy to a region of the gap that is devoid of traps. Above the void region there is still a higher-energy trap density, the population for which is described by Maxwell-Boltzman statistics. This is the case discussed in Section 1.3 in which we found that space-charge-limited currents supersede ohmic currents only provided the voltage is greater than the value $V_{os} = (8e\bar{n}L^2)/(9\Theta K\epsilon_0)$, as given by equation 1.20. The transition to space-charge-limited flow at V_{os} occurs, roughly, when the anode free-charge density has been increased by a factor of two due to charge injection. As we see, V_{os} is a direct function of $\bar{n}$, the no-injection conduction band density. This density is increased by the illumination to such an extent that the crystal is in an ohmic condition after the continuous distribution of traps is filled, and hence proportional, rather than square-law, currents are observed. Square-law currents would be observed under illuminated conditions,

as they are in the dark, if the voltage were increased above the intersection of the dark characteristic and the ohmic curves in figure 5.2.

5.7. Quantitative Analysis of the Observations on Diode 13-4

In this section the theory developed in Section 5.6 and in Chapter 1 will be used to analyze quantitatively the properties of diode 13-4.

First, we have from equation 1.60 and the text of Section 1.6 the fact that the volt-ampere characteristic for the case where the Fermi level is in an energy region of exponentially increasing traps is a proportionality between J and V^m. The exponent m equals $(T_c/T) + 1$, where T_c is a characteristic temperature for the trap density, defined through equation 1.50. From the observed exponent for V of 4.7, we deduce that $T_c = 11{,}100^{\circ}K$ which is larger than T - a condition making valid most of the equations of Section 1.6.2.

From figure 5.2 we can deduce the depth of W_{TU}, the upper limit of the continuous trap density. To do this we note that W_F passes W_{TU} when the dark characteristic changes from 4.7-law behavior to square-law behavior. From the current observed at this point on figure 5.2, we calculate n_a from $n_a = (2JL)/(3e\mu V)$, a form derived from the insertion of equation 1.16 into equation 1.3. Having n_a, we can solve equation 1.24 for $(W_C - W_F)$ to calculate the trap depth from $(W_C - W_F) = kT\ln$

(N_c/n), since now $W_F \approx W_{TU}$ as we have noted. This procedure yields $(W_C - W_{TU}) = 0.567$ev.

Using substantially the same method with the indicated conduction-band density at the lowest voltage studied (before any appreciable injection could take place), we deduce the dark Fermi level to be approximately 0.830ev below the conduction band for diode 13-4.

The number of traps filled by excitation from primary centers is calculable by noting that the apparent trap-filling voltage decreases from 4.7 volts to 1.4 volts under low-level illumination. Using equation 1.22 $(V_{TFL} = eL^2N_t/2K\epsilon_0)$, we see that this 3.3 volt difference implies that the traps filled by light equal $2.09 \times 10^{13} cm^{-3}$. As the level of illumination is increased, the efficiency of trap-filling by this means lessens, as evidenced by the much decreased rate of change of V_{TFL} with light. At a factor of ten times the low-level illumination, the apparent number of traps filled by the light is 2.15×10^{13} per cm^3.

The difference in the Fermi levels under light and dark conditions is given directly by kT times the ratio of illuminated diode current to dark diode current, since:

$$\frac{I_{illuminated}}{I_{dark}} = \frac{n_{illuminated}}{n_{dark}} = \exp[(W_{FL} - W_{FD})/kT]$$

where W_{FL} and W_{FD} represent the illuminated and dark Fermi-level energies, respectively. This current ratio is a factor of 10^4, indicating that $(W_{FL} - W_{FD})$ equals 0.234ev. Since we already have deduced the upper level of the trap density to be 0.567ev below the conduction band and the dark Fermi level to be 0.830ev below the band, the action of the light evidently puts the Fermi level within 0.019ev (or about kT) of the end of the continuous trap density. Contained in this span of energy are about 0.9×10^{13} states per cm^3, calculable from the necessary voltage-injected charge to fill the traps.

The dark-characteristic square law at higher voltages with a θ value of 1.6×10^{-5} calculated in Section 5.5 is indicative of a shallow trapping level as described in Section 1.3. The depth is unknown except for limits which could be set, as were done in the case of diode 13-5 in Section 5.4. Since this procedure was demonstrated in that case it will not be illustrated here. The deductions as to the band-gap states made in this section are collected for clarity and reference in figure 5.4.

5.8. Summary of Trapping Properties Derived from Space-Charge-Limited Current Observations

The complete analyses of the volt-ampere behavior of diodes 13-5 and 13-4 in Sections 5.4 and 5.7 respectively, both give evidence for a density of shallow trapping states. The θ

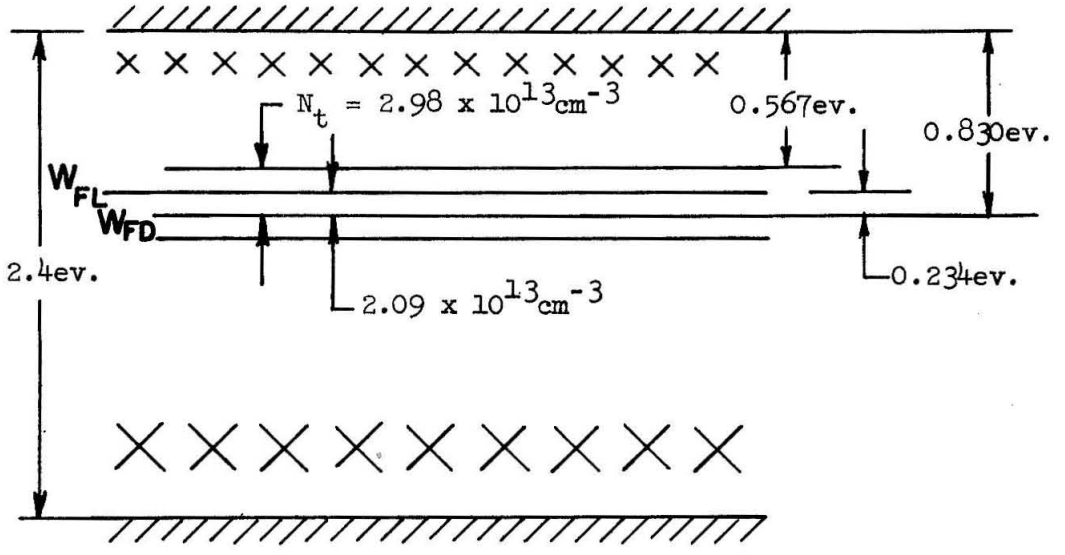

Figure 5.4

Calculated electronic trapping levels and densities for diode 13-4.

implied for the states, however, differs by a factor of 100, being smaller in the chlorine-copper doped sample (diode 13-4). In the case of the pure sample (diode 13-5) fair correspondence was obtained with two other crystals so that there is reasonable certainty as to the value for θ. There is certainly a large margin for error in the determination of θ, considering the uncertainty in such quantities as length of sample and electron mobility, but a factor of 100 is felt to be indicative of a physical difference in the level detected.

What one would like to do, of course, is to determine the physical origin of this trapping level (or "of these levels," dependent on the configuration). To do this demands a great deal of research with a variety of differing samples, only a small amount of which has yet been done. Bube [1, p. 299] gives an account of the meager information thus far available in this field. The shallow levels, appearing consistently in the pure and chlorine-copper doped samples, point to some imperfection inherent in the CdS lattice structure. We have concluded that there are more than $10^{15} cm^{-3}$ shallow traps in the case of the pure sample, but this is still only one in 10^{7} lattice sites which is not a very large density. A lattice-imperfection source for the trapping levels would make the observed variation in θ seem very reasonable, since the traps would be dependent on the techniques and procedures observed in crystal growing.

Diode failure, due to unknown causes as described in Section 5.5, did not permit increasing the voltage to the point where the trapping levels would be traversed by the Fermi level. This is a necessary condition for gaining information on the density and configuration of states from the observation of space-charge-limited currents. Further analysis of these particular levels would better proceed through study of such effects as photoconductive dependence on light intensity, as described in [17]. A search of the literature has revealed little quantitative data on the shallow levels, although their detection is mentioned by Wright [4] and by Ruppel and Smith [29]. Figure 1 in the latter reference, which is reproduced as figure 5.5 in this work, provides some interesting information on shallow levels in CdS but was not analyzed completely by the authors. Since it has a bearing on the results presented here, we shall calculate the crystal properties indicated. From figure 5.5, using the dimensions given in the text of [29] and in the caption for the curve, we calculate a θ due to the shallow traps of approximately 10^{-5}, which matches the value obtained on diode 13-4. As we see in figure 5.5, Ruppel and Smith were able to increase the voltage sufficiently to bring the Fermi level in the range of the shallow traps.* The behavior at these

* Trap-filling is more likely to precede breakdown in a thin sample than in a thicker one. Using equation 1.16 and equation 1.22, we may express the anode (maximum) field at the trap-filling voltage as: $E_a = -3V/2L = 3eN_tL/2K\epsilon_0$. Hence, the maximum field at the trap-filling voltage increases with the length of the sample for a given trap density. Ruppel and Smith's crystal was about 40% shorter than the crystals studied here, which may account for their results.

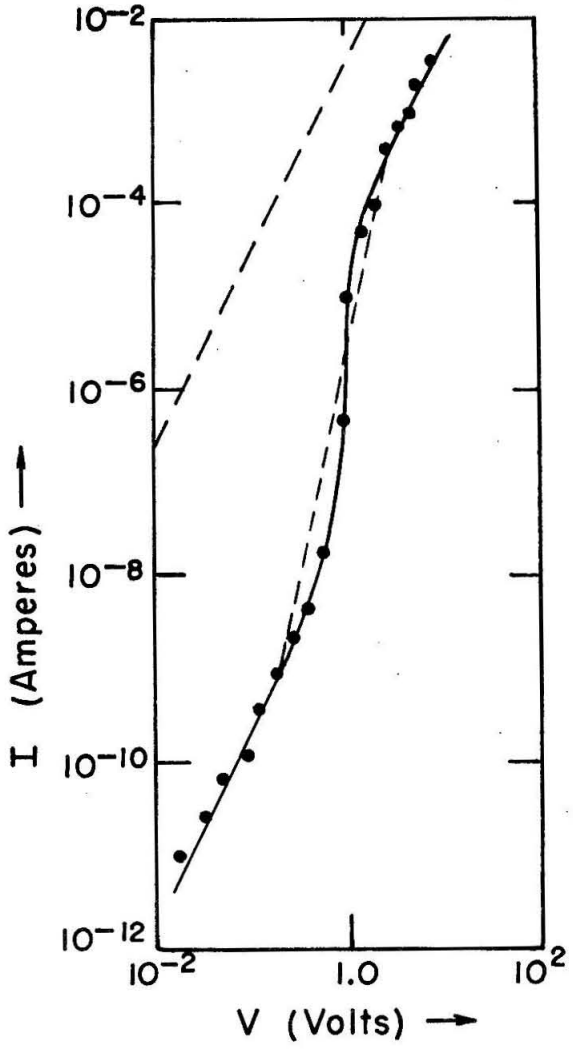

Figure 5.5

D-C characteristic under forward bias of a CdS analogue diode with indium cathode and tellurium anode. The dashed line above the characteristic represents the trap-free space-charge-limited behavior. The dotted line on the data points corresponds to equation 1.39 ($J = \alpha V^m$ with $m = 2 + \log \theta_2/\theta_1$), applied to this diode (contact area = $1mm^2$, thickness = 10μ).

..... reprinted, by permission, from Ruppel and Smith [12]

voltages indicates passage of the Fermi level through a discrete trapping level with even shallower traps above it. This case is the one considered in detail in Section 1.5. In figure 5.5, θ changes from 10^{-5} to 10^{-2} at either side of the trap-filling region. If, from the analysis of Section 1.4, V_{TFL1} (the trap-filling voltage for the lower level) is taken to occur roughly at the point of departure from the higher voltage square law, then the evident value for V_{TFL1} in figure 5.5 is about 2.5 volts. This would imply, again from the arguments of Section 1.4, that there should begin to be significant deviation from the low-voltage square law at $V \approx 0.3$ volts. The data of figure 5.5 is consistent with this prediction. The dotted line connecting the asymptotes at these two points represents the approximate trap-filling law as given in equation 1.39. This equation is seen to underestimate the maximum steepness of the line drawn through actual data points. Since the approximate law specifies a constant power for voltage over the trap-filling region, and we know that the power will increase as trap filling proceeds, this situation is expected.

The trap-filling behavior indicates a discrete trap density of about $2 \times 10^{13} cm^{-3}$ being filled. Using the analysis of Section 1.5 and equation 1.24 in the same manner as in previous calculations for a single level, we calculate that the trap depth is 0.570ev. Again no further information is available about the traps resulting in $\theta = 10^{-2}$ at the upper

end of the curve, since they are not filled in the characteristic shown.

The trap depth of 0.570ev just deduced fails by a small margin to be within the limit $((W_C - W_T) < 0.56ev)$ derived in Section 5.4 for the shallow trapping-states in diode 13-5. In Chapter 6, however, we shall be able to make an even more limiting inequality which will definitely exclude the same source being operative for the traps observed in this work and those in reference 29. The shallow traps we have observed are consistent in depth with traps deduced by Bube to be present in pure CdS crystals through study of the effect of temperature on photoconductivity [8]. Bube finds states in pure CdS at roughly 0.17 and 0.35ev below the band, which are present in concentrations from 10^{13} to $10^{16} cm^{-3}$, dependent on the crystal. In Section 5.4, N_t was shown to be greater than $2 \times 10^{15} cm^{-3}$. This density, coupled with the 0.56ev limit for the trap depth of the shallow levels, is consistent with the above deductions from reference 8.

Smith and Rose give evidence for a continuous density of traps at a range in energy [18] which matches closely the energy range of the energetically-continuous trapping levels, deduced from the data of diode 13-4. In reference 18, the continuous level was interpreted to be of approximately equal density extending from 0.55 to 0.80ev below the conduction band, almost exactly the same range as deduced in Section 5.7 (the

estimate there was 0.567 to 0.830ev). The crystals studied by Smith and Rose were also chlorine-copper doped, and of the same type as used in the experiments described here. From the marked linearity for the log-log plot of figure 5.2, the deduced exponential density variation with energy for the traps, in contrast to the continuous density proposed in [18], is fairly certain. The actual numbers do not imply as rapid a dependence as "exponential" might conjure up. The size of kT_c is approximately 0.1ev so that over the 0.263ev range of trapping-state energies, the density variation is about 10 to 1. Using crystals of the type of diode 13-4 on another occasion, Smith [17] detected deep traps but interpreted them in terms of a discrete density situated about 0.8ev below the conduction band. Comparing our results with these two references to the deep traps we find that the magnitude of the total trap density configuration is $3 \times 10^{13} cm^{-3}$ as deduced in this work, $5 \times 10^{13} cm^{-3}$ in reference 18 and $3 \times 10^{14} cm^{-3}$ in reference 17. In reference 18, a check on the value of N_t was made through photoconductive response time studies, a method felt by the author (Rose) to be less accurate than the analysis of space-charge-limited current behavior. The photoconductive study implied an N_t of $0.5 \times 10^{13} cm^{-3}$.

Since these energetically-distributed, deep levels are not detected in the undoped crystals, it is certainly reasonable to ascribe them to the added copper. The chlorine is not likely

to be responsible, since it is known to create very shallow states [16]. To check this, it would be informative to know the copper density independently. This would add to one's confidence in identifying the levels, but this information was not available.

5.9. Conclusions

As predicted in the introduction to this chapter, an extremely varied current-voltage behavior can be interpreted in terms of space-charge-limited current flow in a crystal with traps. Observations of such flow are a sensitive, experimental method for the determination of various crystal properties. Not only trapping densities, but also trap depths can be deduced in this fashion, provided sufficient charge injection takes place to move the Fermi level into the energy range in which the traps exist. The effects of the variation of illumination as well as of voltage have been shown to be consistent with the physical picture postulated for the over-all interior trap density. Correspondence with other methods of trap detection and identification, such as photoconductive studies, has been shown to be good. It has also been seen that significant trapping-state populations exist even in crystals assumed to be pure. Hence, currents of the magnitude given by equation 5.1 are not to be expected, unless crystals are made thin enough to reach a trap-filling voltage before a breakdown effect.

Complete identification of the source of the traps detected will demand a large body of experimental work with crystals of known imperfection types and densities. At present, only a few trapping levels in CdS, or in fact, in any other materials, are identified with reasonable certainty. For some trapping levels, such as those distributed continuously in energy (detected in diode 13-4), even the nature of the source is speculative. As Bube points out [1, p. 302], one could, for example, take the viewpoint that the energetically-distributed traps stem from small regions of short-range order which are interspersed throughout the crystal. The "conduction band" for these regions may act as trapping centers for the free electrons of the rest of the crystal, provided that these free electrons exist at higher energies. It is also possible, however, to explain these levels as an energetically near-continuum of states for a discrete trapping center. Neither alternative is yet excluded.

Measurements of the space-charge-limited current characteristics permit only the deduction of the static properties of traps. To determine the kinetic properties of traps, other methods, such as will be used in Chapter 6, are necessary.

CHAPTER VI

Capacitance Measurements on the Diodes

The variation of space-charge-limited currents investigated in Chapter 5 was interpreted in terms of the influence of trapping centers in the crystal. The space-charge-limited currents were long term equilibrium values which gave no information on the kinetics of trap filling and trap emptying. In this chapter, some knowledge of these properties will be sought. In addition, the measurements reported in this chapter will reinforce confidence in the model for crystal behavior we have proposed in Chapters 1 and 2 by providing direct evidence of trapping states distributed uniformly in space. Deductions of the trap concentrations and configurations in the analysis of space-charge-limited currents of Chapter 5 were all by inference from the comparison of observed behavior with the theory of Chapter 1. In this chapter, measurements will be reported on the terminal capacitance exhibited by the diodes. Since capacitance is directly related to stored charge, these measurements come closer to being a direct detection of the actual trapped charge than did those of the last chapter.

The capacitance measurements reported here will be found to be in close agreement with the analysis of Chapter 2. The deductions made from these measurements thus represent a new means of obtaining information about trapping kinetics.

6.1. Technique of Making Measurements

Measurements were made of the capacitance of the diodes both under controlled illumination and in the dark, at frequencies ranging from 16kc/s to 5mc/s. These limits were set by the pass band of the radio-frequency bridge available. Positive, negative and zero d-c bias conditions were used on the diodes to test the variation in capacitance produced by voltage. Capacitance values were read directly from a Wayne-Kerr radio-frequency bridge circuit, whose balancing output was connected to a fairly elaborate null-detection apparatus. A schematic diagram of the equipment is shown in figures 6.1a and 6.1b.

Below 50kc/s, the bridge null-detector output was fed into an amplifier which was connected to a Donner wave-analyzer tuned to the exciting frequency. The Donner analyzer consists of a very narrow (20cps) band pass filter followed by a high gain amplifier, rectifier and meter. This allows virtual exclusion of all noise, except that in the narrow range of frequencies surrounding the applied signal, and permits a very sensitive null detection. Above 50kc/s a superheterodyne radio receiver was used as the null detector. A convenient way to establish the null with the radio receiver was to display the modulated intermediate frequency from the receiver on an oscilloscope, and to balance the impedance bridge to a zero in the modulation. The signal from the bridge was coupled into the receiver through the external antenna jack on the superheterodyne receiver.

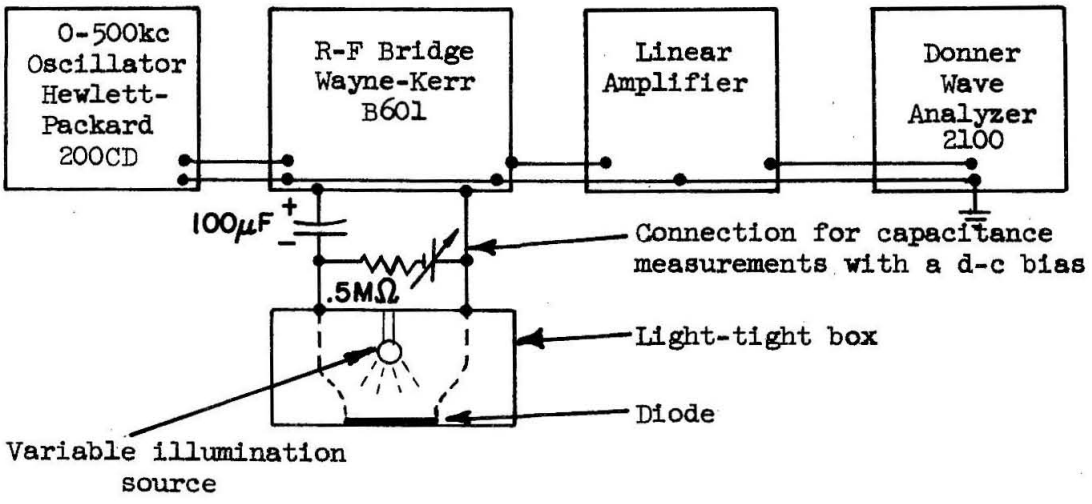

Figure 6.1a. Apparatus used to measure capacitance at low frequencies. ($f < 50kc$)

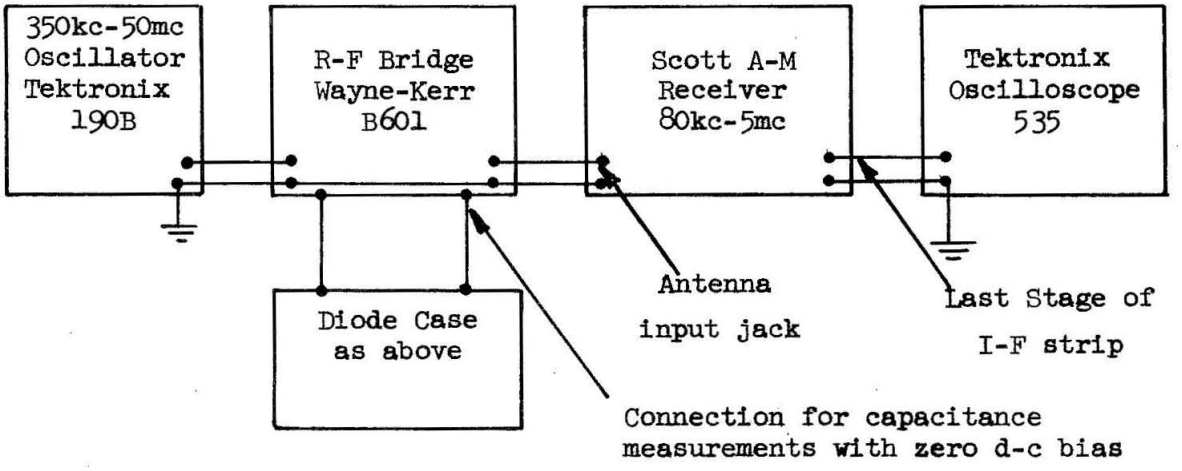

Figure 6.1b. Apparatus used to measure capacitance at higher frequencies. ($f > 80kc$)

These procedures permitted an accurate measurement of capacitance with excitation voltages at the unknown as low as twenty millivolts (peak to peak). Impressed signals less than this did not produce a clear null indication. On the basis of measurements of known capacitance, it is felt that the precision of the measurements is about plus or minus 0.2 picofarads at the higher frequencies, and slightly better than this in the lower ranges of frequency.

6.2. Effects of Trap Filling on Capacitance: Qualitative Treatment

Data on the measured capacitance versus applied frequency for three different thin platelet diodes under various conditions of illumination are presented in figures 6.2 and 6.3. A complete discussion of the curves drawn to fit the data of these figures will be given in Section 6.4. It is proposed here that the variation noted on these curves is indicative of the nature of the trapping states in the crystals. A complete, quantitative, theoretical treatment of the effects of trapping on capacitance has been given in Chapter 2. In this section we shall attempt to clarify the concepts of that chapter, and to develop a physical picture. The discussion to be given will simplify the actual picture by neglecting consideration of the free charge. The magnitude of the free-charge density will be so small, as will be shown experimentally, that only the trapped-charge density will be significant. In succeeding sections of this chapter,

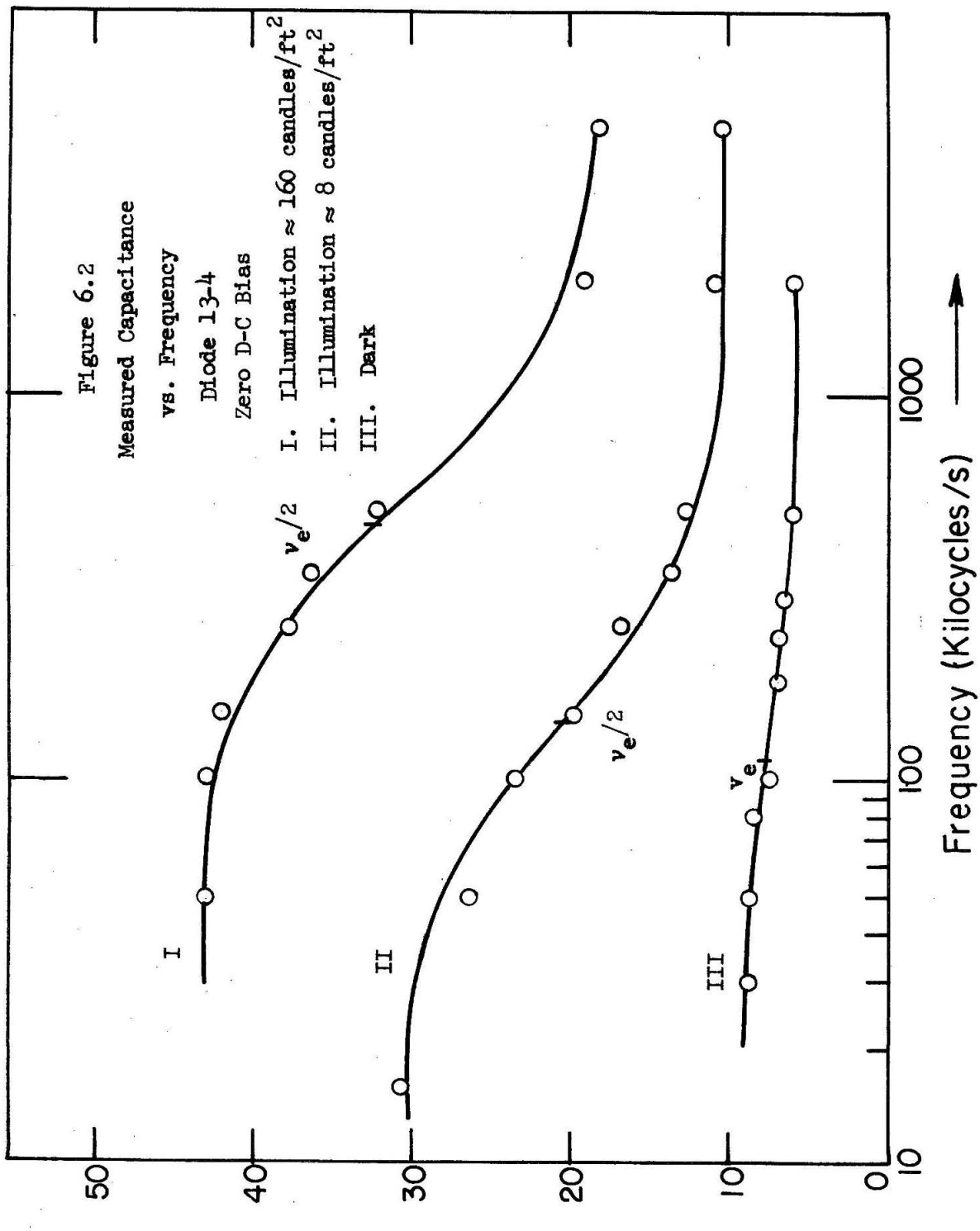
Figure 6.2
Measured Capacitance
vs. Frequency
Diode 13-4
Zero D-C Bias
I. Illumination ≈ 160 candles/ft²
II. Illumination ≈ 8 candles/ft²
III. Dark
I
II
III
$\nu_e/2$
$\nu_e/2$
ν_e
Measured Capacitance (Picofarads)
Frequency (Kilocycles/s)
0
10
20
30
40
50
10
100
1000

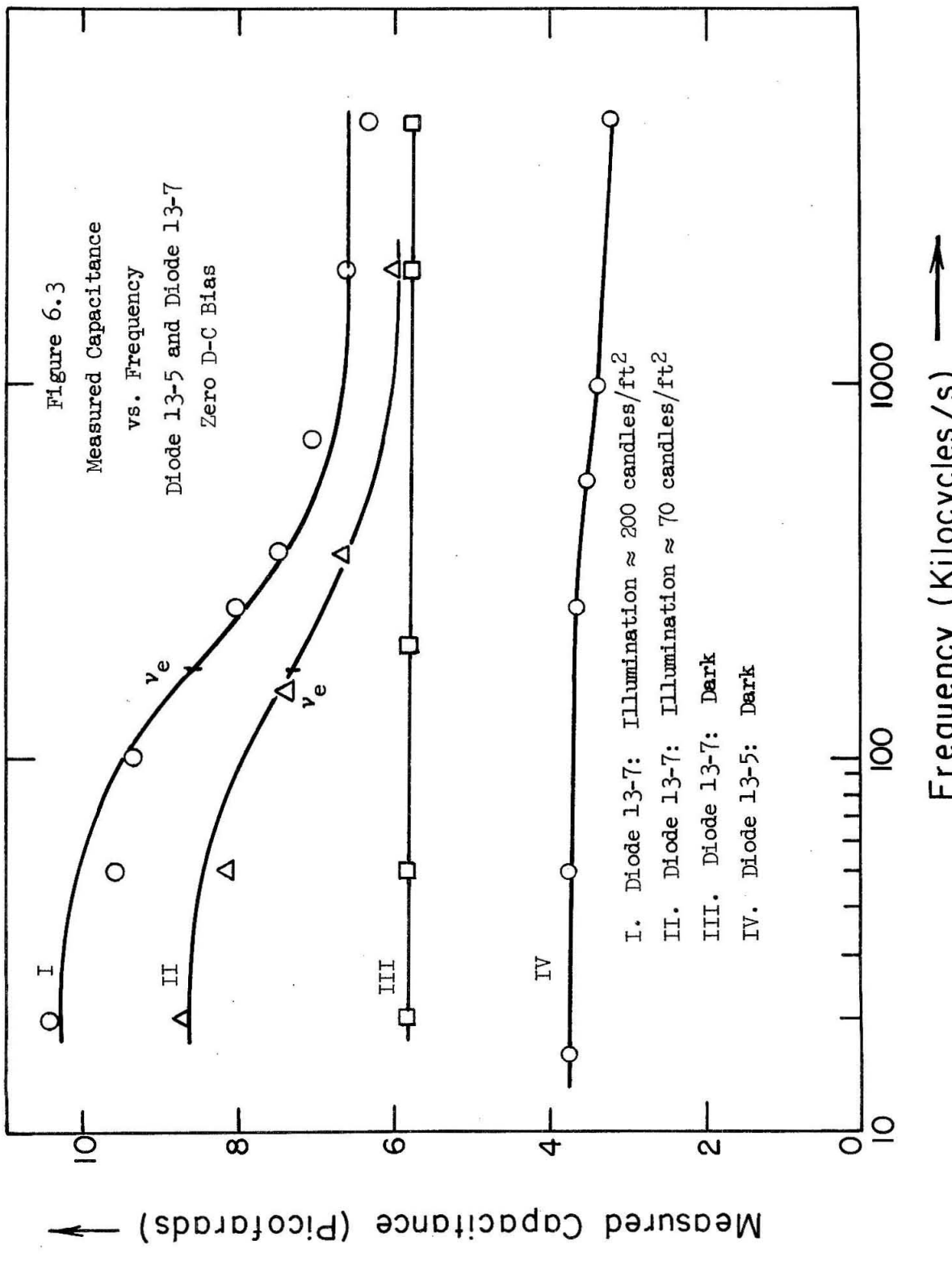
Figure 6.3
Measured Capacitance
vs. Frequency
Diode 13-5 and Diode 13-7
Zero D-C Bias
Measured Capacitance (Picofarads)
Frequency (Kilocycles/s)
10
100
1000
0
2
4
6
8
10
I
II
III
IV
ν_e
ν_e
I. Diode 13-7: Illumination ≈ 200 candles/ft^2
II. Diode 13-7: Illumination ≈ 70 candles/ft^2
III. Diode 13-7: Dark
IV. Diode 13-5: Dark

we shall analyze the data presented in figures 6.2 and 6.3 and present other results from an experimental investigation of the effects of trapping on measured capacitance.

The terminal capacitance measured by a bridge circuit may conveniently be divided into two parts corresponding to the charge stored internal to the crystal and that stored at its surfaces. If one dealt with perfect crystals at very low voltages, the entire capacitance would be the latter: that is, all charge storage would be at the crystal surfaces. The presence of trapping states in the crystal, however, allows there to be significant charge storage interior to the crystal. This fact was graphically demonstrated by Smith [18] who detected the trapped charge itself by dropping a CdS crystal that had been carrying currents onto the pan of a gold leaf electrometer. Smith and Rose also demonstrated a kinetic property of the trapped charge, by showing that space-charge-limited currents near to the theoretical trap-free crystal value could be attained by pulsing the crystal with current so quickly that the traps remained essentially empty [10].

The charge stored interior to the crystal will also make itself evident by increasing the capacitance measured on an a-c bridge. So long as there is time for the trap population to follow the changing applied signal this interior charge reservoir will be effective in increasing the capacitance. As the signal frequency is increased, however, one must reckon

with the time it takes to fill or to empty the traps, and thus to create or to annihilate the electrical flux lines connecting the interior charge with an electrode. As this time becomes comparable with the cycle time of the applied voltage, the traps begin to become insensitive to the voltage - either remaining terminals for flux lines emanating from positive charge held fixed at the metallic electrodes, or else remaining empty.* Thus, at high frequencies, when the traps have assumed a stable population by the process outlined above, a further increase in measuring frequency will result in a constant measured capacitance. This capacitance should be that due to charge storage on the electrodes, with the crystal acting only as a dielectric separator for the charge. If the crystal is capable of injecting electrons from only one contact, the capacitance measured under reverse d-c bias (bias which inhibits injection) should also be that due to the electrodes alone, and hence should match the high frequency value measured under injecting conditions.

6.3. Experimental Observations of Trapping Capacitance

In order to test the validity of our assumption that the added capacitance at lower frequencies is due to trapped charge, a number of tests were performed.

---

* Lampert and Rose analyzed the transient behavior of ohmic contacts to insulating crystals by considering, as we do here, the change in flux linkages between the trapped charge and the charge on electrodes [32].

First, the dependence of capacitance on d-c bias was investigated. Noting from Chapter 4 that charge injection in the dark is impossible when a negative bias is applied to the gold contact, we can expect that any increase in capacitance due to trap filling will disappear under reverse bias. As in Chapter 5, we denote this non-injecting d-c polarity as reverse bias, to be distinguished from the charge-injecting case, or forward bias. The variation of capacitance with d-c bias voltage under forward-bias conditions might take on a number of forms dependent on the inter-relationships between trapping kinetics and the Fermi level inside the crystal. The expected behavior has been discussed briefly in Section 2.4, and is sketched in figure 2.5.

Figure 2.5 should be compared with figure 6.4 which represents actual data taken on diode 13-4 at a single frequency for various values of d-c bias. This figure corroborates a number of the features predicted in the preceding section and in Chapter 2. First, as expected, the measured capacitance is constant under reverse d-c bias and lower in value than under forward bias. Second, the capacitance rises along a curving path for low forward biases, and then assumes a roughly constant value above 6 volts. The constant value indicates trapping by a level having a population density in a ratio to the free-charge density that is independent of voltage (Section 2.4). As we saw in Chapter 5, this constant-ratio condition demands that the crystal Fermi level be situated in a region devoid of traps and enough below the trapping energy that Maxwell-Boltzman

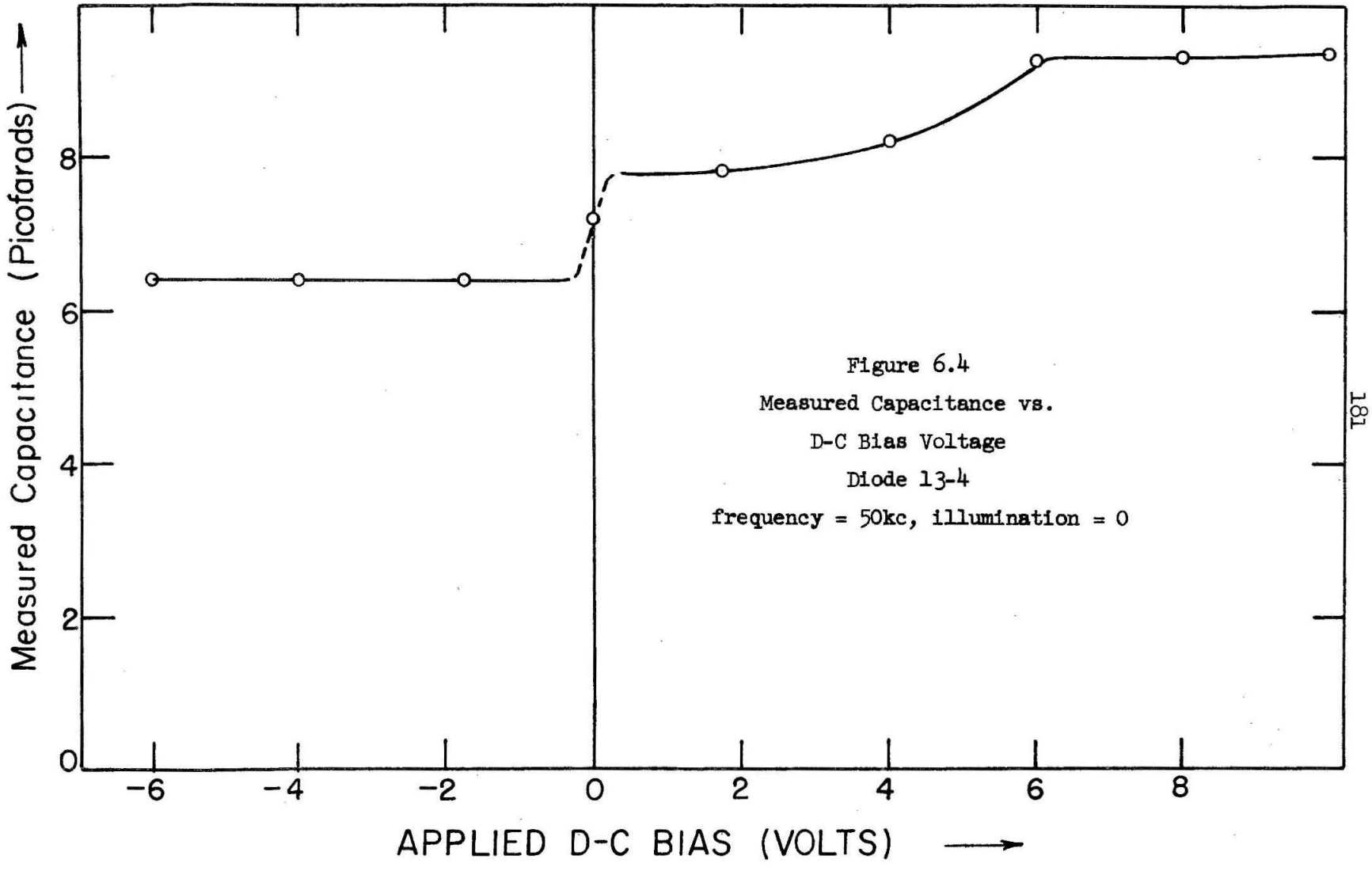

Figure 6.4
Measured Capacitance vs.
D-C Bias Voltage
Diode 13-4
frequency = 50kc, illumination = 0

statistics are a good approximation for the population density. From the space-charge-limited characteristic for diode 13-4 discussed in Section 5.8, we concluded that at about 6 volts of forward bias the Fermi level moved from the midst of trapping levels, detected in that crystal as being distributed in energy, to an energy region that was essentially devoid of traps. Thus, the two observations of the behavior of diode 13-4 are in agreement. In figure 6.4, the region close to the origin of the abscissa is sketched as a dotted line in agreement with the prediction of figure 2.5. Experimental data was omitted here because the electrolytic capacitor used for the d-c bias measurements (figure 6.1) needed about a half volt of reverse bias for accurate operation of the bias circuit.

A second check on our model of trapping capacitance variation arises from the following consideration. If the decrease in capacitance with frequency is due to the ineffectiveness of traps because of kinetic limitations, as we have supposed, then the high-frequency capacitance should assume a constant value after all of the traps have ceased to be responsive to the applied a-c signal. This high frequency capacitance value should, therefore, be just the capacitance due to charge storage on the electrodes. In the preceding paragraph, we have reasoned that the capacitance under reverse d-c bias conditions should also assume the value characteristic of the crystal electrodes. Such a correspondence is found, approximately, between the high

frequency dark value for diode 13-4 in figure 6.2, and the back-biased dark value given for the same diode in figure 6.4. These values actually differ by about 0.5 picofarad: however, it is felt that this difference results from an insufficient time allotted for complete equilibrium in the dark in the data of figure 6.4. The capacitance values, like the space-charge-limited current values of Chapter 5, are light sensitive and equilibrium takes long intervals of time. To test this conclusion further, the data plotted in figure 6.5 were taken. These measurements not only affirmed the conclusion we have presented for capacitance values at illumination levels matching those of the data in figure 6.2, but also gave evidence of another phenomenon. We shall discuss this more fully in Section 6.6. At this time, we merely point out that the rising capacitance values, noted in figure 6.5 at low reverse biases under illuminated conditions, suggest that charge injection apparently is taking place in this region despite the bias condition.

A third test of the hypothesis, that interior charge storage in volume-distributed traps is responsible for the changes in capacitance observed, is contained within figures 6.2 and 6.3. We note there that the variation from maximum to minimum of capacitance at a given illumination is always less than a factor of three. For low level illumination on diode 13-4, the ratio is close to a factor of three, but not quite that great. This observation checks with the prediction of Section 2.1, based upon the maximum capacitance one can

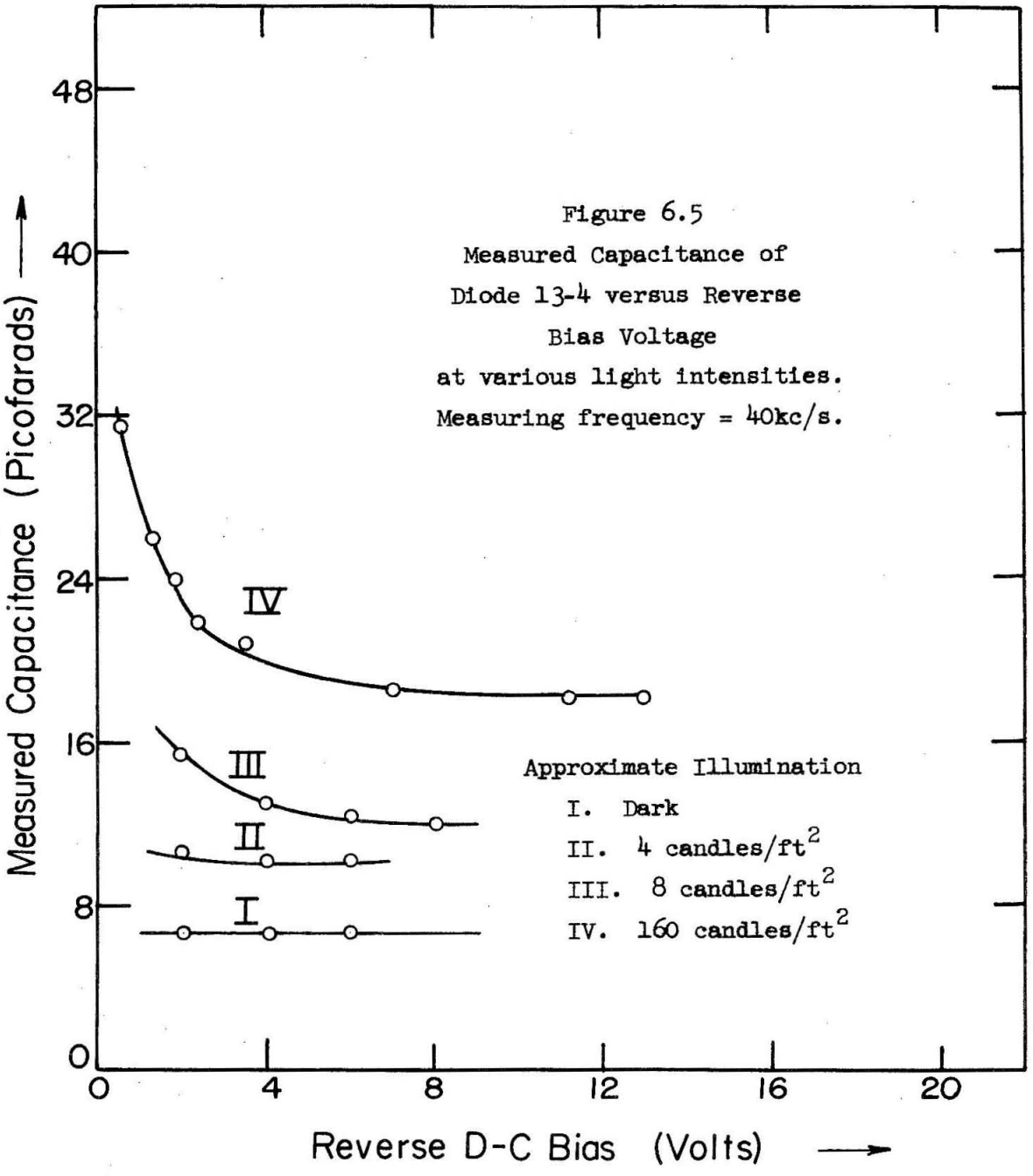

Figure 6.5
Measured Capacitance of
Diode 13-4 versus Reverse
Bias Voltage
at various light intensities.
Measuring frequency = 40kc/s.

observe in a distributed charge system, having a maximum density near the injecting electrode, when it is coupled to a planar sheet of charge. In discussing the frequency dependence in Section 6.4, we shall have more to say about the actual ratios observed between maximum and minimum capacitance. We shall also comment more generally, at that time, about the effect of illumination on capacitance.

6.4. Quantitative Analysis of the Capacitance Measurements

In this section we shall make quantitative deductions from the data which have been discussed briefly in Section 6.3. Certain physical parameters that are pertinent to trapping kinetics will be determined, as well as the numerical densities of the traps taking part in the capacitance measurements.

The first measurements we shall consider are those presented in figure 6.2 and figure 6.3, which show the frequency variation of the measured capacitance. The theoretical analysis of Chapter 2 predicted a variation of C_t with frequency of the form: $C_t = C_t'/(1 + \omega^2/\nu_e^2)$, as given in equation 2.15, and plotted in figure 2.3. The frequency dependence exhibited by figure 2.3 appears to be a good representation of the experimental data given in figure 6.2, and of the intense-illumination data given in figure 6.3. The theoretical curve predicts that the frequency variation in

C_t will be completed in roughly two decades range in frequency, centered approximately at the probability-of-escape frequency ν_e for the influential trapping levels. This is seen to match the approximate range of variation in the experimental data. To check further on the over-all correspondence of the data to equation 2.15, the theoretical curve of figure 2.3 was fitted to the experimental points of figure 6.2 and 6.3 in the manner we shall now describe. The maximum variation noted in measured capacitance was multiplied by the ordinates in figure 2.3, and the resultant values were plotted to a logarithmic scale in frequency, which matched physically the scale of the data to be fitted. This plot was then positioned on the actual measured points to obtain the best fit for the data taken. The solid lines on figures 6.2 and 6.3 were drawn in this fashion. The curve fitting made it possible to obtain a representative value for ν_e simply through notice of the position of this frequency on the calculated curve, relative to the measured data. A discussion of the observed values for ν_e, as noted on the experimental data will be given in Section 6.5.

The curves, drawn as we have described, are seen to be a very good fit to the experimental points. Since no account was taken of transit-time effects (Section 2.3) in drawing them, charge transport from electrodes to traps apparently does not limit until after kinetic limitations have already nullified the effect of the traps on capacitance. Curve IV in figure 6.3, representing the data taken on diode 13-5, does not appear to vary as described in equation 2.15 and could, perhaps, be

reflecting a transit-time limitation in its behavior. Unfortunately, only the data presented in figure 6.3 is available for this diode, since it was inadvertently destroyed before further measurements could be made.

No variation for the capacitance of diode 13-7 in the dark was detectable, which would indicate an insufficiency of injected, trapped charge in the dark for detection by the apparatus. This experimental observation suggests that we calculate the minimum trapped-charge density that was detectable by the measuring technique used. As stated in Section 6.1, the lowest practical excitation voltage across the diodes was 10mv peak. Assuming a threshold for detection of 0.2pf, which is our expected error in the capacitance measurements, we calculate a corresponding detectable trapped charge of 2×10^{-15} coulombs. This is only about 1.25×10^{4} electrons. The volume of the thin platelet crystals was in the range of $5 \times 10^{-6} cm^3$. Hence, the trapped-charge density that could be detected is 2.5×10^{9} electrons per cm^3 under the best of circumstances. Actually a factor of 10 times this amount would be more nearly the charge density necessary for an unequivocal measurement. Since only the electrode capacitance was measured in the dark, the injected charge density that could be trapped in diode 13-7 was evidently less than about 10^{10} per cm^3 in the frequency range studied. As we see in figure 6.2, the greatest amount of trapped charge, which was detected, contributed 25pf to the over-all capacitance. For

the signal intensity used in these measurements, (V_{peak} = 12mv) this capacitance corresponds to 2.4×10^{11} electrons per cm^3.

In the introductory preface to Chapter 2, it was stated that the free-electron density would be essentially negligible in its effect on measured capacitance when compared to the trapped-charge density in actual crystals. To give experimental evidence for this fact, we note here that the resistance of the diodes, as well as their capacitance, was measured as a function of frequency by balancing the bridge circuit. The lowest value for the resistance so measured was in the range of 100 kilohms. As an order-of-magnitude calculation of the free-charge density, we may use this figure in the conductivity formula, $\sigma = e\mu n = L/AR$, to obtain $n \approx 2 \times 10^9 cm^{-3}$. From our discussion above, such a density is on the verge of detectability and is therefore insignificant. Also, the lowest resistance values were always consonant with the highest frequency, as might be expected, since this condition matches the minimum depopulation of the conduction band by trapping. As seen from the data, the capacitance in this range of frequency always approached C_e, the value stemming only from charge storage on the electrodes. This behavior is again consistent with the indetectability of free charge by capacitance measurements.

The electrode capacitance C_e is seen to have appreciable sensitivity to illumination for diode 13-4, indicating a sizable photodielectric effect. This capacitance, which is

evident either under reverse bias (figure 6.5), or at high frequencies (figure 6.2), changes roughly by a factor of 3 in the range of illumination studied. Bube [1, page 420] gives a summary of the essentially meager experimental work done to date in studying this effect, and also comments on the theories advanced to explain it. The photodielectric effect was not a subject of intensive study in the experiments done here, because of a relatively poor capability for quantitative optical studies. Experimental apparatus for quantitative work should include, at minimum, a light source that is well calibrated both spectrally and in intensity. The light intensity for the source used was only very roughly calibrated and its power spectrum was relatively broad.

A few qualitative statements can, nonetheless, be made, based on the measurements that are available. First, there is at least order-of-magnitude agreement with the factor of three change in relative permittivity, noted in this work, and with some data presented by Bube [1] based on the work of Garlick. Garlick studied the temperature variation of the permittivity of ZnS powders and noted a maximum change with temperature of roughly three times the nominal low temperature value. Of course, for this to have relevance, it must be assumed that the same sources are operative for both the thermal and optical variations in K. Somewhat suprisingly, the apparent change in permittivity under illumination for

diode 13-7 (figure 6.3) is very slight. To determine whether this was, perhaps, due to too low a light intensity, a different light source (150 watt bulb) was used to illuminate diode 13-7. This did result in an increased C_e, which indicates that this diode, too, showed a photodielectric effect under sufficient illumination. The conjecture, attributed to Garlick by Bube, that the increased average dipole moment under illumination of electrons trapped at higher energies is responsible for the photodielectric effect, appears to fit our data. We have already spoken in Chapter 5 of the way in which the average energy of the trapped electrons is increased by illumination, which ties in with this last reasoning. The electrons elevated from the primary centers to the deep traps (0.57 to 0.83ev below W_C), deduced in Chapter 5 to be present in diode 13-4, may be responsible for the large photodielectric effect in this sample. Since evidence for these deep levels was not found in diode 13-7, the relatively slight photodielectric effect in this unit is consistent with this supposition. More research into this effect is certainly desirable.

Returning now to the discussion of the fit of the measured capacitance to the theory of Chapter 2, we take notice of the observed values for the low frequency trapping capacitance. From the theory of Section 2.1, for a pure a-c signal applied, the maximum value for C_t' is C_e ($C_t' = C_t$

at low frequencies for a single injecting electrode) and $2C_e$ for C_t'' ($C_t'' = C_t$ at low frequencies for two injecting electrodes). The electrode capacitance C_e is, as has been discussed, a different value at each different illumination.

For diode 13-4 in the dark (curve III in figure 6.2), C_t' is roughly $(1/2)C_e$. The evidence from figure 6.5 is that the gold contact is not injecting in this case so that the maximum trapping capacitance is $C_{tm} = C_e$. The reason for $C_t' < C_{tm}$ could be either a non-uniform charge density due to space-charge-limited charge injection (Section 2.4) or an observed injection efficiency $\eta < \eta_m$ (Section 2.2.2). Under moderate illumination (Curve II of figure 6.2), C_t'' is approximately $2C_e$, which indicates two injecting contacts, as corroborated by the data of figure 6.5. Under heavy illumination (Curve I of figure 6.2) C_t'' approximately equals $(3/2)C_e$. This reduction of C_t'' from C_{tm} could be the result of an η less than η_m due, perhaps, to a diminished voltage injection efficiency for free charge. For the heavy illumination case, in order to achieve a C_t equal to $2C_e$, as theoretically possible, both contacts would have to supply a trapped-charge density of 2.5×10^{11} electrons cm^{-3}. It could well be that the apparent photoemission from the gold fails to provide this density and thus limits the observed C_t. It is also possible that non-uniformity in interior charge density results from the heavy illumination on one side of the crystal, and that this acts to limit the capacitance. A space-

charge-limited effect seems implausible to explain $C_t'' < C_{tm}$ for the heavy illumination case after the evidence of curve II.

For diode 13-7, C_t'' is approximately equal to C_e under heavy illumination (curve I of figure 6.3), and is less than C_e in all other cases. This indicates a single injecting contact with η being dependent on illumination. Data under reverse-bias conditions for this diode, similar to figure 6.5, did not show any rise in capacitance at low reverse d-c biases until higher illumination values than those given in figure 6.3. Thus, the two observations are again consistent, indicating a blocking contact for the gold-film electrode on diode 13-7 in the illumination range studied.

6.5. Interpretation of the Deduced Values for the Probability-of-Escape Frequency

As described in Section 6.4, in fitting equation 2.15 to the measured capacitance data, one can determine the value of the probability-of-escape frequency ν_e. For a single injecting contact, ν_e will be equal to the applied radial frequency which halves the low frequency value of C_t. We have shown, in Section 2.2.2, that under conditions of charge injection from both contacts, the frequency variation of C_t is roughly centered about $\nu_e/2$ (equation 2.18). This occurs in the double-injection case with no bias, because the trapped-charge density must respond effectively at twice the rate of change of the applied voltage. Thus, curves I and II in figure 6.2,

which (from the evidence discussed in Section 6.4) represent charge injection from both contacts, show a frequency drop characteristic of $\nu_e/2$ while those of curve III on figure 6.2 and curves I and II of figure 6.3 are characteristic of ν_e itself. The frequencies corresponding either to ν_e or to $\nu_e/2$ are marked on each curve of figures 6.2 and 6.3 for which the detected behavior made such a deduction possible. The actual values for ν_e are given by the radian frequencies which correspond to 2π times the frequencies noted on figures 6.2 and 6.3. This follows from the analysis of Chapter 2.

We shall first consider the value of ν_e noted in figure 6.3 for diode 13-7. The space-charge-limited current data of Chapter 5 indicated trapping in this diode by a discrete level or by levels sufficiently high in energy to be subject to Maxwell-Boltzman statistics.* Hence, if we assume that the thermal equilibrium value for ν_e applies in the capacitance experiments, we may use equation 2.10 to calculate the product $S_t \exp[-(W_C - W_T)/kT]$ from the observed value of ν_e. Thus,

$$S_t \exp[-(W_C - W_T)/kT] = \nu_e/vN_c \qquad (6.1)$$

The value of ν_e observed for diode 13-7 is (from figure 6.3)

* In Chapter 5, the discussion of crystals whose behavior indicated only a discrete-energy trapping level was framed in terms of the properties of diode 13-5. Since this unit was inadvertently destroyed, continued research on diode of this trapping character is reported for diode 13-7.

$\nu_e = 2\pi \times 1.8 \times 10^5 = 1.13 \times 10^6 s^{-1}$. Insertion of this result in equation 6.1 yields: $\nu_e / v N_c = 8.2 \times 10^{-20}$ at $300^\circ K$ ($v \approx 10^7 cm/s$ at $300^\circ K$). In order to proceed to a determination of the capture cross-section S_t, we must obtain a value for the depth of the level. As we have noted in Chapter 5, it was not possible to obtain the trap depth from the space-charge-limited behavior. However, a maximum value for the trap depth was calculated in Section 5.4. Using the result of that calculation ($(W_C - W_T) < 0.56ev$) in equation 6.1, we calculate a value $S_t = 6.3 \times 10^{-12} cm^2$. Such a cross-section is exceedingly large: in fact, as Rose has pointed out [30], the largest value one could logically expect for S_t for a singly-charged trapping center at room temperature is $10^{-13} cm^2$. A cross-section of this dimension results from consideration of the distance that the Coulomb field of a charge-capturing center will reach out to depress the energy potential in space a value kT below its surrounding value. Thus, we may assume that the traps are in reality shallower than 0.56ev.

A commonly-reported value for S_t [2] is $10^{-15} cm^2$, which would be expected from the physical dimensions of the atoms or ions. If this were the cross-section for the traps under consideration in diode 13-7, it would imply from equation 6.1 that $(W_C - W_T) = 0.24ev$. Conversely, if the largest value of $10^{-13} cm^2$ existed for the trapping cross-section (the trapping center would then have to be positively charged), we could

calculate a maximum value for $(W_C - W_T)$ using equation 6.1. For diode 13-7, this allows us to write: $(W_C - W_T) \leq 0.36$ev. Hence, the capacitance data indicate a smaller limit for the depth than the 0.56ev derived as the maximum from the space-charge-limited current considerations of Section 5.4. The capacitance considerations have thus led both to an upper bound for the trap depth and a probable value for it, assuming that the center is uncharged.

In the data for diode 13-4 (figure 6.2) we note an increase in the value of ν_e obtained under increased illumination; whereas the value of ν_e obtained for diode 13-7 (figure 6.3) was independent of illumination. In Section 2.2.1, it was pointed out that if the ratio of total, free charge to total, trapped charge in a crystal is specified by Fermi-Dirac statistics, then the resultant ν_e and γ as used in equation 2.9, will be dependent on the position of the Fermi level. Hence, we conclude from the capacitance measurements that Fermi-Dirac statistics are needed to specify n/n_t at low voltages in diode 13-4, and furthermore that the Fermi level is sensitive to the applied illumination. This finding is entirely consistent with our investigation of the space-charge-limited current behavior of diode 13-4, discussed in Section 5.5. A continuous distribution of traps surrounding the Fermi level at low voltages (and subject, therefore, to Fermi-Dirac statistics) were deduced to be present from the measurements reported in

Chapter 5. The effect of illumination on the position of the Fermi level for diode 13-4 is summarized in figure 5.3.

Figure 6.2 shows that ν_e changes roughly by a factor of 8 from its dark value to the frequency obtained under heavy illumination. We may define an effective trap depth and capture cross-section for the over-all trapping process in diode 13-4 through insertion of the measured ν_e into equation 2.10. With this definition, the change in ν_e with Fermi level may either be reflected by a change in effective cross-section or in the effective trap depth. The latter course seems most meaningful in light of the source of the variation. The observed factor of eight increase in ν_e indicates only an 0.05ev decrease in the effective trap depth. In Section 5.8, the evidence from space-charge-limited current behavior indicated that light intensities in the range of the maximum used were capable of raising the interior Fermi level by roughly 0.25ev. We must assume, therefore, that most of the trapping states detected by the capacitance measurements exist appreciably above the dark Fermi level. Hence, the frequency dependence obtained is a function chiefly of the shallow trapping centers.

The lowest value obtained for ν_e ($\nu_e = 7.5 \times 10^5$ per s) implies a magnitude: $S_t \exp[(-W_C - W_T)/kT] = 5.3 \times 10^{-20} cm^2$ for the product defined in equation 6.1. At maximum illumination this product climbs to approximately $4.2 \times 10^{-19} cm^2$. If, as

with diode 13-7, we assume a geometrical capture cross-section of $10^{-15}cm^2$, we may calculate the effective trap depth for the three levels of illumination in figure 6.2. In the dark, this value is 0.25ev; it decreases to 0.23ev at medium illumination and to 0.20ev at high illumination.

6.6. Conclusions

The experimental work reported in this chapter has verified the predictions of Chapter 2 in the following manner:

1. The variation with frequency of the capacitance observed has been consistent with the predicted variation with frequency for the terminal capacitance exhibited by trapped charge whose density is subject to a rate equation of the form of 2.11 ($dn_t/dt = -(n_t - \gamma n)\nu_e$).
2. The variation of capacitance in magnitude has been within the limits expected for trapping states distributed uniformly in space. Furthermore, the variation in magnitude has been predictable in terms of the effects of environment upon trap populations.

From these observations, the interpretation of the experimental results in terms of the kinetic properties of trapping states appears to be justified.

The frequency dependence of the measured capacitance yields directly a value for the probability-of-escape frequency ν_e. To obtain a value for the trap depth from this, we noted in Section 6.5 that a knowledge of the capture cross-section for the trapping level was necessary. A similar situation occurs in the study of traps through the observation of luminescent glow-curve data [1, p. 292], a technique used extensively in deducing trapping properties in phosphors and employed by Bube [8] in a study of the trapping states in CdS.

To make glow-curve measurements, crystal traps are initially filled at liquid nitrogen temperatures by illumination. The traps are then emptied into the conduction band by heating the crystal at a constant rate. In the experimental method used by Bube [8], the current passing through ohmic contacts made to the crystal was monitored under constant voltage conditions in order to provide a measure of the conduction-band population. Peaks, which correspond to traps being emptied into the conduction band at a maximum rate, are observed in the plotted curve of current versus crystal temperature. A fairly straightforward analysis relates the temperature at these peaks to a function of the depths and capture cross-sections for the traps which are responsible for them. Glow-curve measurements do not provide accurate, independent values for the depth and cross-section of a given trapping level. In order to obtain both of these parameters in his study of the

trapping properties of CdS, therefore, Bube used the further assumption that $W_F \approx W_T$ at the peak current. This assumption depends for its validity on a number of conditions, including the supposition that the electron population in the crystal maintains a continuous thermal equilibrium between all energy states despite increasing temperature. Trap depth is easily deduced under the condition $W_F \approx W_T$ from the insertion of the free-electron density, implied by the observed current, into the Maxwell-Boltzman formula $n = N_c \exp[-(W_C - W_F)/kT]$. The equation relating trap depth and capture cross-section to the temperature at the peak current may then be used to calculate S_t. Because trap depth enters this equation exponentially, however, the assumption used to obtain the depth critically affects the magnitude for S_t.

Bube's data for pure CdS crystals indicate principal shallow-trap densities at 0.17 and 0.35ev in pure crystals and at 0.06ev in doped crystals. These depths are consistent with the shallow levels deduced from the observations discussed in this chapter. The capture cross-sections Bube ascribes to these levels is about $10^{-18}cm^2$, which is appreciably lower than the $10^{-15}cm^2$ we had assumed in this chapter. Use of a cross-section of $10^{-18}cm^2$ in the calculations of Section 6.5 would raise the effective trap depth deduced for diode 13-7 roughly to 0.07ev below the conduction band. It is idle to speculate further on the correspondence between Bube's

results and those reported here, however, because first, the degree of similarity between Bube's crystals and those studied here is unknown, and second, because neither the experimental technique used in this work nor the one used by Bube provides a dependable means for the separate determination of trap depth and capture cross-section. The two methods of trap study, luminescent glow-curve measurements and capacitance observations, used together on a single crystal would eliminate ambiguity in the separation of these trap properties, because each provides an independent relationship between capture cross-section and trap depth. We have already discussed the possible physical sources for the shallow levels (Section 5.6), and will not mention them further here.

The experiments on capacitance reported in this chapter were all performed on the thin platelet diodes. The inverse dependence for capacitance on thickness would have made the capacitive effect due to the trapped charge undetectable for the larger crystals. In other measurements of the capacitance of single-crystal CdS units reported by Kallman et al [33], crystal thicknesses were 20 to 30 times those used for the work reported here. One would therefore not expect to detect the trapped charge in their measurements. Kallman does report enormous increases in capacitance under illumination for these thicker CdS crystals, which were contacted by two gold electrodes. The authors explain this in terms of an effective change in crystal

thickness due to high conductivity in regions of the interior of the CdS crystals. The crystals we have studied did not exhibit any phenomena consistent with this physical picture.

The brief discussion on evidence for the photodielectric effect, given in Section 6.4, does not mention the fact, brought out by Bube [1, p. 429], that some researchers, including Kallman [33], believe that the effect is confined to powders. The evidence of figures 6.2 and 6.5 indicates the contrary, as also does the variation in C_e for diode 13-7 under heavy illumination, reported in Section 6.4.

The evidence for an apparent photoemission from the gold film into the CdS, presented in figure 6.5, is in agreement with the hypothesis of Williams and Bube [15]. These authors explain the observed photovoltaic voltage in junctions made to CdS by gold, copper, silver and some other metals, in terms of photon-stimulated emission from the metallic films into the CdS crystals. The observed behavior of the capacitance in figure 6.5 may be explained in terms of photoemission from the gold electrode as follows. Photoemitted electrons would form a virtual cathode near the gold contact. One would expect to be able to modulate the photoemitted current by applying a voltage less than that value tending to draw the entire virtual cathode density across the crystal. For higher collection voltages, no modulation would be possible. The situation is perfectly analogous to the operation of a vacuum

diode in the emission-limited region. The only difference is in the stimulus for the emission - light for the case described here and heat in the thermionic emission case. If the injected charge density, and therefore the trap population, can not be modulated by the applied signal, no trapping capacitance is measured. Thus, in figure 6.5, an increased reverse d-c bias acts to quench the trapping capacitance. The increased photoemission is evident in the increased d-c voltage required for quenching the trapping capacitance at higher illumination values.

In assessing the effectiveness of capacitance studies to gain information about trapping kinetics, we find both benefits and drawbacks. The benefits include the possibility of variation of a number of parameters. The observed dependence of the measurements on these parameters (d-c bias, a-c signal magnitude and frequency, illumination, temperature) can do much to develop a physical picture of the trapping process. One can also detect an extremely small quantity of trapped charge through capacitance measurements; the threshold estimated in Section 6.4 was only about a thousand electrons. The chief disadvantage of this technique is the fact that a number of experimental points are necessary to determine one kinetic parameter, such as ν_e. Frequency information is then achieved only through curve fitting, which is apt to be a tedious process. In general, capacitance measurements provide a valuable adjunct to the other techniques available for the study of trapping kinetics.

CONCLUSIONS

We shall begin this section with a short summary of the major topics discussed in each of the chapters and of the conclusions we might draw from our discussion of these topics. Further observations, pertinent to the over-all report, will then be made.

In Chapter 1, it was shown that a simplified analysis which helps preserve the physical picture of events may be used in a straight-forward fashion to treat mathematically the properties of space-charge-limited currents in trap-filled insulators. The mathematical approach used there avoided a direct solution of the exact equations but retained the pertinent features of the dependence of current on voltage. Chapter 2 presented a mathematical treatment of the expected dependence of capacitance on trapping properties for an insulator under charge-injection conditions. The predictions of that chapter led one to believe that a study of the variation of capacitance with parameters such as bias voltage, illumination, and frequency could provide a valuable adjunct to the more usual techniques employed in the study of trapping kinetics. The procedures followed in the fabrication of analogue diodes in CdS were discussed fully in Chapter 3.

In Chapter 4, an experimental analysis of the properties of the blocking contact to CdS under high reverse bias was reported. The data corresponded to Schottky-type field emission

over the blocking contact, although a possible tunnel mechanism through the barrier was not ruled out. The requisite high effective-donor-state density near the surface for tunnel emission made this process implausible. Such a high state density was not detected in any of the other experiments. In Chapter 5, experimental data were presented which were in direct agreement with the theory of Chapter 1. Chapter 5 thereby reinforced confidence in the physical picture of a volume-distributed trap population which underlay the theory of Chapter 1. A number of properties of trapping centers were deduced in Chapter 5 and correspondence with published data was shown to be very good. The experimental results of Chapter 6 were consistent with the analysis of Chapter 2 and therefore allowed further deductions of the properties of the trapping states in CdS. The new technique for obtaining a probability-of-escape frequency, explained in Chapter 6, gave results that were both plausible and of the same order of magnitude as values deduced in a different fashion by other investigators.

The correspondence observed between experiment and theory leaves little doubt that the physical picture emphasizing volume-distributed traps, as developed in Chapter 1, results in a valid description of the behavior of the crystals studied. Thus, we may assume that space-charge-limited currents have been observed in the CdS crystals, contrary to the premise of control by a surface trapping layer as postulated by Rhys-Roberts and Tredgold [7]. The capacitance measurements of Chapter 6, in

particular, are not consonant with surface trapping in either magnitude or variation.

The experimental results of Chapter 5 make it apparent that one should attempt to exceed the trap-filling voltage $V = eN_tL^2/2K\epsilon_0$ (equation 1.18) in order to achieve any appreciable, space-charge-limited current levels in an analogue device having dimensions of the order of the diodes studied in this work. The trap-filling voltage must be exceeded without applying a field which will cause a dielectric breakdown in the material. A breakdown field at $V = V_{TFL}$ would be the limiting case of a useful analogue device. In order to have any dynamic range and to allow for local inhomogeneities, the field should be held to some fraction of the breakdown value when all the traps are filled. This constraint can be used together with an estimated lower limit for the crystal trap densities to calculate an approximate thickness limitation for a solid-state analogue device, as we shall now demonstrate.

The average field at $V = V_{TFL}$ is expressed from the trap-filled voltage formula as $\underline{E} = eN_tL/2K\epsilon_0$. We can solve this equation for the thickness: $L = 2K\epsilon_0\underline{E}/eN_t$. To calculate a maximum thickness for the crystal we need only to insert a maximum permitted $\underline{E}$ and a minimum expected N_t in this formula. In Chapter 4, evidence corresponding to that reported by Williams [28] indicated an apparent dielectric

breakdown in CdS at a field of about 10^6 volts/cm. From what we have said above, the maximum value for $\underline{E}$ might therefore be set at 10^4 volts/cm. To choose a minimum for N_t, we need to consider the present technology of materials. Utilizing the vast amount of experience accrued in the technology of germanium crystal growth, specialists have been able to grow crystals of that material having trap densities as low as 10^{11} cm^{-3} [34]. This perfection has not been reached for the larger band-gap materials: with silicon the best material has about 10^{13} traps/cm^3.* Bube [8] suggests that a perfection comparable to this might be obtained in CdS. A trap density of 10^{13} cm^{-3} corresponds to a single trap in almost 10^9 lattice sites for CdS and therefore certainly represents a high degree of perfection. Assuming a trap density of this magnitude together with an electric field of 10^4 volts/cm, we calculate a maximum thickness of roughly 10 microns for a crystal showing trap-free space-charge-limited currents over a useful dynamic range. Poorer materials, such as the crystals studied in this report, decrease this thickness by the ratio of the actual N_t to 10^{13} cm^{-3}. For example, a trap density of 10^{16} cm^{-3} results in a thickness maximum of only 100 angstroms. Thus, we see that any practical solid state analogue device will necessarily be very small indeed. Because of this, fabrication techniques will be extremely critical, especially for three-element devices.

---

* G. C. Dacey - personal communication

The fine control of thickness and geometry, possible with vapor-deposition techniques, has led to an attempt to adapt this process to analogue device manufacture. Work has been reported by Weimer on the construction of an analogue three-element unit in CdS made completely by vacuum deposition of the electrodes and CdS in powder form [35]. The correspondence of behavior between single crystals and powders must be thoroughly investigated to determine what portion of the information now available will be useful if this form of fabrication is employed. Polycrystalline material will certainly have a larger trap density than the estimate of $10^{13} cm^{-3}$ which, if one specified $V < V_{TFL}$, would necessitate an even smaller thickness than the 10 microns calculated above. Vapor-deposited fabrication, however, might so reduce the permissible size for the device that the variation of output current with the cube of reciprocal electrode spacing (equation 1.14) could compensate for the reduced θ due to an increased trap density.

If analogue devices were to be made of single crystal material, it is probable that epitaxial growth techniques could be profitably employed. Using epitaxial growth, a three-element device might be made by using a thin platelet seed crystal having a vapor-deposited metallic grid structure. Smith and Ruppel [29] did construct a three-element crystal amplifier on a thin platelet crystal but their geometry was far from ideal for a practical device.

The exploitation of insulating materials with high trap densities in unconventional ways may be possible with crystals of more manageable dimensions. An unconventional device could, for example, employ the variation of trapped charge with frequency, as investigated in Chapter 6, to provide a frequency-variant capacitance. If the source for a given trapping level could be correctly identified and synthesized, such a device might be tailor-made for a specified frequency range. Thickness, for a given capacitance, would be proportional to electrode area in this case. Variation with bias voltage of capacitance, as described in Chapter 6, could also be used to obtain an element with a gross (factor-of-three) change in capacitance over a small range in bias.

One of the properties of the diodes, noted for each unit but not studied extensively, was the polarity and intensity variation of the open circuit photovoltage (meter resistance = 100 megohms). This effect was definitely centered at the gold contact and differed both in magnitude and polarity in sets of diodes made from apparently identical crystals. The majority of the diodes had a photovoltage which resulted in the gold-film contact becoming more positive with increasing illumination. In a few of the thin platelet diodes, however, the indium terminal became positive with illumination. The magnitude of the photovoltage ranged up to 550mv when the gold contact became positive and to 305mv when the indium contact became positive. A photovoltaic effect causing the gold contact to

become positive could result from photoemission of electrons into the CdS from the gold film. This hypothesis, due to Williams and Bube [15], is corroborated by two effects which we have noted. The first is the behavior of trapping capacitance under reverse bias (Section 6.7), and the second is the fact that for some diodes an increased thickness of gold film resulted in an increased positive photovoltaic effect. The film thicknesses ranged from 500 to 1000 angstroms. A negative photovoltaic effect would be possible if the dominant light absorption were in the interior of the CdS. This would effectively raise the interior Fermi level and cause an electron flow into the gold. As has been noted, an indium-contact-positive photovoltage was observed only in the thin platelet diodes for which the surface preparation prior to electrode deposition was held to a minimum. To fit the picture described above, we might assume, therefore, that a poor surface at the CdS acted to inhibit electron emission from the gold film. The capacitance variation of diode 13-7 was consistent in this respect. Diode 13-7 showed a gold-film-negative photovoltage and also failed to exhibit the variation in capacitance with reverse bias typified by figure 6.5. That variation, in turn, was explained in Section 6.7 as having resulted from the photoemission of electrons from the gold film. These conjectures point up the fact that further study of this effect might yield useful information on the properties of blocking contacts to CdS. Optical effects in CdS that have been studied to date are summarized in a review article by Lambe

and Klick [36]. This reference also has a fairly comprehensive bibliography on other properties of the material.

Another subject which might bear further study is the properties exhibited by some of the larger area diodes made from the crystals that were cut and lapped. Several of the diodes made from chlorine-doped crystals of this type showed properties which were superficially similar to conventional p-n junction diodes of silicon and germanium. There was no evidence of space-charge limitations in their behavior. Further knowledge of the extent of the similarity of such diodes to grown or alloyed junction silicon and germanium units could prove helpful in a study of the properties of metallic contacts to CdS.

LIST OF SYMBOLS

		Section in Which Symbol Is Defined
A	Diode cross-sectional area	1.4
A_e	Richardson thermionic-emission factor	4.3
C	Capacitance	1.4
C_e	Electrode capacitance	2.1
C_m	Measured capacitance	2.1
C_t	Trapping capacitance	2.1
C_{tm}	Maximum value of C_t	2.1
C'_t	Low frequency value of C_t for a single injecting contact	2.2
C''_t	Low frequency value of C_t for two injecting contacts	2.2
c_e	Transition probability for trap emptying	2.2
c_f	Transition probability for trap filling	2.2
E	Electric field magnitude	1.2
$\underline{E}$	Average value for E	5.8
E_a	Value of E at the anode	1.2
E_{asd}	E_a under space-charge-limited conditions with a discrete-energy trap density	1.3
e	Magnitude of the electronic charge	1.1
h	Planck's constant	4.1
I	Current	5.7
J	Current density	1.1
K	Relative permittivity	1.2
k	Boltzman's constant	1.3
L	Crystal thickness	1.2
m	An exponent for voltage	1.4
m_e	Effective mass of a free electron	4.1
m_r	Rest mass of an electron	4.1
N_c	Effective density of states in the conduction band	1.3

N_d	Density of donor states	4.1
N_e	Trapping-state density defined for continuously-distributed traps	1.6
N_t	Density of trapping states	1.3
N_t'	Minimum value determined experimentally for N_t	5.4
n	Free-electron density	1.1
$\overline{n}$	Value of n under no-injection conditions	1.2
$\underline{n}$	Average value for n	1.3
n_a	Value of n at the anode	1.2
n_f	Fundamental of Fourier-analyzed waveform for n	2.2
n_m	Maximum value for n	2.4
n_t	Trapped-electron density	1.2
$\overline{n}_t$	Value of n_t under no-injection conditions	1.3
$\underline{n}_t$	Average value for n_t	1.3
n_{ta}	Value of n_t at the anode	1.3
n_{te}	Trapped charge effective in enhancing C_t	2.1
n_{tf}	Fundamental of Fourier-analyzed waveform for n_t	2.2
R_E	Rate of trap emptying	2.2
R_F	Rate of trap filling	2.2
Q	Quantity of electronic charge	1.4
Q_e	Charge stored on crystal electrodes	2.1
Q_t	Charge stored in crystal traps	2.1
Q_{TFL}	Value of Q_t at the trap-filling voltage	1.4
S_t	Trapping-state capture cross-section for a free electron	2.2
T	Absolute temperature	1.3
T_c	Characteristic "temperature" for an exponential trap distribution	2.1
T_{tr}	Electron transit time	2.2
t	Time	2.1
V	Applied voltage	1.1
V_B	Barrier height potential	4.3
V_f	V at incipient field emission	4.1

V_j	V at which two solutions to the space-charge-limited current characteristic are joined	1.4
V_m	Maximum value of the a-c applied voltage	2.2
V_{os}	V at which ohmic behavior gives way to space-charge-limited behavior	1.3
V_{TFL}	V at which all traps are filled by injected charge	1.4
V_{TFL1}, V_{TFL2}	Values of V_{TFL} for discrete levels when more than one trapping level are present	1.5
v	Free-electron thermal velocity	2.2
v_f	Free-electron drift velocity	2.3
W	Electron energy	1.3
W_a	Electron potential well depth	4.4
W_C	Energy at lower edge of conduction band	1.3
W_F	Fermi-level energy for electrons	1.4
W_G	Energy interval in the forbidden gap	4.1
W_T	Energy of discrete trapping level	1.3
W_{FD}	Quasi-Fermi level for electrons in the dark	5.7
W_{FL}	Quasi-Fermi level for electrons in the light	5.7
W_{Fn}	Quasi-Fermi level for electrons	5.6
W_{Fp}	Quasi-Fermi level for holes	5.6
W_{TL}, W_{TU}	Energies characteristic of various trap configurations	1.6
w	Electron barrier width for electrons having a given energy	4.3
x	Distance	1.2
x_c	Critical distance defined for tunneling	4.2
x_m	Distance from emitting surface to potential maximum in image-force considerations	4.4
α	A constant multiplier	1.4
β	Ratio of the cathode field to the average field in the crystal	4.2
γ	Low frequency equilibrium ratio between n and n_t	2.2
ϵ_0	Permittivity of free space	1.1
η	Proportionality constant between V and n_m	2.2

θ	Ratio of n to n_t for a discrete trapping level under equilibrium conditions	1.3
$\theta_1, \theta_2, \theta_e$	Values of θ characteristic of discrete trapping levels	1.5
λ	Characteristic length for use of image-force potential theory	4.4
μ	Electron mobility	1.2
ν	Parameter defined for algebraic simplification	1.2
ν_a	Value of ν at the anode	1.2
ν_e	Probability-of-escape frequency for an electronic trapping state	2.2
ρ	Resistivity	3.6
ρ_0, ρ_t	Density of trapping states per energy increment	1.6
τ	Lifetime of a free carrier	5.6
ϕ	Emission work function for electrons	4.2
ω	Radian frequency	2.1

REFERENCES

1. Bube, R. H., Photoconductivity of Solids, (1960) John Wiley and Sons, Inc., New York.

2. Rose, A., "Performance of Photoconductors," (1955) Proc. IRE, Vol. 43, (1850-1869).

3. Parmenter, R. H., and Ruppel, W., "Two Carrier Space-Charge-Limited Current in a Trap Free Insulator," (1959) J. Appl. Phys., Vol. 30, (1548-1558).

4. Wright, G. T., "Some Properties and Applications of Space-Charge-Limited Currents in Insulating Crystals," (1959) Proc. Inst. Elect. Engineers (British), Vol. 106, part B, (915-922).

5. Wright, G. T., "A Proposed Space-Charge-Limited Dielectric Triode," (1960) J. British IRE, Vol. 20, (337-355).

6. Smith, R. W., "Ohmic Contacts to Single Crystals of CdS," (1955) Phys. Rev., Vol. 97, (1525-1530).

7. Rhys-Roberts, C., and Tredgold, R. H., "A Note on the Theory of Space-Charge-Limited Currents," (1960) Proc. Phys. Soc. London, Vol. 76, (497-501).

8. Bube, R. H., "Photoconductivity and Crystal Imperfections in CdS. Part II: Determination of Characteristic Photoconductivity Quantities," (1955) Chem. Phys., Vol. 23, (18-25).

9. Lampert, M. A., "Simplified Theory of Space-Charge-Limited Currents in an Insulator with Traps," (1956) Phys Rev., Vol. 103, (1648-1656).

10. Rose, A., "Space-Charge-Limited Currents in Solids," (1955) Phys. Rev., Vol. 97, (1538-1544).

11. Shockley, W., and Prim, R. C., "Space-Charge-Limited Emission in Semiconductors," (1953) Phys. Rev., Vol. 90, (753-759).

12. Suits, G., "Exact Volt-Ampere Relation for the Metal-Insulator-Metal Junction," (1957) J. Appl. Phys., Vol. 28, (454-460).

13. Lampert, M. A., and Rose, A., "Volume Controlled, Two Carrier Currents in Solids: The Injected Plasma Case," (1961) Phys. Rev., Vol. 121, (26-37).

14. Mott, N. F., and Gurney, R. W., Electronic Processes in Ionic Crystals, (1940) Oxford University Press, London.

15. Bube, R. H., and Williams, R., "Photoemission in the Photovoltaic Effect in Cadmium Sulfide Crystals," (1959) J. Appl. Phys., Vol. 31, (968-978).

16. Bube, R. H., and Thomsen, S. M., "Photoconductivity and Crystal Imperfections in CdS. Part I. Effect of Impurities," (1955) J. Chem. Phys., Vol. 23, (15-17).

17. Smith, R. W., "Properties of Deep Traps Derived from Space-Charge-Limited Current Flow and Photoconductive Decay," (1959) RCA Rev., Vol. 20, (69-78).

18. Rose, A., and Smith, R. W., "Space-Charge-Limited Currents in Single Crystals of Cadmium Sulfide," (1955) Phys. Rev., Vol. 97, (1531-1537).

19. Holland, L., Vacuum Deposition of Thin Films, (1958) John Wiley and Sons, Inc., New York.

20. Van Heerden, P. J., "Primary Photocurrent in Cadmium Sulfide," (1957) Phys. Rev., Vol. 106, (468-473).

21. Spangenberg, K., Fundamentals of Electron Devices, (1957) McGraw-Hill Co., Inc., New York.

22. Henisch, H. K., Rectifying Semiconductor Contacts, (1957) Oxford University Press, London.

23. Fowler, R. H., and Nordheim, L., "Electrons in Intense Electric Fields," (1930) Proc. Royal Soc., Vol. 119, (173-179).

24. Vermilyea, D. A., "Electron and Photocurrents in Thin Films of ZrO_2," (1954) Acta Met., Vol. 2, (346-348).

25. Parker, P., Electronics, (1950) Edward Arnold Co., London.

26. Cutler, P. H., and Gibbons, J. J., "Model for the Surface Potential Barrier and the Periodic Deviations in the Schottky Effect," (1958) Phys. Rev., Vol. 111, (394-402).

27. MacDonald, J. R., "Theory of the Differential Capacitance of the Double Layer in Unadsorbed Electrolytes," (1954) J. Chem. Phys., Vol. 22, (1857-1866).

28. Williams, R. L., "High Electric Fields in CdS," (1961) Phys. Rev., Vol. 123, (1645-1651).

29. Ruppel, W., and Smith, R. W., "A CdS Analog Diode and Triode," (1959) RCA Rev., Vol. 20, (702-714).

30. Rose, A., "An Outline of Some Photoconductive Processes," (1951) RCA Rev., Vol. 12, (362-348).

31. Rose, A., "Recombination Processes in Insulators and Semiconductors," (1955) Phys. Rev., Vol. 97, (322-330).

32. Lampert, M. A., and Rose, A., "Transient Behavior of the Ohmic Contact," (1959) Phys. Rev., Vol. 113, (1236-1239).

33. Kallman, H., Kramer, B., and Mark, P., "Impedance Measurements on CdS Crystals," (1956) Phys. Rev., Vol. 99, (1328-1330).

34. Dacey, G. C., "Space-Charge-Limited Hole Current in Germanium," (1953) Phys. Rev., Vol. 90, (759-764).

35. Weimer, P. K., "Evaporated Circuits Incorporating a Thin-Film Transistor," 1962 International Solid-State Circuits Conference Technical Paper Digest (32-33).

36. Lambe, J., and Klick, C., "Electronic Processes in Cadmium Sulfide," (1958) Progress in Semiconductors, (Volume 3), John Wiley and Sons, Inc., New York (183-207).